72-15,056

FABER, Sandra Moore, 1944-
PHOTOMETRY OF ELLIPTICAL GALAXIES IN MULTIPLE SYSTEMS.

Harvard University, Ph.D., 1972
Astronomy

University Microfilms, A XEROX Company, Ann Arbor, Michigan

© 1972

SANDRA MOORE FABER

ALL RIGHTS RESERVED

Reproduced with permission of the copyright owner. Further reproduction prohibited without permission.

PHOTOMETRY OF ELLIPTICAL GALAXIES IN MULTIPLE SYSTEMS

A thesis presented

by

Sandra Moore Faber

to

The Department of Astronomy

in partial fulfillment of the requirements

for the degree of

Doctor of Philosophy

in the subject of

Astronomy

Harvard University

Cambridge, Massachusetts

December, 1971

Reproduced with permission of the copyright owner. Further reproduction prohibited without permission.

PLEASE NOTE:

Some pages have indistinct print. Filmed as received.

University Microfilms, A Xerox Education Company

Reproduced with permission of the copyright owner. Further reproduction prohibited without permission.

ABSTRACT

Elliptical galaxies, globular clusters, and stars have been observed on a 10-color intermediate-band photometric system designed for the study of the integrated spectra of old stellar populations. Measurements of standard stars have been used to calibrate the system absolutely. Observations of 148 stars are used to examine the dependence of certain color indices on temperature and metal abundance. A color index straddling the blanketing discontinuity near 4000 Å is a useful indicator of metal abundance in G dwarfs of roughly solar composition. However, the interpretation of an index monitoring CN absorption as a measure of metal content in K giants is less secure.

10-color observations of 31 elliptical galaxies, largely members of double galaxies or small groups, are presented. To within the accuracy of the present observations, the colors of these elliptical galaxies form a one-parameter family. This single parameter is identified as the galaxy luminosity. The fact that elliptical galaxies of a given luminosity have identical colors suggests their use as standard sources for the investigation of galactic and intergalactic reddening and the cosmological expansion. No variations in galaxy colors that correlated with group properties, types of companions, or the presence of optical line or radio emission were found.

Reproduced with permission of the copyright owner. Further reproduction prohibited without permission.

The strengths of the absorption features CN and Mg "b" plus MgH, together with blanketing caused by metallic lines near 3800 Å, increase monotonically with increasing luminosity. A reddening-free line absorption index monitoring CN and Mg can be used to determine the absolute magnitude of elliptical galaxies with an accuracy of approximately ±0.5 magnitude.

Four red dwarf ellipticals of high surface brightness, three of which have been observed on this 10-color system, appear to constitute a separate class of elliptical galaxy. Several of their properties can be understood in terms of a strong tidal interaction with a nearby, more massive, companion.

The technique of quadratic programming as directed to the problem of galaxy synthesis is described. The method offers significant advantages over the trial-and-error approach usually employed. This technique is applied to the 38-color data of Spinrad and Taylor (1971a) and the 10-color photometry presented here. The results indicate that estimates of mean line strengths in external galaxies by means of population synthesis are well determined. Ages based on the main-sequence turnoff point are uncertain by at least a factor of two. Mass-to-light ratios of the computed populations are uncertain by factors of five to ten.

Reproduced with permission of the copyright owner. Further reproduction prohibited without permission.

ACKNOWLEDGEMENTS

It is a pleasure to thank my thesis advisor, Dr. I. J. Danziger, for his continued support and valuable advice. His suggestion that double galaxies deserved further study originally motivated this investigation. I also thank Kitt Peak National Observatory and Smithsonian Astrophysical Observatory for the use of their observing facilities. The calculations of stellar population models in Chapter 3 were performed on the IBM 360/91 computer at the Goddard Spaceflight Center in Greenbelt, Maryland.

Dr. Eric Becklin and Mr. Glen Veeder communicated data in advance of publication. Dr. Ivan King provided tracings of his spectra of elliptical galaxies and drew my attention to the peculiar nature of NGC 5846A. I also thank Dr. Myron Lecar, Dr. Jay Frogel, and Mr. Duane Carbon for helpful discussions and Dr. N. Visvanathan, Dr. Vera Rubin, Mrs. Jean Goad, Mr. Andrew Faber, and Mr. Fred Chromey for their criticisms of the manuscript. Miss Martha Schwink typed the final draft.

Harvard University paid for most of the travel expenses connected with observing, and the University and Harvard College Observatory shared the cost of the filter set.

The major portion of this research was carried out at the Department of Terrestrial Magnetism, Carnegie In-

Reproduced with permission of the copyright owner. Further reproduction prohibited without permission.

stitution of Washington, in Washington, D.C. I am indebted to the Department for its hospitality and the support of a Carnegie Predoctoral Fellowship. The financial assistance of a National Science Foundation Fellowship is also gratefully acknowledged.

Reproduced with permission of the copyright owner. Further reproduction prohibited without permission.

TABLE OF CONTENTS

INTRODUCTION 3

THE PHOTOMETRIC SYSTEM AND STELLAR OBSERVATIONS. 7

I. INTRODUCTION 7

II. PHOTOMETRIC SYSTEM 7

III. OBSERVATIONS 13

IV. TRANSFORMATIONS TO PUBLISHED SYSTEMS. 15

V. RESULTS. 34

VI. SUMMARY. 49

PHOTOMETRY OF ELLIPTICAL GALAXIES AND GLOBULAR CLUSTERS 51

I. INTRODUCTION 51

II. SELECTION OF PAIRS 55

III. PHOTOMETRIC SYSTEM AND OBSERVATIONS. 57

IV. CORRECTIONS TO OBSERVED COLORS 71

V. COLOR-COLOR AND COLOR-MAGNITUDE DIAGRAMS . . 88

VI. ANALYSIS INTO PRINCIPAL COMPONENTS: GALAXIES 96

VII. ANALYSIS INTO PRINCIPAL COMPONENTS: GALAXIES AND GLOBULAR CLUSTERS 126

VIII. DWARF ELLIPTICALS OF HIGH SURFACE BRIGHTNESS 128

IX. DISCUSSION 135

X. SUMMARY. 137

Reproduced with permission of the copyright owner. Further reproduction prohibited without permission.

QUADRATIC PROGRAMMING APPLIED TO THE PROBLEM OF POPULATION SYNTHESIS 139

I. INTRODUCTION. 139

II. THE SYNTHESIS PROBLEM 140

III. MODELS FOR M 31 145

IV. COMPARATIVE MODELS FOR M 31, M 32, AND M 81. 171

V. ELLIPTICAL GALAXIES 177

VI. DISCUSSION. 191

VII. SUMMARY 194

REFERENCES. 196

Reproduced with permission of the copyright owner. Further reproduction prohibited without permission.

INTRODUCTION

The fact that all members of a star cluster in our galaxy have a common age and original composition has had an enormous impact on the course of astronomical research. As a consequence of this discovery, each cluster became an individual laboratory for the study of stellar formation and evolution, the calibration of absolute magnitudes, and innumerable other problems. In the field of extragalactic studies, the question naturally arises whether members of groups of galaxies also possess common or correlated properties. If the history of studies of stellar clusters serves as a valid comparison, the existence of such properties might be expected to expose new avenues of extragalactic research.

The study reported here was an investigation of group photometric properties among elliptical galaxies. Most objects observed were members of pairs or small clusters. The photometric system monitored several of the most prominent absorption features in the spectra of elliptical galaxies. We examined whether the colors of these galaxies exhibited variations that were correlated in any way with other physical properties of the immediate pair or group to which the elliptical belonged. Such properties included number and morphological type of group members and presence of tidal interactions.

Reproduced with permission of the copyright owner. Further reproduction prohibited without permission.

Elliptical galaxies were selected for observation for several reasons. The differences among objects in various groups could not be large since previous photometry of galaxies (cited in Chapter 2) had not revealed the presence of such effects. Hence the large color variations within an inherently heterogeneous set of objects, such as spiral galaxies, might mask small color differences between groups. Elliptical galaxies, on the other hand, were known to form a fairly homogeneous family. However, the residual variations among the colors of ellipticals were larger than expected from observational errors alone. Whether these residual differences were caused purely by a dependence of color on luminosity could not be ascertained from the available data. The aim of the research was therefore to determine the reality of these variations among elliptical galaxies and, if real, to test whether the variations correlated with other properties of the immediate pair or group.

Additional reasons for the choice of elliptical galaxies as candidates for observation included the absence of large quantities of obscuring material within these objects. Colors of spiral galaxies, in contrast, are affected to an unknown degree by the presence of internal reddening. Moreover, the stellar population within spirals is quite heterogeneous. Hence, interpretation of variations in the integrated colors

Reproduced with permission of the copyright owner. Further reproduction prohibited without permission.

of spiral galaxies in terms of differences in stellar populations is difficult, if not impossible.

The work divides itself logically into three parts. The main body comprises the observations of elliptical galaxies, together with an analysis of the variations in their colors. These topics are discussed in Chapter 2. Chapter 1 describes the formation of the photometric system and discusses observations of 148 stars on this system. The stellar observations were obtained for two reasons. The 10-color system used to study the elliptical galaxies is a hybrid of two already-existing photometric systems. Therefore, stellar observations were necessary to determine the transformations between the system established here and the data already published. Furthermore, the interpretation of the galaxy color variations in terms of differences in stellar populations is immensely easier if observations of stars of various spectral types and compositions, made on the same photometric system, are available for comparison. Therefore, the dependence of stellar colors on measured metal abundances is also discussed in Chapter 1.

The last aspect of the work, the development of an objective, impartial method for fitting a model stellar population to the observed energy distributions of galaxies, was a logical outgrowth of the elliptical galaxy observations. It

Reproduced with permission of the copyright owner. Further reproduction prohibited without permission.

became apparent early in the investigation that the differences in colors among elliptical galaxies were real but small. An interpretation of these changes in terms of differences in stellar content was possible only if the uncertainties in the computed models themselves were smaller than the variations implied by the differences in the observed galaxy colors. Therefore an accurate assessment of the model uncertainties was necessary. Although the attempt to account for differences in the colors of elliptical galaxies in terms of population variations only partially succeeded, the method developed for population synthesis proved to be extremely useful. These results are described in Chapter 3.

In order to reduce the effort needed to reorganize the thesis for publication, each chapter has been written as a logically independent unit capable of standing alone as a single paper. However, additional material has been included, being appropriate to a dissertation but not to a journal article. For ease in reading, all references have been collected into a single bibliography at the rear.

Reproduced with permission of the copyright owner. Further reproduction prohibited without permission.

CHAPTER I

The Photometric System and Stellar Observations

I. INTRODUCTION

The present paper reports on observations of stars on a 10-color photometric system designed to study old stellar populations in globular clusters and elliptical galaxies (Chapter II). The system combines five filters from the David Dunlap Observatory system of McClure and van den Bergh (1968a) with six filters from Wood's (1966, 1969) 12-color system. The stellar observations presented here determine the transformations between the photometric calibration in this paper and the data already published by McClure and van den Bergh and by Wood. Observations of additional stars having known abundances are used to study the behavior of certain line indices as a function of abundance variations in G and K dwarfs and giants.

II. PHOTOMETRIC SYSTEM

The ten filters in the photometric system monitor several of the most prominent absorption features in the spectra of elliptical galaxies. Table 1 presents the data on the passbands determining the system. The nominal values of the effective wavelengths and halfwidths are those given by McClure and van den Bergh (1968a) and by Wood (1969). The filter trans-

Reproduced with permission of the copyright owner. Further reproduction prohibited without permission.

Reproduced with permission of the copyright owner. Further reproduction prohibited without permission.

TABLE 1

PROPERTIES OF PHOTOMETRIC SYSTEM

Filter	Source	Effective Wavelength[1]	Nominal Effective Wavelength[1]	Filter Half-width	Nominal Filter Half-width	Feature Monitored
35	DDO, Wood	3450 Å	3490 Å	390 Å	372 Å	Balmer discontinuity
38	DDO	3803	3800	140	172	
41	DDO	4167	4166	79	83	Line-blanketing discontinuity
42	DDO	4257	4257	82	73	CN absorption
45	DDO	4517	4517	84	76	G-band
52	Wood	5162	5169	54	56	MgH + Mg"b"
55	Wood	5545	5470	214	233	Continuum
62	Wood	6222	6220	108	79	TiO
67	Wood	6702	6696	131	155	Continuum
74	Wood	7415	7331	188	100	Continuum

1. Includes response function of entire observing system.

mission curves are shown in Figure 1. All measurements were made with an S-20 photocathode.

Photometric observations are of greatest utility if they express information concerning the absolute flux of energy received from a source. Accordingly, the system in this paper has been calibrated absolutely through observation of standard stars measured by Oke (1964) and Hayes (1970). The standard star measurements were in turn reduced to the new calibration of α Lyr by Oke and Schild (1970). Let $F_\nu(\nu)$ be the flux per unit frequency interval outside the atmosphere on the system determined by the new absolute calibration of α Lyr. Let $R(\nu)$ represent the response function of the entire observing system, including the effects of mirror reflectivity, photomultiplier response, and filter transmission. A magnitude on the present photometric system represents the mean magnitude of the source on the Oke-Schild system weighted by the response function of the observing apparatus. Hence

$$m_v = -2.5 \log \frac{\int F_\nu(\nu) R(\nu) d\nu}{\int R(\nu) d\nu} \qquad (1)$$

The contribution to $R(\nu)$ arising from the filters can be measured directly. The contributions from telescope optics, Fabry lens, and photomultiplier tube are most easily estimated by measurement of standard sources at the telescope itself. The method employed here closely resembled the technique described by Wood (1969), whose 12-color system was similarly calibrated.

Reproduced with permission of the copyright owner. Further reproduction prohibited without permission.

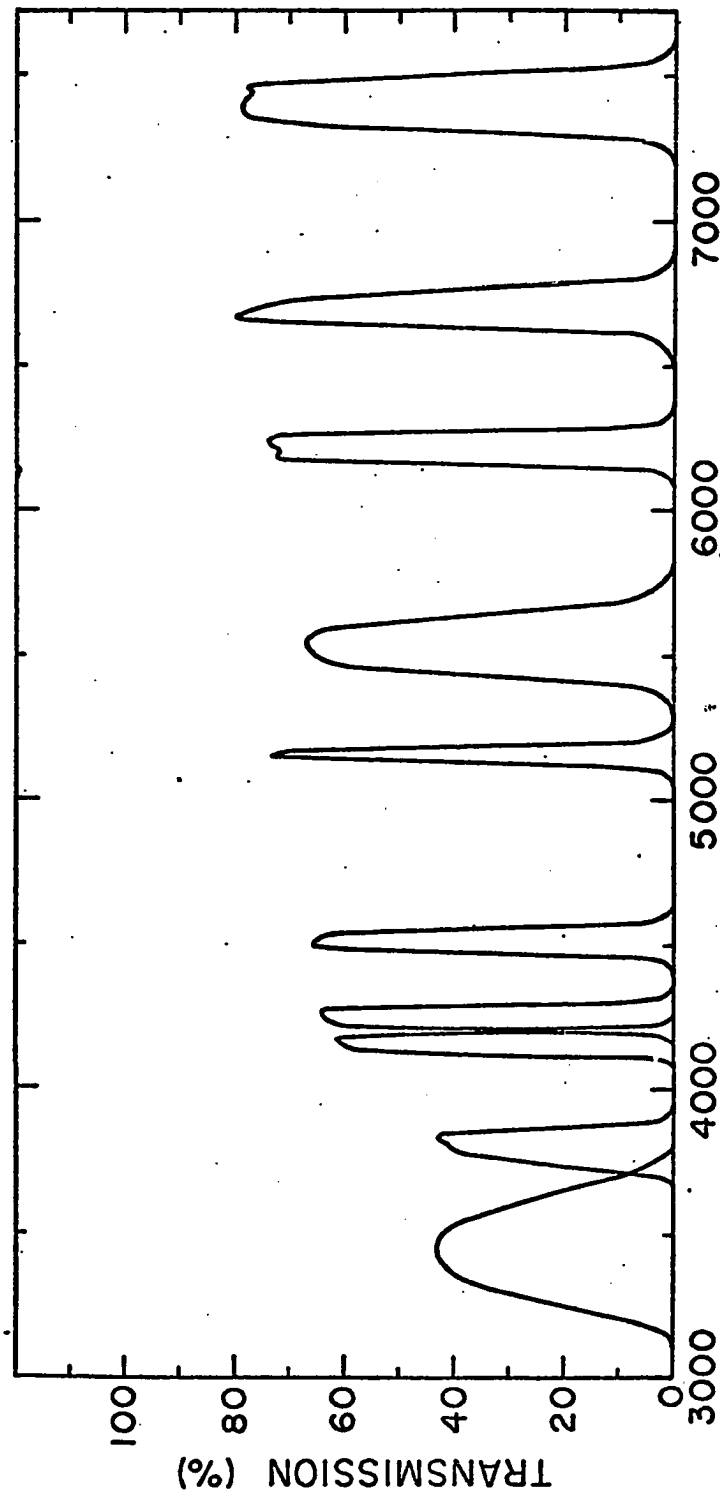

Fig. 1. Filter transmission curves.

Reproduced with permission of the copyright owner. Further reproduction prohibited without permission.

The five primary standard stars are shown in Table 2. When available, Oke's (1964) data, reduced to the new calibration of α Lyr, determined $F_\nu(\nu)$. However, Oke has not published fluxes for the stars η Hya and 58 Aql at wavelengths longer than 5840 Å. For these stars, the red measurements of Hayes (1970), reduced to the new calibration of α Lyr, were adjoined to the blue measurements of Oke by forcing the mean difference in flux in the wavelength region $\lambda\lambda$4167-5840 to be zero. This operation provided values of $F_\nu(\nu)$ for all standards out to a wavelength of 7850 Å.

The calibration of filter 38 is difficult because of line absorption by several Balmer lines of hydrogen in this region. For this reason, Oke has not published values of $F_\nu(\nu)$ in the interval $\lambda\lambda$3704-4032. An approximate calibration for filter 38 was obtained from the hot standard ζ Oph (O9.5V), for which the Balmer discontinuity and line absorption are small. $F_\nu(\nu)$ longward of 4032 Å was linearly extrapolated to 3922 Å. The gap across the Balmer jump was then bridged by a straight line. All other standard measurements through filter 38 were then tied to ζ Oph.

The standard magnitudes calculated with expression (1) can be compared with the final magnitudes of the standard stars reduced in the same manner as those of the program stars. Such a comparison (Table 2) is a measure of the internal con-

Reproduced with permission of the copyright owner. Further reproduction prohibited without permission.

Reproduced with permission of the copyright owner. Further reproduction prohibited without permission.

TABLE 2

STANDARD STAR MAGNITUDES

	ξ^2Cet		η Hya		109 Vir		ζ Oph		58 Aql*	
Filter	Observed	Computed	Observed	Computed	Observed	Computed	Observed	Computed	Observed	Computed
35	5.070	5.082	4.074	4.068	4.710	4.715	2.359	2.373	6.816	6.778
38	4.456		3.985		3.993		2.412	2.412	5.986	
41	3.952	3.960	3.855	3.855	3.453	3.456	2.374	2.377	5.482	5.436
42	3.966	3.976	3.880	3.875	3.471	3.474	2.384	2.388	5.498	5.445
45	4.028	4.040	3.973	3.970	3.516	3.519	2.433	2.442	5.517	5.478
52	4.181	4.185	4.171	4.173	3.644	3.647	2.477	2.497	5.576	5.534
55	4.260	4.263	4.289	4.284	3.720	3.726	2.534	2.548	5.605	5.564
62	4.415	4.416	4.486	4.485	3.853	3.857	2.648	2.656	5.691	5.645
67	4.516	4.511	4.618	4.624	3.941	3.944	2.727	2.726	5.742	5.696
74	4.628	4.636	4.759	4.755	4.038	4.042	2.802	2.799	5.804	5.743

* Not used as a standard.

sistency of the calibration. Table 2 shows that the agreement is closer than 0.01 magnitude in most cases except for the standard 58 Aql, for which the observed magnitudes average 0.04 magnitude larger than the computed value. This discrepancy was discovered early in the work, and 58 Aql was subsequently deleted as a standard.

Colors on this system are first formed relative to filter 55 and denoted (x-55).

III. OBSERVATIONS

All observations were obtained on the Number 4 16-inch and Number 2 36-inch telescopes at Kitt Peak National Observatory. All peripheral equipment was also provided by the Observatory. The output of an ITT FW-130 photomultiplier, refrigerated with dry ice, was recorded in the pulse-counting mode with a fast amplifier-discriminator and a digital counter. Coincidence corrections never exceeded 2 per cent. One observation consisted of two ten-second integrations in each filter, except for the faintest stars, for which as many as five integrations were recorded. Sky was measured when necessary for the fainter objects.

The internal mean errors for all stars are given in Table 3. Errors for stars with visual magnitudes fainter than 7.0 are approximately 50 per cent larger than the tabulated

Reproduced with permission of the copyright owner. Further reproduction prohibited without permission.

TABLE 3

INTERNAL MEAN ERRORS OF STELLAR OBSERVATIONS

	(35-55)	(38-55)	(41-55)	(42-55)	(45-55)	(52-55)	(62-55)	(67-55)	(74-55)
All stars	$0^m.006$	$0^m.005$	$0^m.005$	$0^m.004$	$0^m.004$	$0^m.004$	$0^m.004$	$0^m.004$	$0^m.004$

Reproduced with permission of the copyright owner. Further reproduction prohibited without permission.

values. Table 4 presents the observational data for 148 stars.

IV. TRANSFORMATION TO PUBLISHED SYSTEMS

Figure 2 compares colors on this system with the corresponding DDO indices for stars in common with McClure and van den Bergh (1968a). Deviant points are labeled. With the exception of the values of the index (38-41) for two supergiants, all discrepant points correspond to stars of very late spectral type, two of which (HR 6146, 8775) are variables. BD + 4° 3561 and HD95735 are M dwarfs. The transformation between (38-41) of the DDO system and (38-41) of the present system is somewhat inaccurate, especially for the redder stars. A luminosity effect at earlier types is also apparent. These discrepancies are almost certainly caused by the fact that the 38 filter used in the present study is considerably narrower and more asymmetric than the DDO 38 filter.

If the labeled points are excluded, the resulting least-squares transformations between the DDO system and the system in this paper are as follows:

$$\underset{\pm\ 0.021}{(35\text{-}41)_{DDO}} = \underset{\pm\ 0.001}{0.000\,(35\text{-}41)_F^2} + \underset{\pm\ 0.007}{0.977\,(35\text{-}41)_F} - \underset{\pm\ 0.003}{0.815},$$

$$\underset{\pm\ 0.024}{(38\text{-}41)_{DDO}} = \underset{\pm\ 0.017}{-0.067\,(38\text{-}41)_F^2} + \underset{\pm\ 0.035}{1.048\,(38\text{-}41)_F} - \underset{\pm\ 0.004}{0.116},$$

Reproduced with permission of the copyright owner. Further reproduction prohibited without permission.

Reproduced with permission of the copyright owner. Further reproduction prohibited without permission.

TABLE 4

OBSERVATIONS OF STARS

HR No.	Sp. Type	n	(35-55)	(38-55)	(41-55)	(42-55)	(45-55)	(52-55)	(62-55)	(67-55)	(74-55)
			m	m	m	m	m	m	m	m	m
HD26	K0	3	2.373	2.272	1.405	1.266	0.642	0.285	-0.235	-0.340	-0.439
HD2665	Pop.II Gt.	5	1.808	1.288	0.821	0.841	0.521	0.179	-0.192	-0.313	-0.443
163	G8III	5	2.234	1.891	1.007	1.006	0.541	0.235	-0.191	-0.308	-0.417
HD5223	R3	4	3.009	3.140	2.121	1.573	0.780	0.297	-0.486	-0.624	-0.745
HD5544	G8II-III	5	3.141	2.857	1.638	1.380	0.757	0.355	-0.255	-0.416	-0.556
224	K5III	5	4.402	3.778	2.329	2.111	1.082	0.653	-0.300	-0.625	-0.939
483	G2V	7	1.571	1.323	0.611	0.634	0.319	0.165	-0.110	-0.165	-0.215
509	G8Vp	5	1.752	1.579	0.787	0.841	0.420	0.266	-0.143	-0.229	-0.311
563	K1p	6	2.548	2.180	1.143	1.002	0.595	0.248	-0.201	-0.325	-0.430
660	G0V	6	1.462	1.201	0.604	0.635	0.331	0.191	-0.110	-0.184	-0.248
718	B9III	54	0.809	0.195	-0.308	-0.294	-0.231	-0.079	0.154	0.256	0.367
799AB	F7V	6	1.347	1.000	0.435	0.435	0.234	0.110	-0.070	-0.104	-0.126
867	gM6	2	3.888	2.533	1.245	1.420	1.182	-0.032	-0.157	-0.930	-2.969
937	G0V	7	1.565	1.284	0.584	0.596	0.305	0.158	-0.098	-0.150	-0.184
996	G5V	6	1.690	1.482	0.710	0.733	0.366	0.206	-0.126	-0.196	-0.249
HD22879	F9V	6	1.269	0.972	0.490	0.515	0.292	0.127	-0.099	-0.146	-0.202
1136	K0IV	6	2.477	2.316	1.194	1.113	0.540	0.351	-0.206	-0.321	-0.406
HD25329	K1V	4	2.060	1.866	1.031	1.060	0.534	0.353	-0.202	-0.318	-0.456
1346	K0III	6	2.644	2.400	1.363	1.121	0.609	0.287	-0.202	-0.328	-0.409
1373	K0III	6	2.704	2.477	1.380	1.132	0.610	0.284	-0.202	-0.326	-0.408
HD28068	G1V	5	1.610	1.371	0.652	0.663	0.328	0.180	-0.116	-0.187	-0.237
HD28099	G0V	5	1.687	1.471	0.685	0.697	0.340	0.200	-0.123	-0.176	-0.240
1409	K0III	6	2.814	2.575	1.447	1.172	0.634	0.296	-0.211	-0.341	-0.420
1411	K0III	5	2.596	2.346	1.306	1.094	0.592	0.282	-0.199	-0.319	-0.398
HD28344	G2V	6	1.567	1.308	0.601	0.622	0.321	0.174	-0.106	-0.157	-0.191
1542	O9.5Ia	3	-0.178	-0.122	-0.134	-0.116	-0.086	-0.031	0.103	0.169	0.241
HD30649	G0IV	4	1.414	1.130	0.560	0.598	0.317	0.158	-0.103	-0.164	-0.222
1543	F6V	8	1.290	0.927	0.382	0.371	0.204	0.099	-0.050	-0.075	-0.086
1577	K3II	7	4.318	3.735	2.404	2.067	1.149	0.578	-0.326	-0.603	-0.801
1641	B3V	7	-0.093	-0.235	-0.416	-0.398	-0.304	-0.108	0.195	0.325	0.467
1666	A3III	3	1.291	0.549	-0.100	-0.099	-0.101	-0.027	0.080	0.143	0.201

Reproduced with permission of the copyright owner. Further reproduction prohibited without permission.

TABLE 4 continued

OBSERVATIONS OF STARS

HR No.	Sp. Type	n	(35-55)	(38-55)	(41-55)	(42-55)	(45-55)	(52-55)	(62-55)	(67-55)	(74-55)
			m	m	m	m	m	m	m	m	m
1729	G0V	7	1.594	1.321	0.606	0.625	0.322	0.170	-0.107	-0.166	-0.206
1791	B7III	3	0.230	-0.123	-0.369	-0.344	-0.275	-0.094	0.182	0.293	0.422
1805	K3III	7	4.113	3.671	2.293	1.891	1.002	0.566	-0.310	-0.545	-0.714
1907	G8IIIp	7	2.475	2.170	1.169	1.141	0.613	0.304	-0.215	-0.353	-0.480
2002	G8III	7	2.766	2.468	1.448	1.209	0.654	0.345	-0.223	-0.367	-0.460
2035	G8III	5	2.563	2.239	1.219	1.184	0.640	0.315	-0.220	-0.357	-0.493
2047	G0V	2	1.474	1.206	0.563	0.586	0.300	0.150	-0.103	-0.154	-0.202
2091	M3.5II	3	4.682	3.592	2.272	2.191	1.296	0.414	-0.119	-0.760	-1.928
2219	G8III	12	2.729	2.454	1.335	1.219	0.647	0.305	-0.226	-0.363	-0.478
2286	M3III	3	4.722	3.685	2.290	2.202	1.216	0.468	-0.085	-0.700	-1.711
2421	A0IV	3	1.131	0.325	-0.251	-0.237	-0.197	-0.063	0.137	0.225	0.318
2721	G0V	12	1.413	1.134	0.541	0.574	0.301	0.143	-0.103	-0.153	-0.204
2763AB	A3V	3	1.231	0.554	-0.134	-0.139	-0.132	-0.038	0.098	0.171	0.239
2782AB	O9III	3	-0.531	-0.398	-0.370	-0.339	-0.255	-0.097	0.179	0.283	0.400
3369	G9III	11	2.817	2.565	1.441	1.185	0.651	0.286	-0.216	-0.347	-0.450
3410	A0V	3	1.041	0.324	-0.249	-0.235	-0.199	-0.071	0.125	0.212	0.298
3454	B3V	107	-0.214	-0.303	-0.434	-0.408	-0.315	-0.118	0.197	0.328	0.470
3664	G6III	10	2.106	1.740	0.929	0.940	0.515	0.210	-0.181	-0.290	-0.397
3787	A3III	4	1.305	0.443	-0.117	-0.113	-0.111	-0.034	0.079	0.140	0.197
3852A	A5V+F8III	6	1.654	1.087	0.466	0.400	0.231	0.107	-0.044	-0.070	-0.075
3882	gM8e	4	3.827	1.529	1.020	1.898	2.057	0.306	-0.738	-1.955	-4.156
3905	K2III	12	3.614	3.286	1.951	1.553	0.818	0.483	-0.267	-0.445	-0.557
3951	G2V	7	1.755	1.515	0.696	0.706	0.351	0.201	-0.122	-0.189	-0.231
HD86986	A1V	7	1.393	0.471	-0.109	-0.103	-0.089	-0.027	0.073	0.124	0.174
HD88230	K7V	3	3.572	3.147	1.908	2.040	0.937	0.790	-0.350	-0.639	-0.975
3994	K0III	4	2.817	2.605	1.445	1.162	0.612	0.300	-0.209	-0.337	-0.421
4098AB	G1V	20	1.484	1.232	0.593	0.637	0.323	0.166	-0.109	-0.173	-0.233
4112	F8V	5	1.352	1.042	0.472	0.485	0.257	0.122	-0.079	-0.121	-0.150
4133	B1Ib	4	-0.430	-0.382	-0.355	-0.326	-0.260	-0.101	0.168	0.287	0.412
4267	M5III	4	3.968	2.650	1.295	1.458	1.186	0.009	-0.161	-0.923	-2.900
4287	K0III	4	3.017	2.779	1.544	1.316	0.692	0.339	-0.243	-0.400	-0.490

Reproduced with permission of the copyright owner. Further reproduction prohibited without permission.

TABLE 4 continued

OBSERVATIONS OF STARS

HR No.	Sp. Type	n	(35-55)	(38-55)	(41-55)	(42-55)	(45-55)	(52-55)	(62-55)	(67-55)	(74-55)
			m	m	m	m	m	m	m	m	m
4301AB	K0II-III	4	2.927	2.586	1.493	1.259	0.689	0.313	-0.233	-0.383	-0.494
HD95735	M2V	3	3.608	2.954	1.961	2.198	1.070	0.693	-0.156	-0.695	-1.490
4357	A4V	4	1.256	0.588	-0.092	-0.100	-0.107	-0.020	0.105	0.165	0.235
4362	M3III	4	4.693	3.689	2.331	2.236	1.240	0.479	-0.134	-0.717	-1.619
4365	K3III	4	3.264	2.848	1.721	1.497	0.802	0.436	-0.281	-0.472	-0.629
4386	B9V	4	0.816	0.142	-0.321	-0.302	-0.242	-0.085	0.154	0.257	0.365
4468	B9V	2	0.723	0.107	-0.332	-0.311	-0.249	-0.092	0.154	0.257	0.374
4534	A3V	4	1.166	0.579	-0.140	-0.149	-0.144	-0.037	0.118	0.191	0.275
4540	F8V	99	1.491	1.167	0.502	0.512	0.259	0.123	-0.088	-0.131	-0.160
4550	G8VI	4	1.722	1.534	0.810	0.860	0.438	0.258	-0.184	-0.282	-0.393
4695	K0III	4	3.291	2.922	1.623	1.450	0.774	0.404	-0.270	-0.460	-0.616
HD109995	A0V	5	1.297	0.375	-0.218	-0.193	-0.172	-0.072	0.092	0.162	0.231
4845	G0V	7	1.336	1.070	0.507	0.539	0.284	0.129	-0.099	-0.150	-0.203
4883	G0III	9	1.754	1.339	0.683	0.684	0.380	0.156	-0.129	-0.197	-0.258
4894AB	G8III+F6	4	2.512	2.152	1.196	0.983	0.530	0.257	-0.192	-0.306	-0.385
4932	G8III	8	2.550	2.309	1.234	1.039	0.555	0.246	-0.191	-0.304	-0.383
4983	G0V	7	1.472	1.199	0.541	0.564	0.282	0.143	-0.096	-0.146	-0.182
HD114762	F9V	5	1.269	0.986	0.466	0.498	0.266	0.110	-0.099	-0.151	-0.211
HD115043	G1V	4	1.515	1.253	0.582	0.614	0.304	0.159	-0.118	-0.168	-0.212
5080	gM7e	3	3.605	1.836	1.188	1.748	1.970	0.075	-0.390	-1.582	-4.122
5154	M2III	4	4.758	3.852	2.440	2.301	1.220	0.598	-0.204	-0.705	-1.324
HD119850	M4V	2	3.489	2.899	1.878	2.094	1.020	0.681	-0.180	-0.660	-1.382
5235	G0IV	3	1.647	1.333	0.569	0.549	0.274	0.133	-0.097	-0.147	-0.173
5264A	A3III	8	1.299	0.487	-0.140	-0.130	-0.123	-0.039	0.089	0.153	0.216
5270	Pop.II Gt.	35	2.260	1.579	1.002	0.953	0.644	0.204	-0.260	-0.393	-0.561
HD126327	M8e	4	4.148	2.003	1.164	1.773	1.960	0.212	-0.480	-1.584	-3.877
5409AB	G2III	5	1.765	1.441	0.707	0.719	0.380	0.166	-0.141	-0.178	-0.272
5435A	A7III	8	1.346	0.629	-0.008	-0.014	-0.047	-0.006	0.061	0.105	0.152
5447	F2V	9	1.141	0.746	0.247	0.226	0.124	0.050	-0.032	-0.037	-0.045
5480	G8III	5	2.653	2.360	1.342	1.130	0.621	0.253	-0.219	-0.348	-0.442
5511	A0V	128	0.989	0.272	-0.267	-0.250	-0.204	-0.076	0.131	0.219	0.316

Reproduced with permission of the copyright owner. Further reproduction prohibited without permission.

TABLE 4 continued

OBSERVATIONS OF STARS

HR No.	Sp. Type	n	(35-55)	(38-55)	(41-55)	(42-55)	(45-55)	(52-55)	(62-55)	(67-55)	(74-55)
5535	G8III-IV	5	2.615	2.323	1.253	1.157	0.607	0.287	-0.227	-0.367	-0.483
5544A	G8V	2	1.781	1.598	0.764	0.811	0.380	0.220	-0.151	-0.235	-0.308
5568A	K5V	4	3.003	2.831	1.505	1.539	0.637	0.647	-0.283	-0.444	-0.596
5568B	M1V	4	3.655	3.063	1.977	2.168	1.091	0.684	-0.220	-0.721	-1.439
5589	M5III	4	4.318	3.189	1.835	1.835	1.147	0.230	-0.046	-0.735	-2.304
5681A	G8III	4	2.517	2.241	1.180	1.110	0.585	0.257	-0.208	-0.340	-0.450
5709	K0III	4	2.726	2.452	1.314	1.211	0.625	0.291	-0.235	-0.375	-0.494
5802	K0p	5	2.499	2.312	1.241	1.078	0.554	0.253	-0.207	-0.321	-0.410
HD140283	F5VI	5	1.129	0.804	0.434	0.418	0.277	0.080	-0.113	-0.162	-0.240
5854	K2III	7	3.391	3.111	1.800	1.443	0.752	0.420	-0.252	-0.415	-0.520
5911	G2V	4	1.409	1.183	0.586	0.613	0.312	0.159	-0.115	-0.175	-0.228
5914	F9V	6	1.396	1.071	0.516	0.554	0.291	0.126	-0.108	-0.163	-0.216
5968	G2V	4	1.503	1.234	0.583	0.620	0.313	0.155	-0.116	-0.172	-0.205
6146	M6III	2	3.946	2.529	1.259	1.467	1.321	-0.009	-0.247	-1.047	-3.109
HD148816	F9V	4	1.283	0.988	0.483	0.519	0.283	0.121	-0.099	-0.147	-0.206
6175	O9.5V	5	-0.174	-0.121	-0.159	-0.149	-0.100	-0.057	0.114	0.193	0.268
6212AB	G0IV	3	1.705	1.405	0.650	0.665	0.329	0.166	-0.115	-0.178	-0.223
6220	G7III-IV	4	2.392	2.153	1.143	1.034	0.543	0.236	-0.197	-0.313	-0.405
HD152792	G0V	3	1.548	1.263	0.621	0.658	0.345	0.153	-0.123	-0.188	-0.251
6418	K3II	4	4.132	3.652	2.241	1.901	1.023	0.523	-0.321	-0.560	-0.734
HD157089	G0V	23	1.384	1.076	0.528	0.566	0.305	0.142	-0.103	-0.154	-0.210
6458	G0V	3	1.501	1.259	0.596	0.647	0.327	0.176	-0.117	-0.181	-0.235
HD157881	K7V	2	3.554	3.151	1.906	2.044	0.929	0.800	-0.352	-0.637	-0.948
HD160693	G0V	3	1.373	1.119	0.538	0.583	0.296	0.149	-0.107	-0.162	-0.219
6623A	G5IV	3	1.990	1.781	0.834	0.813	0.382	0.222	-0.155	-0.228	-0.282
HD161817	A2VI	4	1.409	0.494	-0.053	-0.031	-0.050	-0.019	0.044	0.084	0.114
BD+4°3561	M5V	3	4.003	3.140	2.489	2.813	1.263	0.663	0.087	-0.797	-2.092
6707	F2II	3	1.592	0.791	0.265	0.257	0.149	0.059	-0.046	-0.068	-0.092
HD165195	Pop.II Gt.	3	3.374	2.478	1.612	1.508	1.017	0.337	-0.376	-0.597	-0.848
6775AB	F7V	4	1.292	0.977	0.459	0.484	0.255	0.117	-0.096	-0.146	-0.202
6791	G8IIIp	4	2.529	2.186	1.153	0.978	0.563	0.240	-0.207	-0.327	-0.414

Reproduced with permission of the copyright owner. Further reproduction prohibited without permission.

TABLE 4 continued

OBSERVATIONS OF STARS

HR No.	Sp. Type	n	(35-55)	(38-55)	(41-55)	(42-55)	(45-55)	(52-55)	(62-55)	(67-55)	(74-55)
			m	m	m	m	m	m	m	m	m
7300A	G5IIp	3	2.860	2.580	1.471	1.240	0.696	0.284	-0.241	-0.384	-0.490
7429	K3III	6	3.374	3.085	1.746	1.486	0.749	0.491	-0.273	-0.448	-0.578
7477	G6V	6	2.667	2.411	1.301	1.161	0.617	0.294	-0.218	-0.355	-0.463
7503	G2V	4	1.659	1.421	0.650	0.676	0.331	0.176	-0.122	-0.184	-0.227
7504	G5V	4	1.677	1.475	0.673	0.704	0.336	0.182	-0.128	-0.196	-0.244
7525	K3II	4	4.248	3.692	2.347	2.025	1.113	0.550	-0.328	-0.598	-0.798
7569	G2V	3	1.617	1.363	0.636	0.685	0.334	0.169	-0.121	-0.190	-0.248
7576	K3III	10	3.839	3.466	2.087	1.679	0.875	0.545	-0.292	-0.490	-0.620
7596	A0	62	1.211	0.381	-0.122	-0.106	-0.088	-0.028	0.086	0.137	0.199
7602AB	G8IV	9	2.186	1.983	1.000	1.005	0.498	0.271	-0.186	-0.295	-0.389
7796	F8Ib	7	2.296	1.359	0.718	0.638	0.402	0.167	-0.100	-0.168	-0.193
7949A	K0III	5	2.806	2.538	1.386	1.242	0.662	0.323	-0.225	-0.370	-0.482
HD201626	K0IIIp	9	2.328	2.308	1.404	1.297	0.634	0.278	-0.313	-0.429	-0.565
8204	G5II-III	5	2.425	2.215	1.355	1.160	0.621	0.274	-0.199	-0.300	-0.375
8255	K1III	5	3.037	2.801	1.593	1.325	0.699	0.360	-0.236	-0.390	-0.494
HD209621	R3	4	3.359	3.543	2.540	1.719	1.031	0.336	-0.374	-0.546	-0.639
8622	O9V	4	-0.608	-0.459	-0.415	-0.394	-0.286	-0.106	0.198	0.324	0.469
8775	M2II-III	5	4.758	3.746	2.372	2.239	1.250	0.553	-0.097	-0.680	-1.621
8819AB	G2III	4	2.182	1.807	0.988	0.847	0.477	0.228	-0.166	-0.267	-0.337
8832	K3V	4	2.764	2.649	1.367	1.359	0.605	0.567	-0.245	-0.384	-0.501
HD221170	Pop.II Gt.	5	2.696	1.988	1.262	1.214	0.807	0.276	-0.303	-0.470	-0.670
8961	G8III-IV	5	2.586	2.261	1.256	1.193	0.651	0.365	-0.230	-0.384	-0.521
8969	F7V	4	1.376	1.012	0.459	0.458	0.259	0.120	-0.072	-0.108	-0.143
9088AB	G2V	5	1.544	1.306	0.689	0.747	0.390	0.231	-0.140	-0.229	-0.326

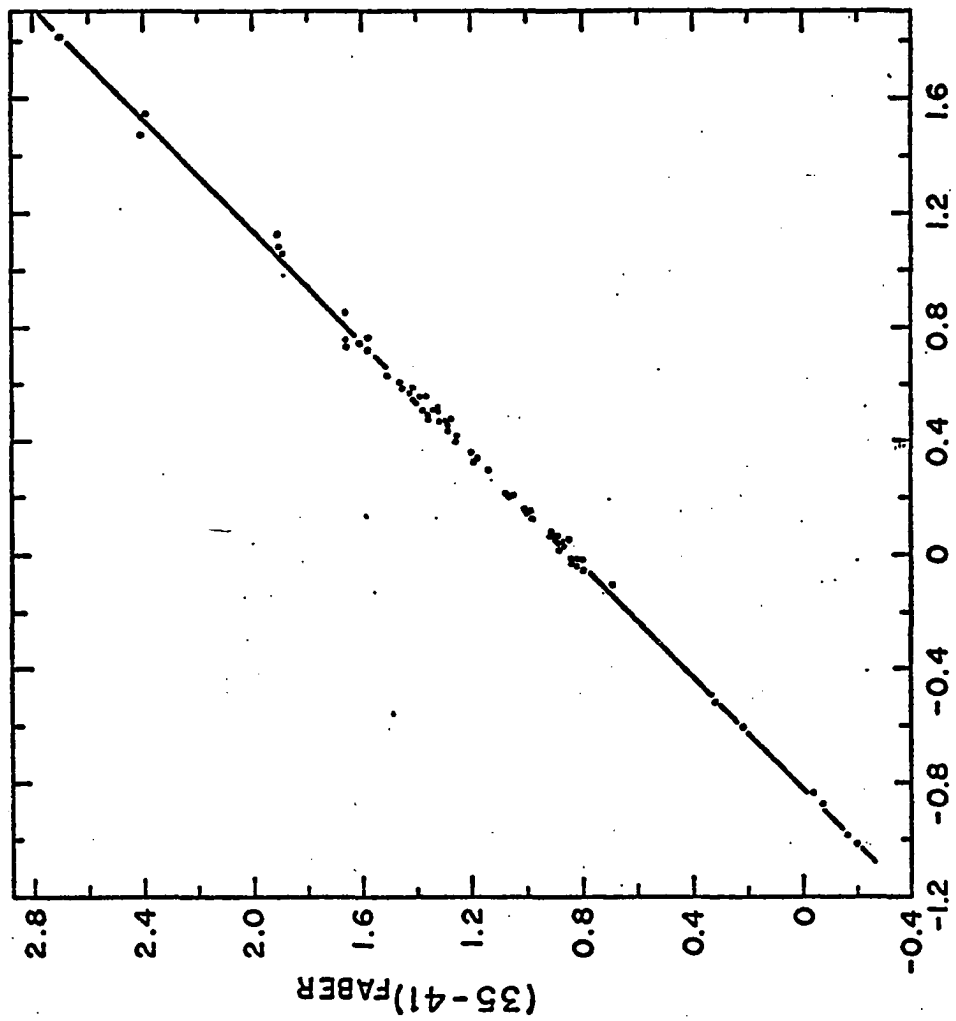

Fig. 2. Comparison of photometric indices measured in this paper with the corresponding DDO indices. Solid lines represent the transformations given in the text.

Reproduced with permission of the copyright owner. Further reproduction prohibited without permission.

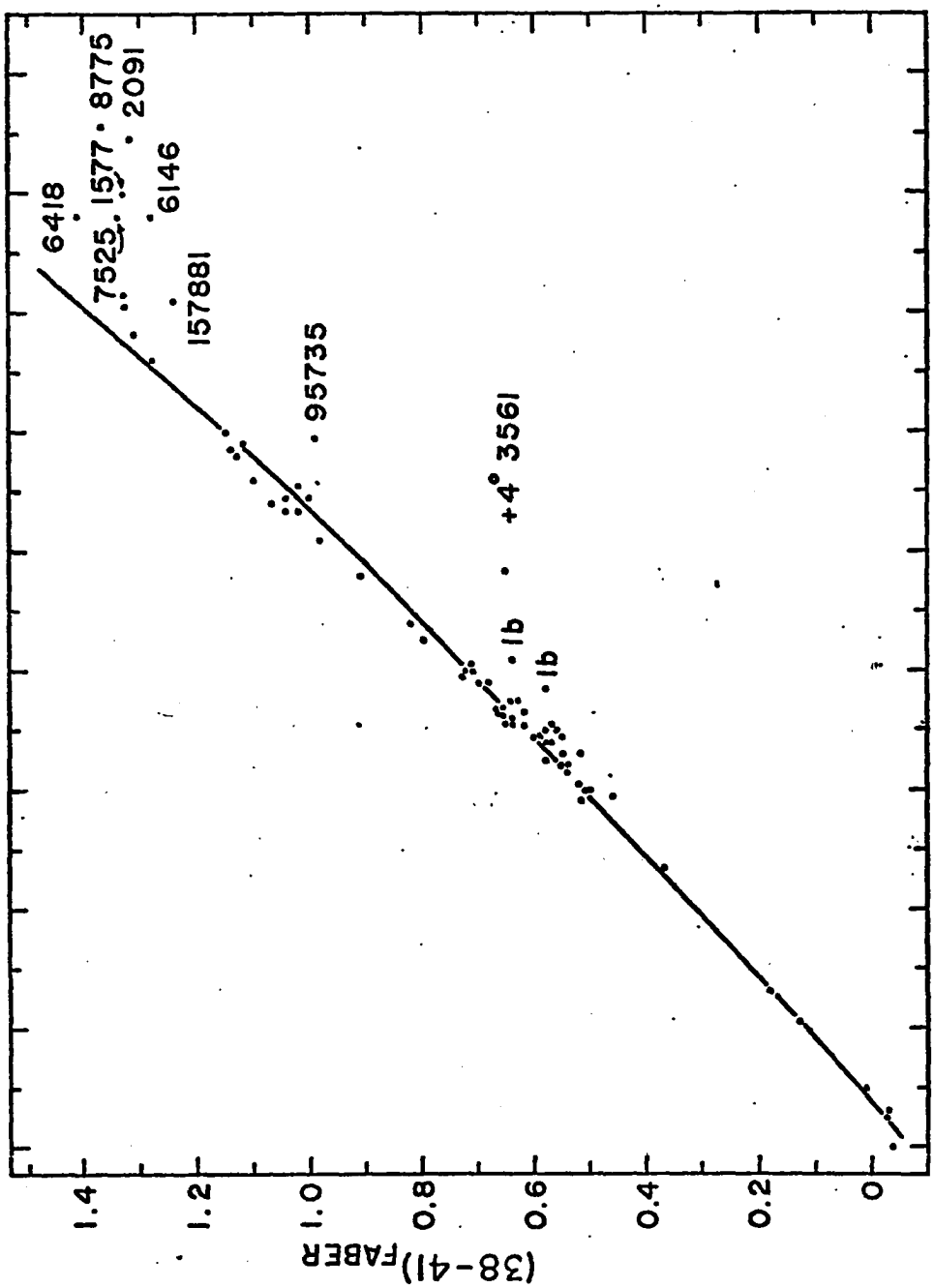

Fig. 2 (continued). Except for the two stars of luminosity class Ib, all labeled points correspond to stars of spectral types K and M.

Reproduced with permission of the copyright owner. Further reproduction prohibited without permission.

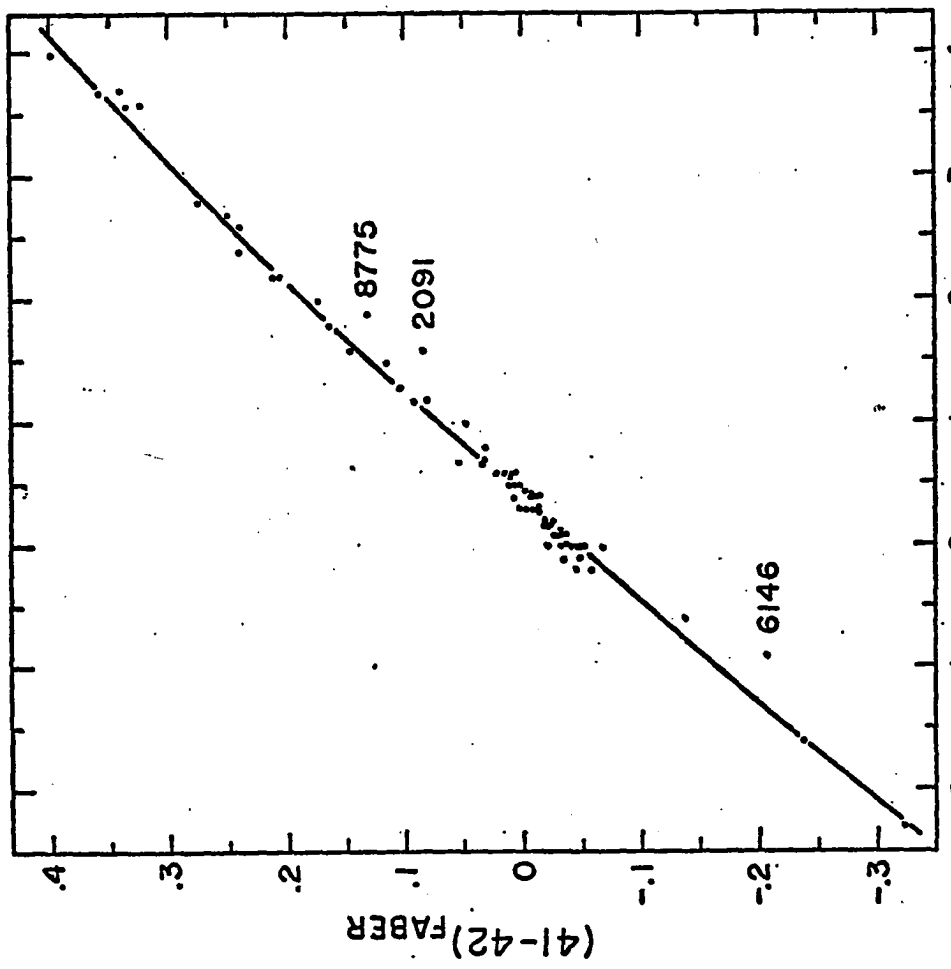

Fig. 2 (continued). The labeled points correspond to M giant stars.

Reproduced with permission of the copyright owner. Further reproduction prohibited without permission.

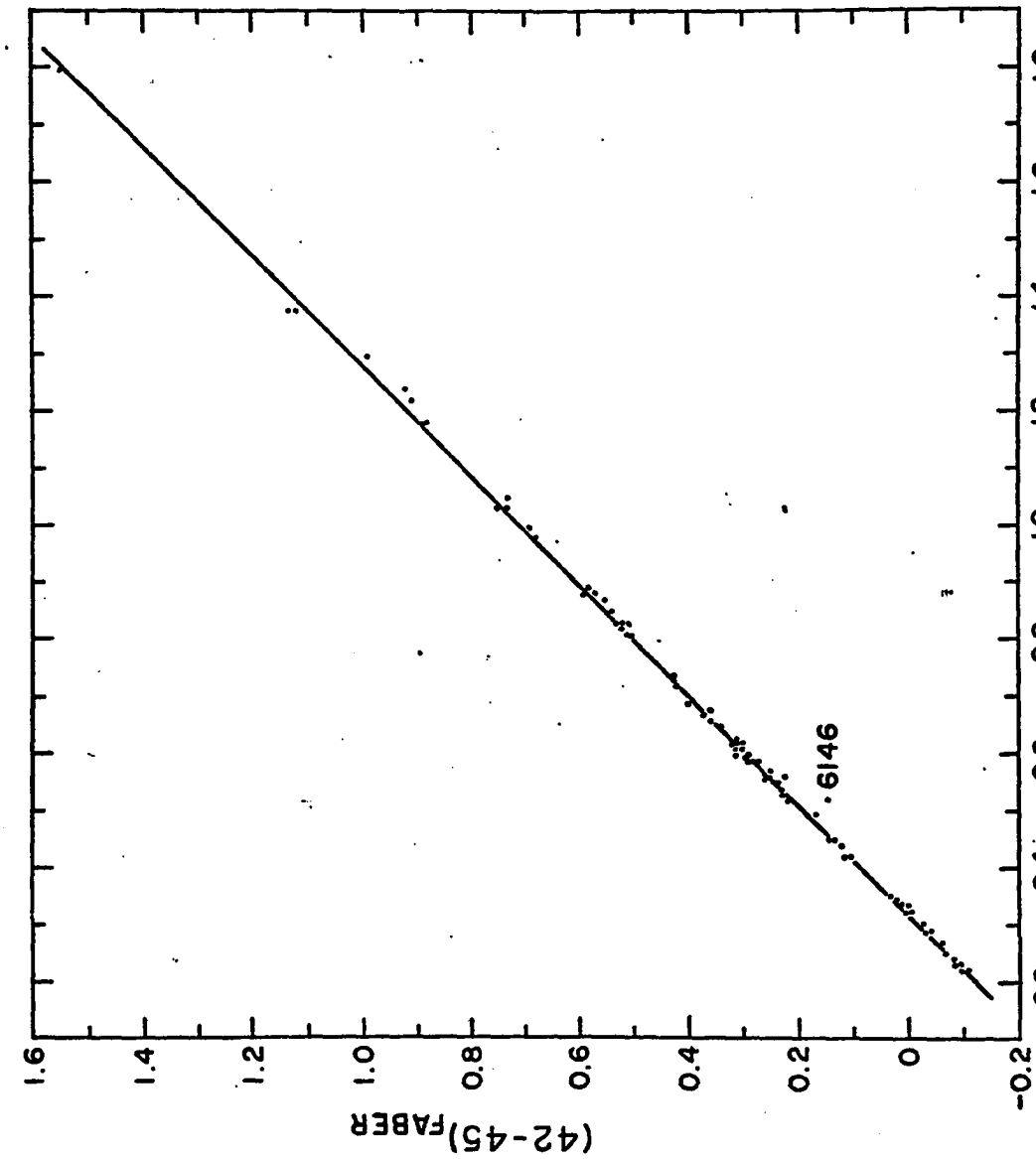

Fig. 2 (continued).

Reproduced with permission of the copyright owner. Further reproduction prohibited without permission.

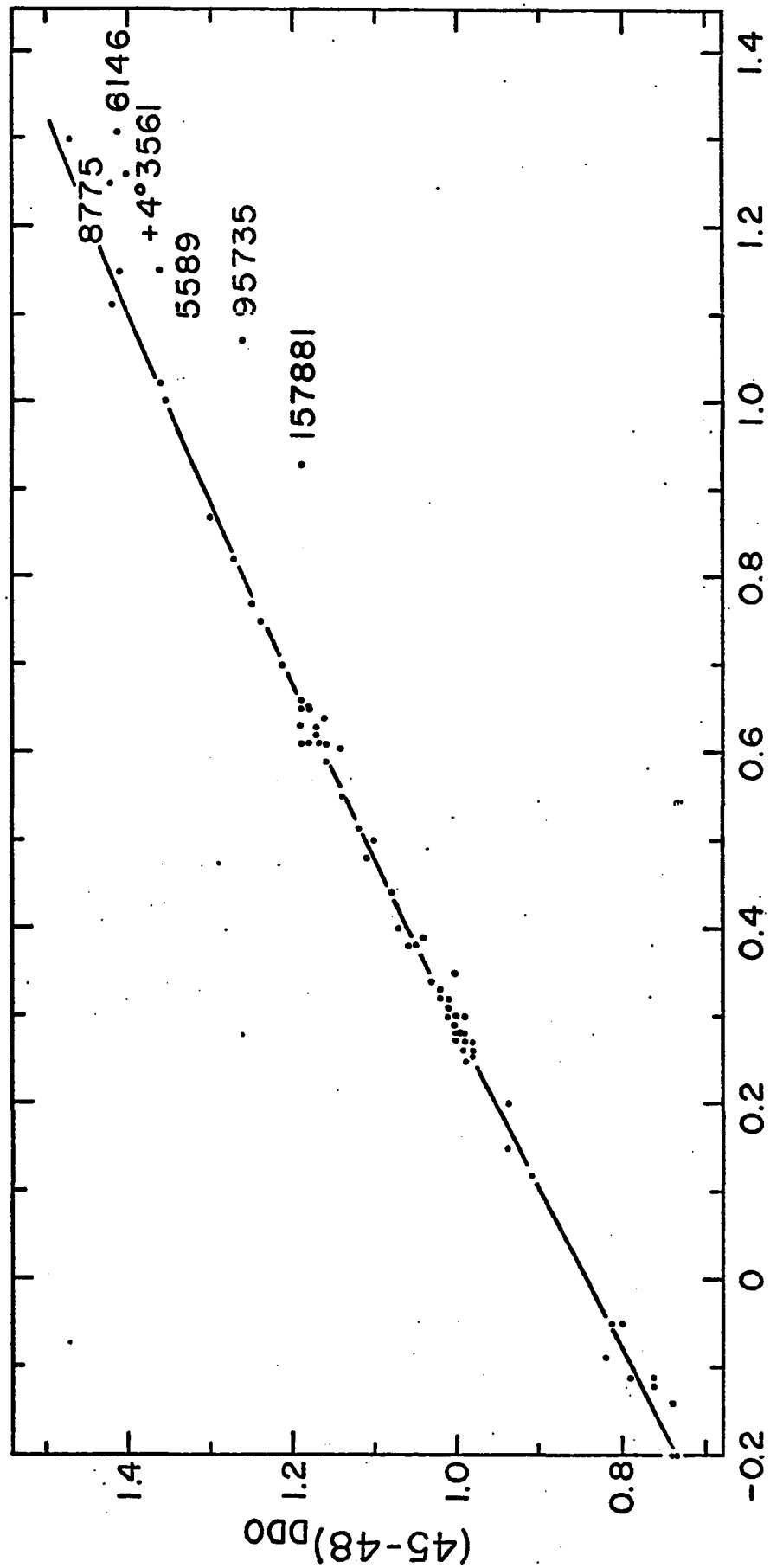

Fig. 2 (continued). The labeled points correspond to late K or M stars.

Reproduced with permission of the copyright owner. Further reproduction prohibited without permission.

$$(41-42)_{DDO} = +0.139(41-42)_F^2 + 0.879(41-42)_F + 0.040,$$
$$\pm 0.011 \quad \pm 0.222 \quad \pm 0.017 \quad \pm 0.000$$

$$(42-45)_{DDO} = -0.009(42-45)_F^2 + 0.971(42-45)_F + 0.321,$$
$$\pm 0.010 \quad \pm 0.005 \quad \pm 0.007 \quad \pm 0.000$$

$$(45-48)_{DDO} = +0.007(45-55)_F^2 + 0.486(45-55)_F + 0.859.$$
$$\pm 0.021 \quad \pm 0.010 \quad \pm 0.007 \quad \pm 0.001$$

Wood's published colors and line indices were converted to eleven colors formed relative to his y filter. These colors are directly comparable to those presented here. Figure 3 compares colors on the two systems, where discrepant points are again labeled. These deviant points appear in most of the color-color plots.

As was the case for the transformations to the DDO system, the stars corresponding to these points are of very late spectral type. HR 867, 4267, 8775, and HD 126327 are variables. If the discrepancies are due to red leaks, the sense is always such that the leak is either in Wood's 55 filter or in the other, non-55 filters of Faber. If the former were true, the deviations for each star from each mean relation should be identical, because the 55 filter is used to form each color. These deviations are not identical. Therefore the leaks, if real, are found in the present data. All filters were traced to 1.2μ to search for such leaks, but none were found. Moreover, if red leaks are the cause of the deviations, the size of the error ought to increase directly with the increasing

Reproduced with permission of the copyright owner. Further reproduction prohibited without permission.

Reproduced with permission of the copyright owner. Further reproduction prohibited without permission.

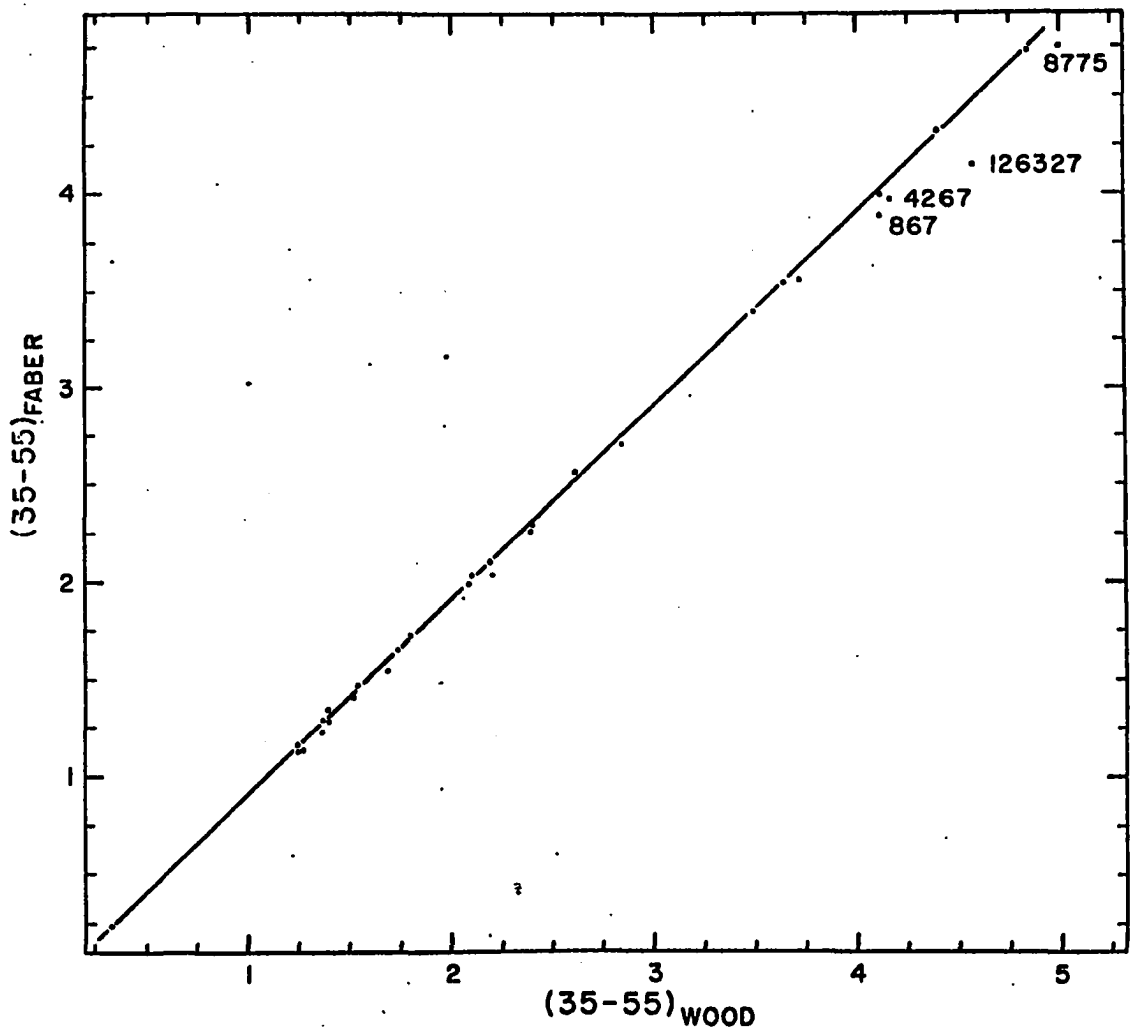

Fig. 3. Comparison of photometric indices measured in this paper with the corresponding Wood indices. Solid lines represent the transformations given in the text. The four labeled points represent M variables.

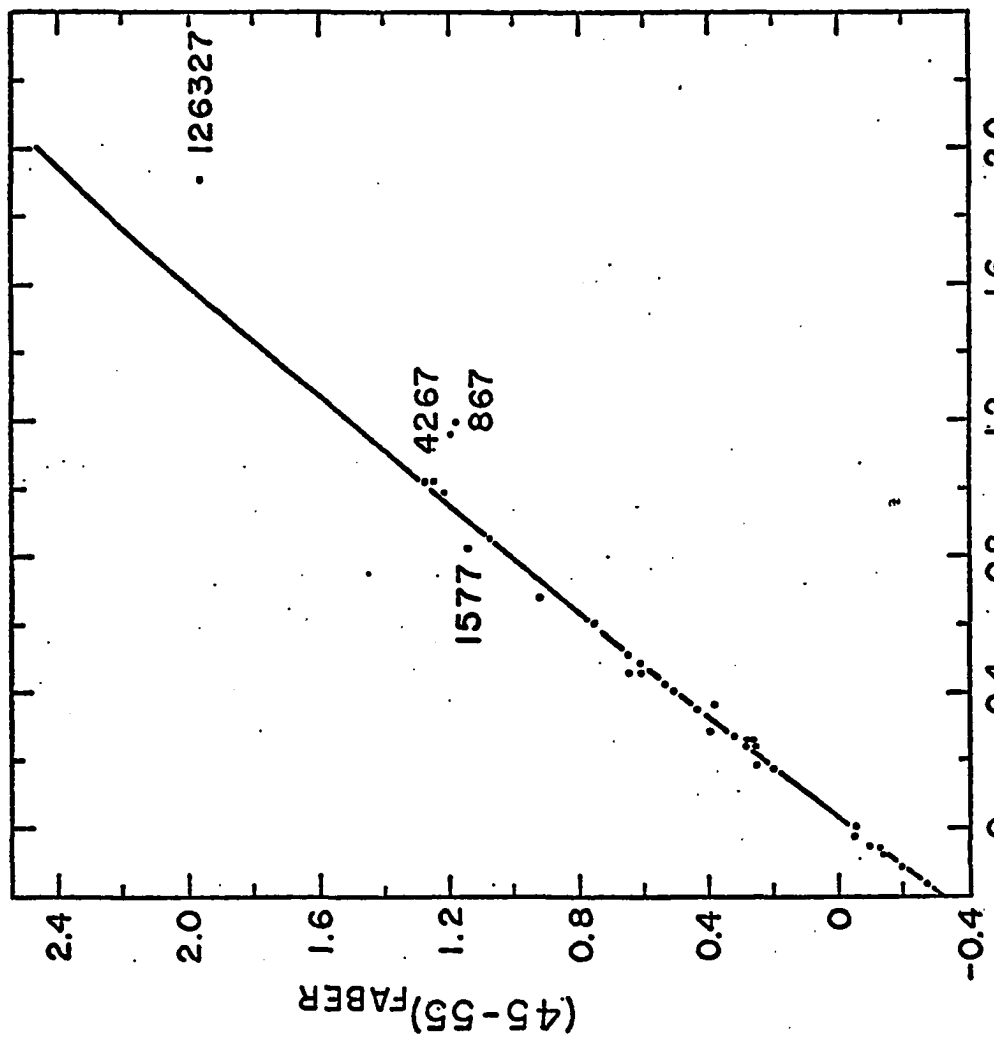

Fig. 3 (continued). The labeled points correspond to K and M giants.

Reproduced with permission of the copyright owner. Further reproduction prohibited without permission.

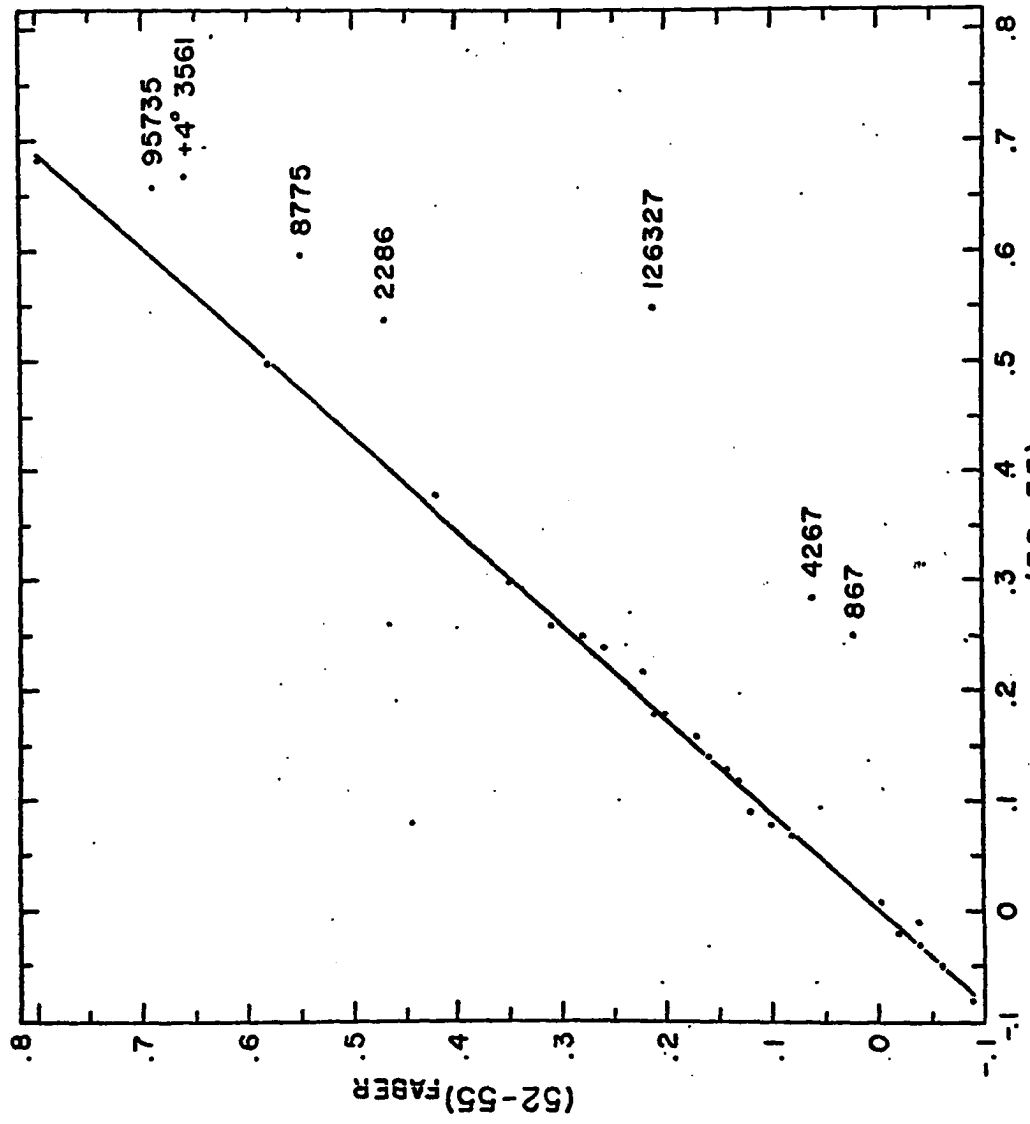

Fig. 3 (continued). The labeled points correspond to M stars.

Reproduced with permission of the copyright owner. Further reproduction prohibited without permission.

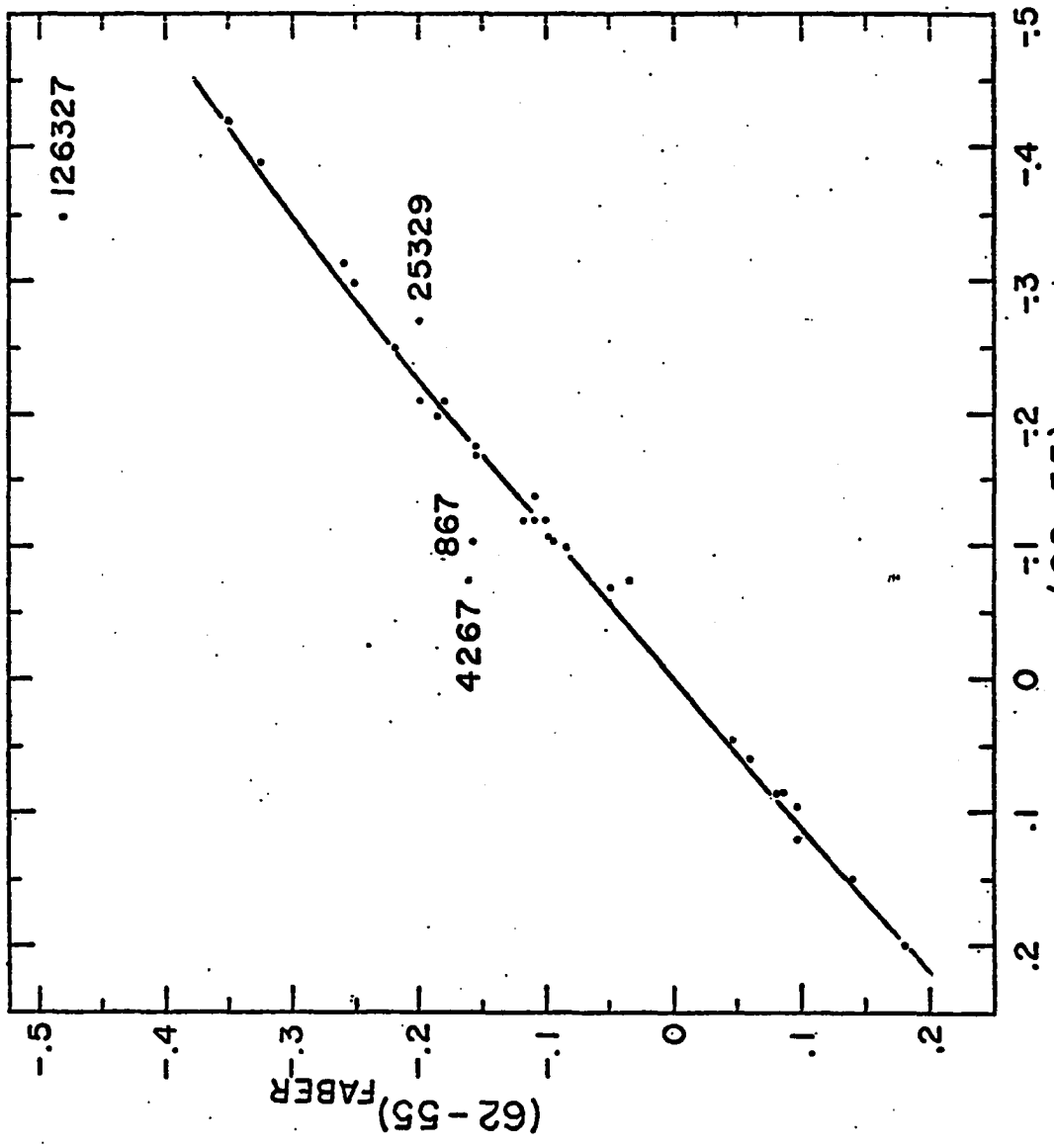

Fig. 3 (continued). The three points above the curve are M giants. HD 25329 has spectral type K1V.

Reproduced with permission of the copyright owner. Further reproduction prohibited without permission.

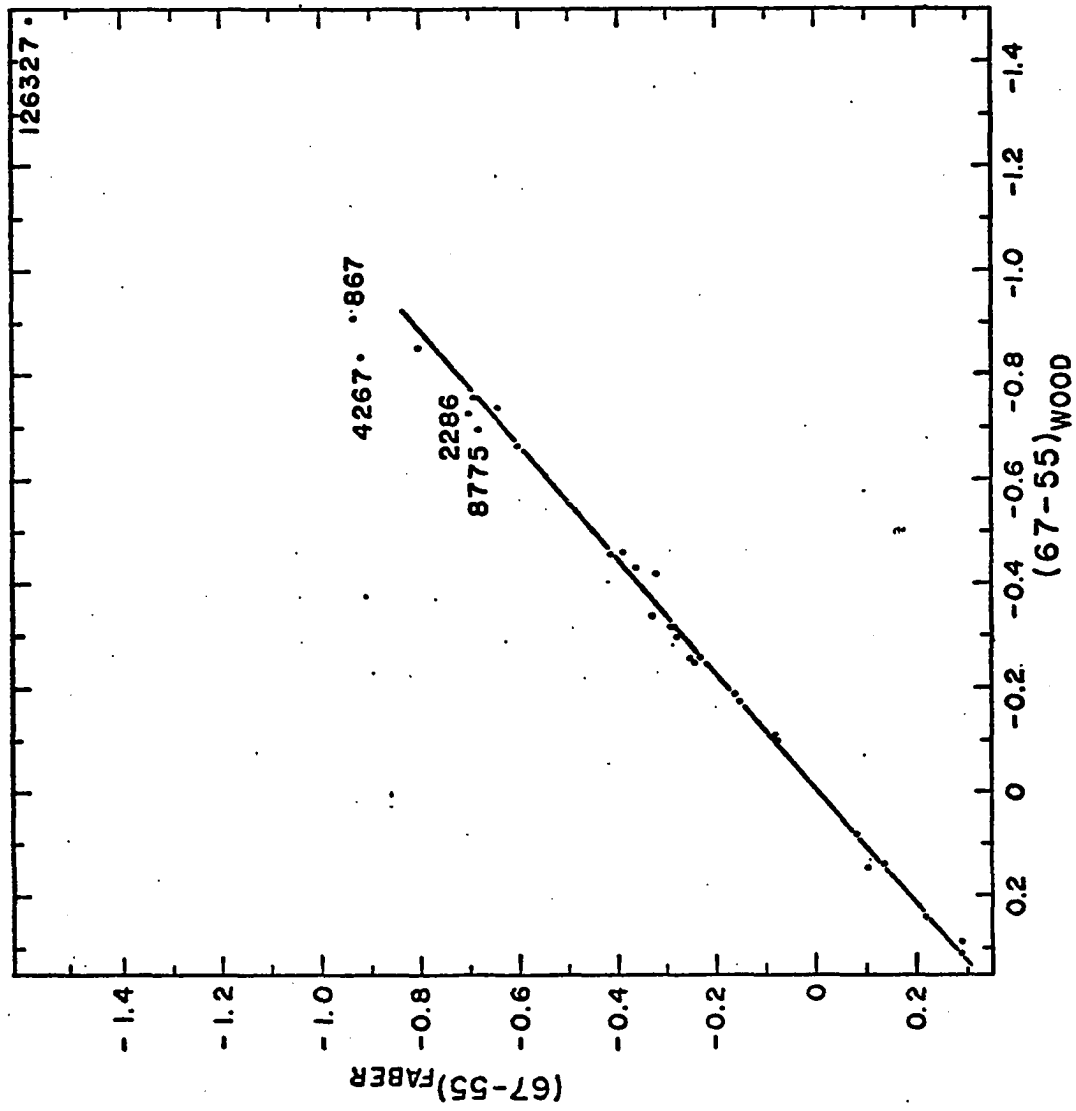

Fig. 3 (continued). The labeled points correspond to M giants.

Reproduced with permission of the copyright owner. Further reproduction prohibited without permission.

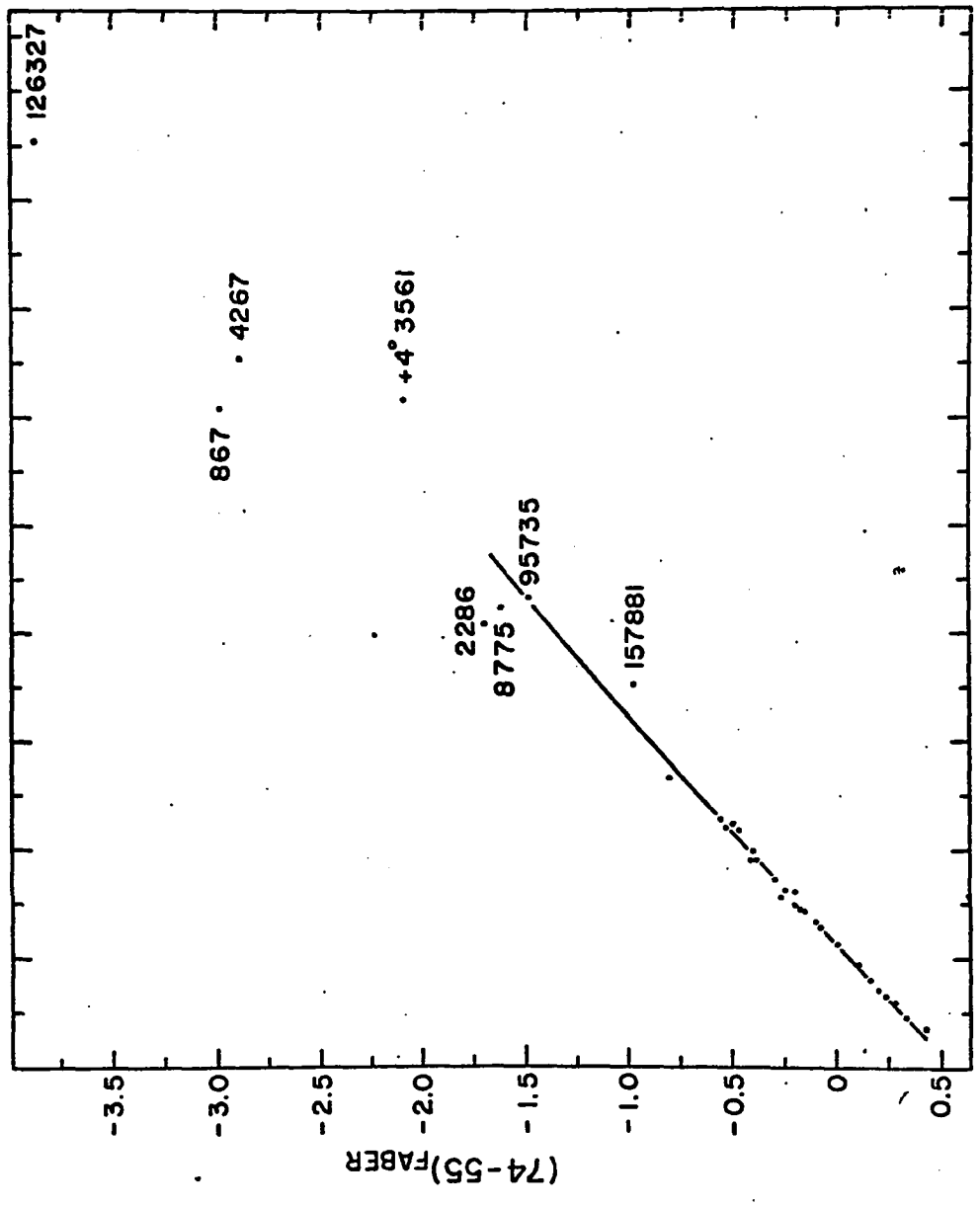

Fig. 3 (continued). The labeled points correspond to late K and M stars.

Reproduced with permission of the copyright owner. Further reproduction prohibited without permission.

redness of the object. In particular, the deviations for HD 126327 (M8e) should be much larger, relative to those for the other stars, than actually measured. A more likely explanation of the deviations is the fact that the filters are not perfectly matched. Strong band-heads of TiO lie in both the 52 and 55 filters, for example, and the differences in half-width and effective wavelength for the two sets of filters are sufficient to account for the differences in the (52-55) index between Wood's data and those presented here.

If the labeled points are omitted, the least-squares transformations between Wood's system and the present system are as follows:

$$(35-55)_W = -0.001(35-55)_F^2 + 1.001(35-55)_F + 0.092,$$
$$\pm 0.022 \quad \pm 0.000 \quad \pm 0.014 \quad \pm 0.018$$

$$(48-55)_W = +0.050(48-55)_F^2 + 0.715(48-55)_F + 0.032,$$
$$\pm 0.030 \quad \pm 0.023 \quad \pm 0.029 \quad \pm 0.002$$

$$(52-55)_W = -0.028(52-55)_F^2 + 0.877(52-55)_F + 0.005,$$
$$\pm 0.011 \quad \pm 0.117 \quad \pm 0.052 \quad \pm 0.001$$

$$(62-55)_W = -0.214(62-55)_F^2 + 1.100(62-55)_F - 0.001,$$
$$\pm 0.013 \quad \pm 1.002 \quad \pm 0.046 \quad \pm 0.001$$

$$(67-55)_W = +0.052(67-55)_F^2 + 1.118(67-55)_F - 0.009,$$
$$\pm 0.022 \quad \pm 0.084 \quad \pm 0.028 \quad \pm 0.001$$

$$(74-55)_W = -0.040(74-55)_F^2 + 1.006(74-55)_F - 0.078.$$
$$\pm 0.035 \quad \pm 0.018 \quad \pm 0.021 \quad \pm 0.002$$

Reproduced with permission of the copyright owner. Further reproduction prohibited without permission.

Figure 4 compares the UBV system with the indices (45-55) and (35-55). Aside from the M6III variable HR6146, the only seriously discrepant object is the metal-poor giant HD 165195. The other eight colors for this object (Figure 6) leave no doubt that this star as observed is indeed extremely metal-poor. Therefore the chance of a misidentification is slight. The 10-color data for this star agree more closely with the six-color photometry presented by Wallerstein et al. (1963) than with the UBV colors given in the same paper.

The transformation relating (45-55) to B-V is:

$$\underset{\pm 0.029}{B-V} = \underset{\pm 0.006}{-0.082(45-55)_F^2} + \underset{\pm 0.006}{1.278(45-55)_F} + \underset{\pm 0.000}{0.225}.$$

V. RESULTS

A number of dwarfs and giants with known abundances were observed in order to investigate variations in line indices as a function of changing metal abundance. The adopted values of the logarithm of the iron-to-hydrogen ratio relative to the sun, [Fe/H], are given in Table 5, together with the source(s) of these estimates. (Many of these values have been tabulated by Cayrel and Cayrel (1966)). When more than two sources are listed, a mean was taken. Values of [Fe/H] from Helfer and Wallerstein (1968) were corrected for interstellar reddening, when necessary, by the amounts suggested by Mannery, Wallerstein, and

Reproduced with permission of the copyright owner. Further reproduction prohibited without permission.

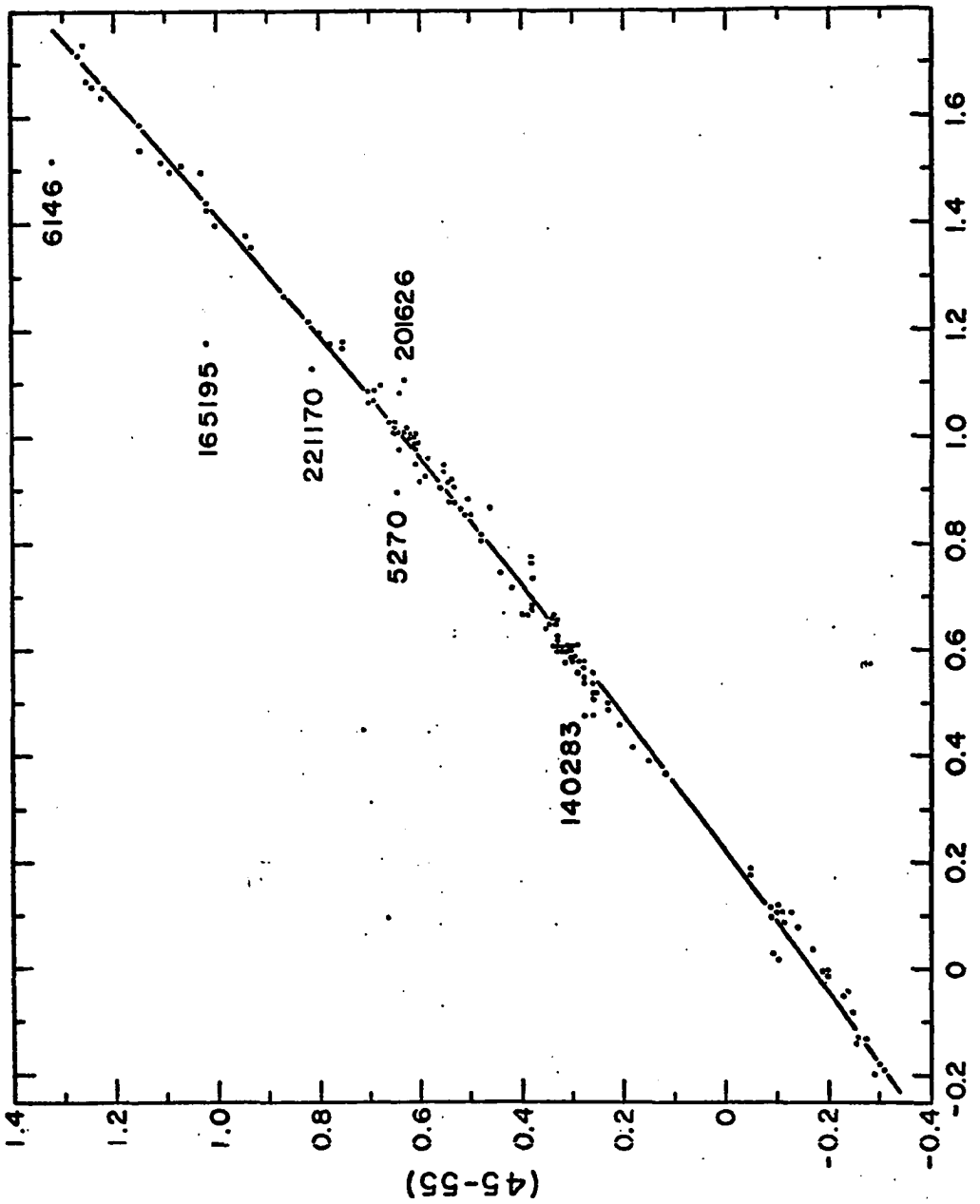

Fig. 4. Comparison of B-V and (45-55). Except for HR 6146 (M6III), the labeled points correspond to metal-poor stars.

Reproduced with permission of the copyright owner. Further reproduction prohibited without permission.

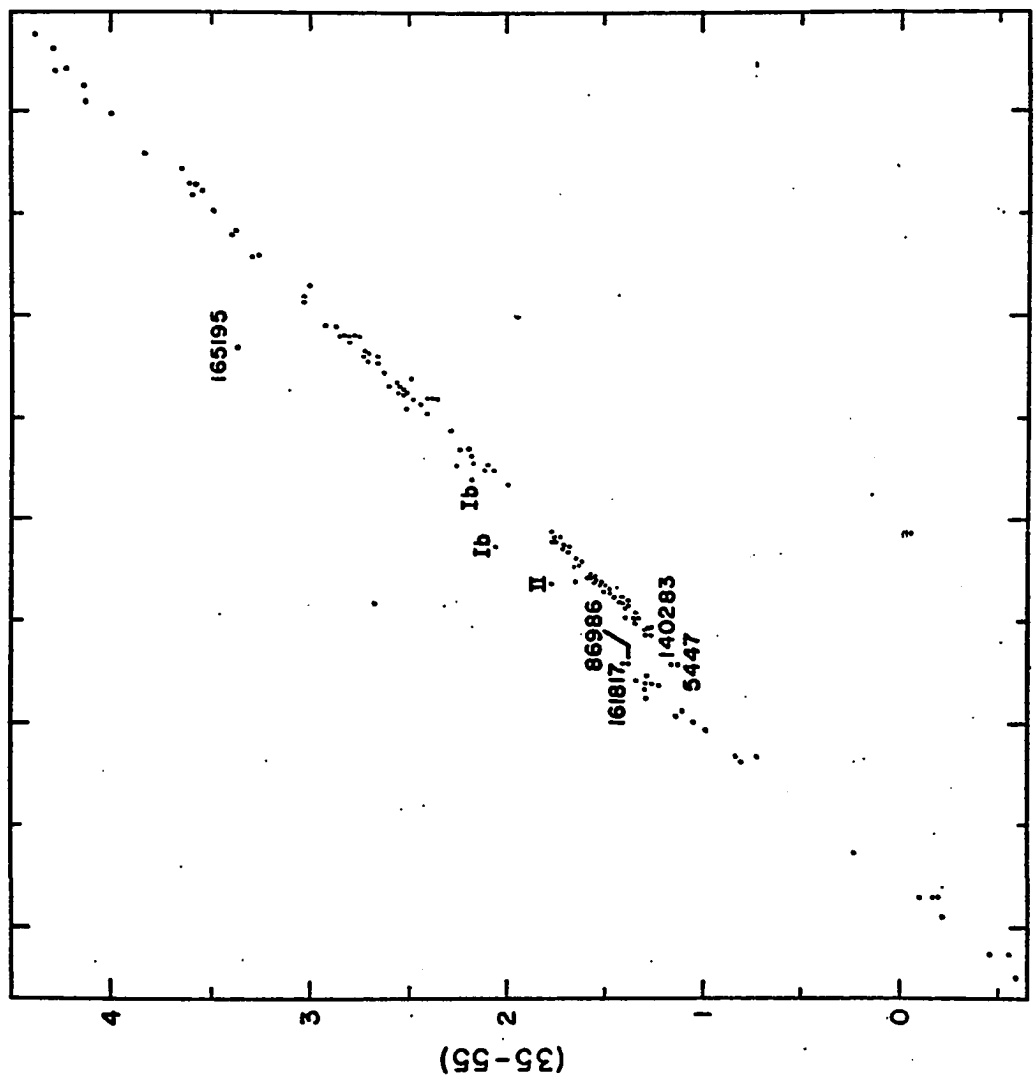

Fig. 4 (continued). Comparison of U-V and (35-55).

Reproduced with permission of the copyright owner. Further reproduction prohibited without permission.

Welch (1968). A value of +0.15 dex for the abundance of the Hyades relative to the sun (Chaffee, et al. 1971) was used to convert original abundances measured relative to the Hyades to the solar scale. This adjustment was necessary for the abundances of K giants determined by Helfer and Wallerstein (1968).

Figure 5 displays the fluxes on the 10-color system for G dwarfs of greatly differing composition. [Fe/H] for each star is shown to the left of the corresponding curve. The stars are arranged in three groups according to mean continuum slope in filters 55, 67, and 74. The ultraviolet excess in the metal-poor stars relative to the flux in the metal-rich stars is clearly apparent. The strength of the absorption due to Mg "b" and MgH near 5200 Å, the G-band absorption near 4300 Å, and absorption in the line-blanketed region near 3800 Å all increase with increasing abundance.

A similar selection of G and K giants is displayed in Figure 6. The metal-poor giants HD 2665, 165195, and 201626 were corrected for reddening by the amounts in E_{B-V} of 0.08 magnitude (Koelbloed 1967), and 0.25 and 0.10 magnitude (Wallerstein, et al. 1964) respectively.

Abundance results for HR 3994 and 7576 are controversial. They are among the group Spinrad and Taylor (1969) have termed super-metal-rich (SMR). Various estimates of the

Reproduced with permission of the copyright owner. Further reproduction prohibited without permission.

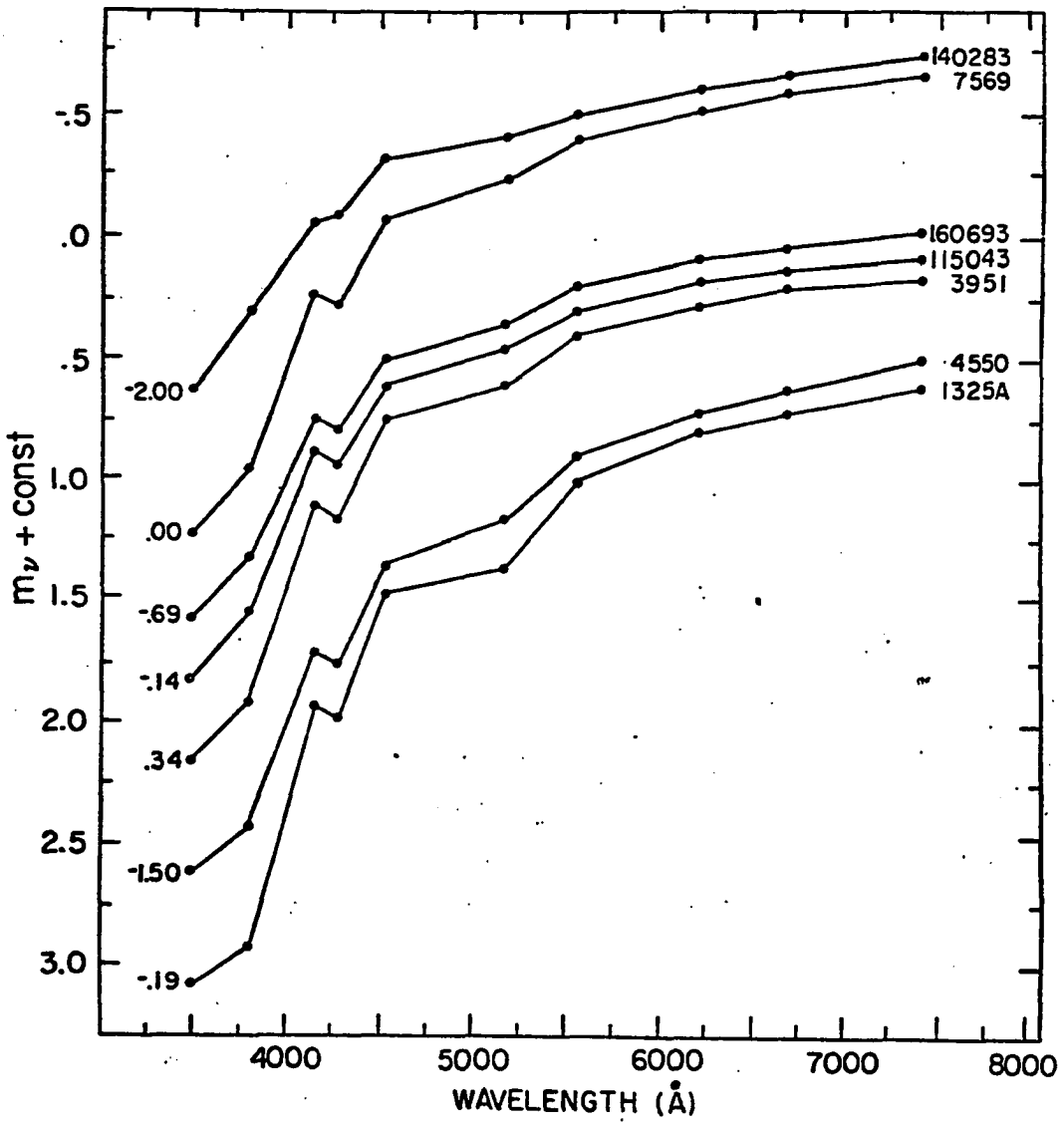

Fig. 5. Comparison of colors for dwarf stars having similar red color indices but different metal abundances. Values of [Fe/H] for each star are shown to the left of each curve. Spectral types range from A8VI (HD 140283) to K1V (HR 1325A).

Reproduced with permission of the copyright owner. Further reproduction prohibited without permission.

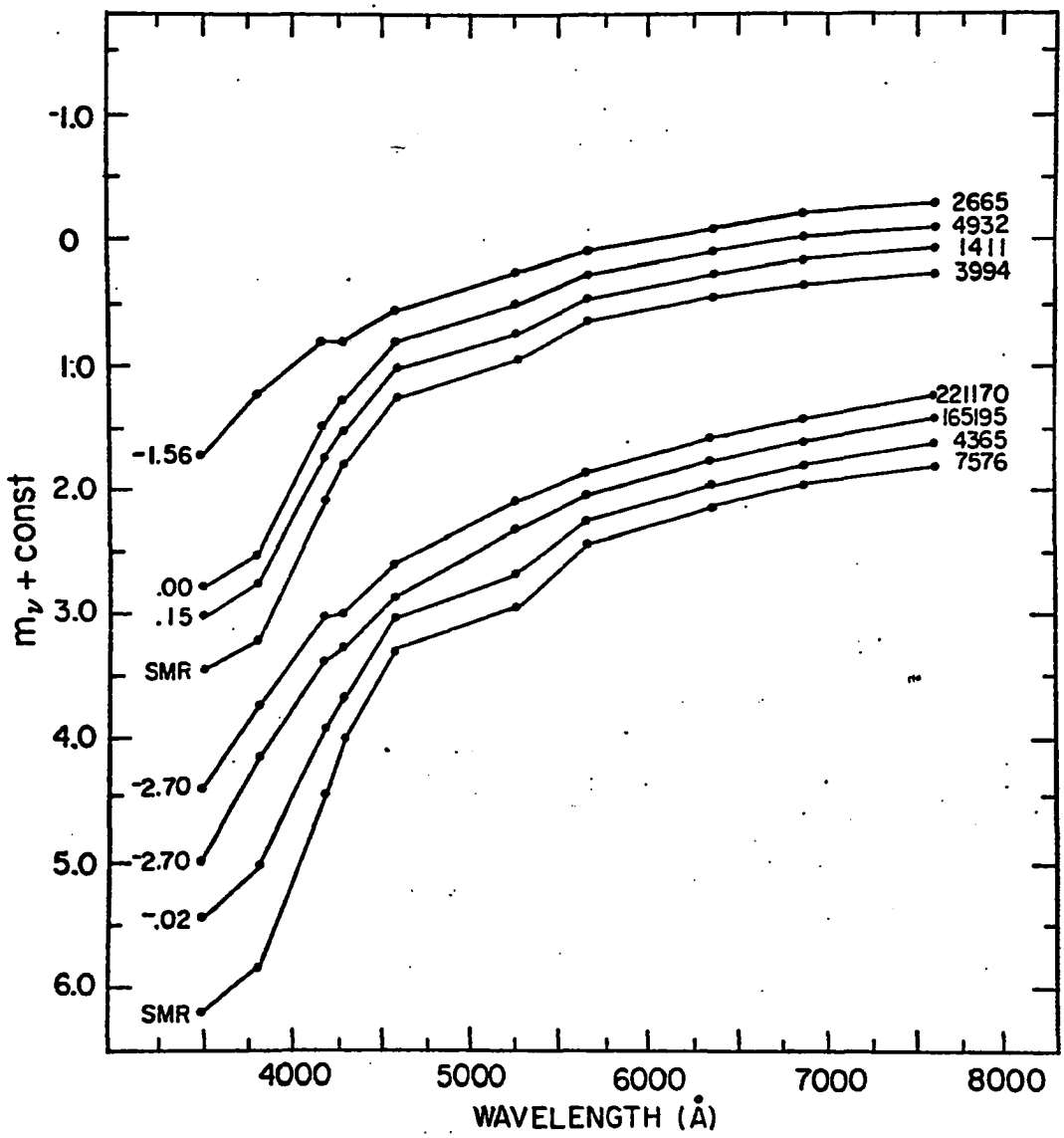

Fig. 6. Comparison of colors for giant stars having similar red color indices but different metal abundances. Colors for HD 2665, 165195, and 221170 have been corrected for reddening, as explained in the text. Values of [Fe/H] for each star are shown to the left of each curve. Various estimates of [Fe/H] for the SMR stars can be found in Table 5.

Reproduced with permission of the copyright owner. Further reproduction prohibited without permission.

abundances for these and other SMR stars can be found in Table 5. Figure 6 demonstrates that in giants, as in dwarfs, the strength of the absorption features and the ultraviolet blanketing increases with increasing metal abundance. These effects appear to be most extreme in the two SMR stars.

McClure and van den Bergh (1968a) and McClure (1970) have shown that the (38-41) and (41-42) indices are sensitive to abundance changes in G and K dwarfs and giants. A large number of dwarfs and giants of known composition have been observed in this study in order to calibrate the photometric effects more precisely in terms of actual metal abundance. As first pointed out by McClure and van den Bergh, the indices

$$(38\text{-}41)^* = (38\text{-}41) - 0.318(B\text{-}V),$$

$$(42\text{-}45)^* = (42\text{-}45) - 0.234(B\text{-}V)$$

are independent of reddening. In Figure 7, (38-41)* is plotted against (42-45)* for G dwarfs with known abundances. The dashed line represents the mean relation between (38-41)* and (42-45)* for stars with $\delta(U\text{-}B) = 0.0$ found by McClure and van den Bergh. When stars of known abundance are placed in the figure, however, the solid line appears to be a closer fit to the set of points with [Fe/H] = 0.0. Following the approach of McClure and van den Bergh, in Figure 8 we have plotted the distance of a point below the mean relation, $\delta(38\text{-}41)^*$, against

Reproduced with permission of the copyright owner. Further reproduction prohibited without permission.

Reproduced with permission of the copyright owner. Further reproduction prohibited without permission.

TABLE 5

[Fe/H] FOR G AND K DWARFS AND GIANTS

HR No.	Sp. Type	[Fe/H]	Sources	HR No.	Sp. Type	[Fe/H]	Sources
HD2665	Pop.II Gt.	-1.56	26	2219	G8III	-0.27	1
163	G8III	-0.60	1	2721	G0V	-0.21	4
483	G2V	+0.20	4	3369	G9III	+0.32	15
509	G8Vp	-0.38	7	3664	G6III	-0.70	1
563	K1p	-0.12	1	3905	K2III	+0.1	2
660	G0V	-0.43	4			+0.6	3
799	F7V	+0.02	8,9	3951	G2V	+0.34	4
937	G0V	+0.14	4	3994	K0III	+0.20	1
996	G5V	+0.38	8			+0.2	2
HD22879	F9V	-0.57	4			+0.60	3
1136	K0IV	-0.04	11,7	4098	G1V	-0.23	4
HD25329	K1V	-1.80	10,12	4112	F8V	+0.23	16
1325A	K0V	-0.19	7	4287	K0III	+0.03	1
1346	K0III	+0.15	5	4301	K0II-III	-0.08	1
1373	K0III	+0.15	5	4365	K3III	+0.08	1
HD28068	G1V	+0.15	5	4540	F8V	+0.33	4
HD28099	G0V	+0.15	5	4550	G8VI	-1.50	17
1409	K0III	+0.15	5	4695	K0III	-0.50	1
1411	K0III	+0.15	5	4845	G0V	-0.32	4
HD28344	G2V	+0.15	5	4932	G8III	0.00	1
HD30649	G0V	-0.20	4	4983	G0V	+0.05	4
1543	F6V	+0.18	13	HD114762	F9V	-0.59	4
1577	K3II	0.00	14	HD115043	G1V	-0.14	4
1729	G0V	+0.22	4	5270	Pop. II Gt.	-2.90	18
1805	K3III	-0.42	6	5447	F2V	-0.90	25
		-0.4	2	5480	G8III	-0.03	1
		+0.4	3	5535	G8III-IV	-0.34	1
1907	G8IIIp	-0.58	1	5544	G8V	0.00	8
2002	G8III	+0.04	1	5681	G8III	-0.42	1
2035	G8III	-0.36	15	5709	K0III	-0.17	1

Reproduced with permission of the copyright owner. Further reproduction prohibited without permission.

TABLE 5

[Fe/H] FOR G AND K DWARFS AND GIANTS

HR No.	Sp. Type	[Fe/H]	Sources
5802	K0p	+0.09	1
5854	K2III	0.00	19
		0.30	20
5911	G2V	-0.28	4
5914	F9V	-0.40	8
5968	G2V	-0.20	4
HD148816	F9V	-0.54	4
6212	G0IV	+0.07	21
HD152792	G0V	-0.45	4
HD157089	G0V	-0.57	4
6458	G0V	-0.36	4
HD160693	G0V	-0.69	4
6623	G5IV	+0.14	22
6775	F7V	-0.45	4
HD165195	Pop. II Gt.	-2.70	18
6791	G8IIIp	+0.17	1
7300	G5IIp	+0.21	15
7429	K3III	+0.39	1
		+0.30	2
		+0.3	3
7503	G2V	+0.22	4
7504	G5V	+0.11	4
7525	K3II	0.00	14
7569	G2V	0.00	4
7576	K3III	+0.11	1
		-0.1	2
		+0.55	3
7602	G8IV	-0.13	22
7949	K0III	-0.25	19
8204	G5II-III	+0.18	23
8255	K1III	+0.08	1
8832	K3V	0.00	24
8961	G8III-IV	-0.63	1
8969	F7V	+0.09	13
9088	G2V	-0.60	4
HD221170	Pop. II Gt.	-2.70	18

Sources for Table 5:

(1) Helfer and Wallerstein (1968).
(2) Strom et al. (1971).
(3) Spinrad and Taylor (1969).
(4) Wallerstein (1961).
(5) Chaffee et al. (1971).
(6) Cayrel (1966).
(7) Pagel (1964).
(8) Herbig (1965).
(9) Boyarchuk (1960).
(10) Heiser (1960).
(11) Hazelhurst (1963).
(12) Krishna Swamy (1968).
(13) Powell (1970).
(14) Schwarzschild et al. (1957).
(15) Greenstein and Keenan (1958).
(16) Boyarchuk (1962).
(17) Jugaku (1966).
(18) Wallerstein et al. (1963).
(19) Gratton (1953).
(20) Griffin (1969).
(21) Helfer et al. (1963).
(22) Spite (1966).
(23) Warner (1965).
(24) Cayrel (1964).
(25) Danziger (1966).
(26) Koelbloed (1967).

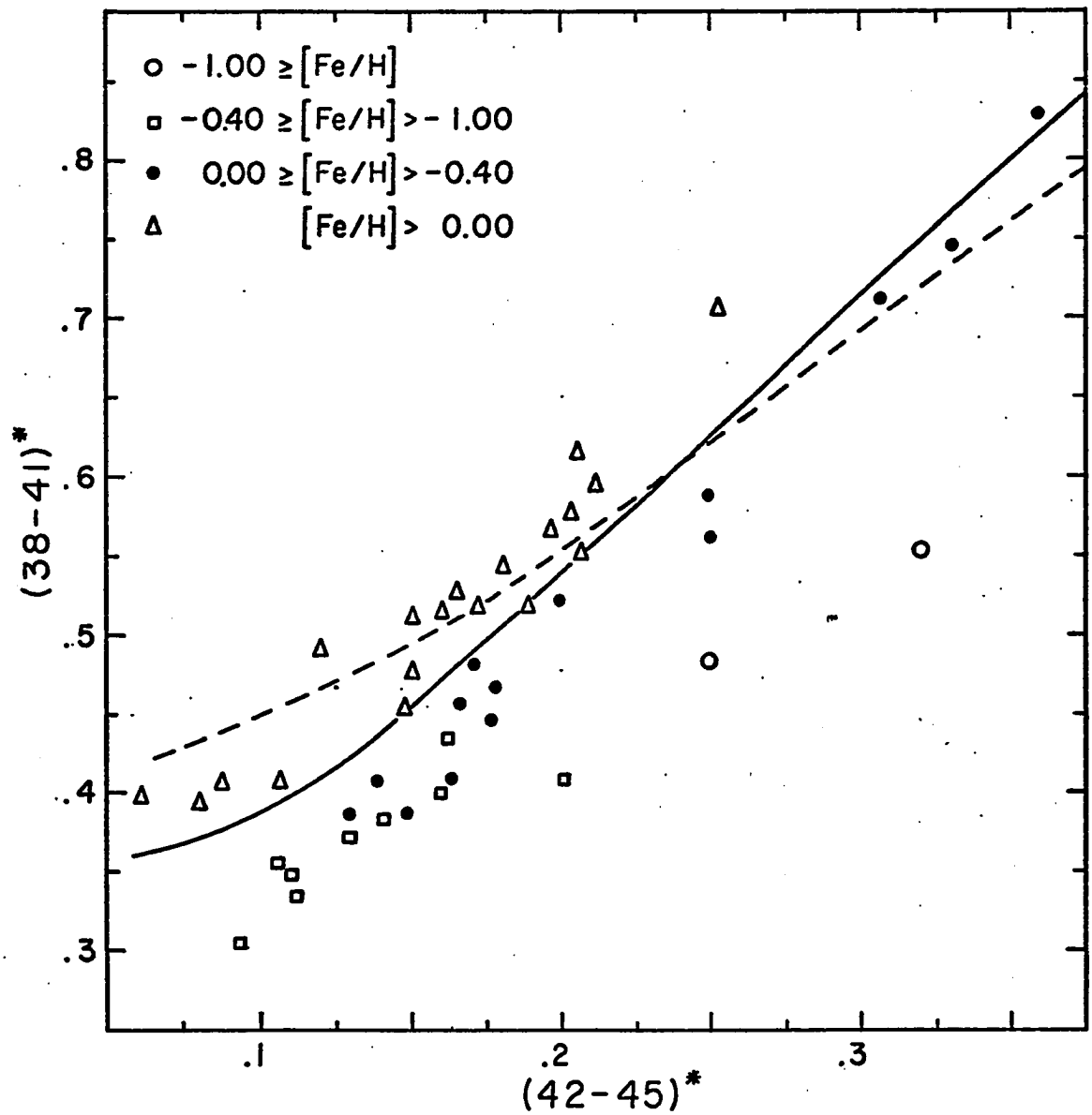

Fig. 7. The reddening-free blanketing index, $(38-41)^*$, plotted against the reddening-free G-band index $(42-45)^*$ for dwarf stars with known metal abundances. The solid line represents the adopted relation between $(38-41)^*$ and $(42-45)^*$ for stars having [Fe/H]=0.0. The dashed line is the provisional relation adopted by McClure and van den Bergh (1968a) for stars having $\delta(U-B)=0.0$.

Reproduced with permission of the copyright owner. Further reproduction prohibited without permission.

Reproduced with permission of the copyright owner. Further reproduction prohibited without permission.

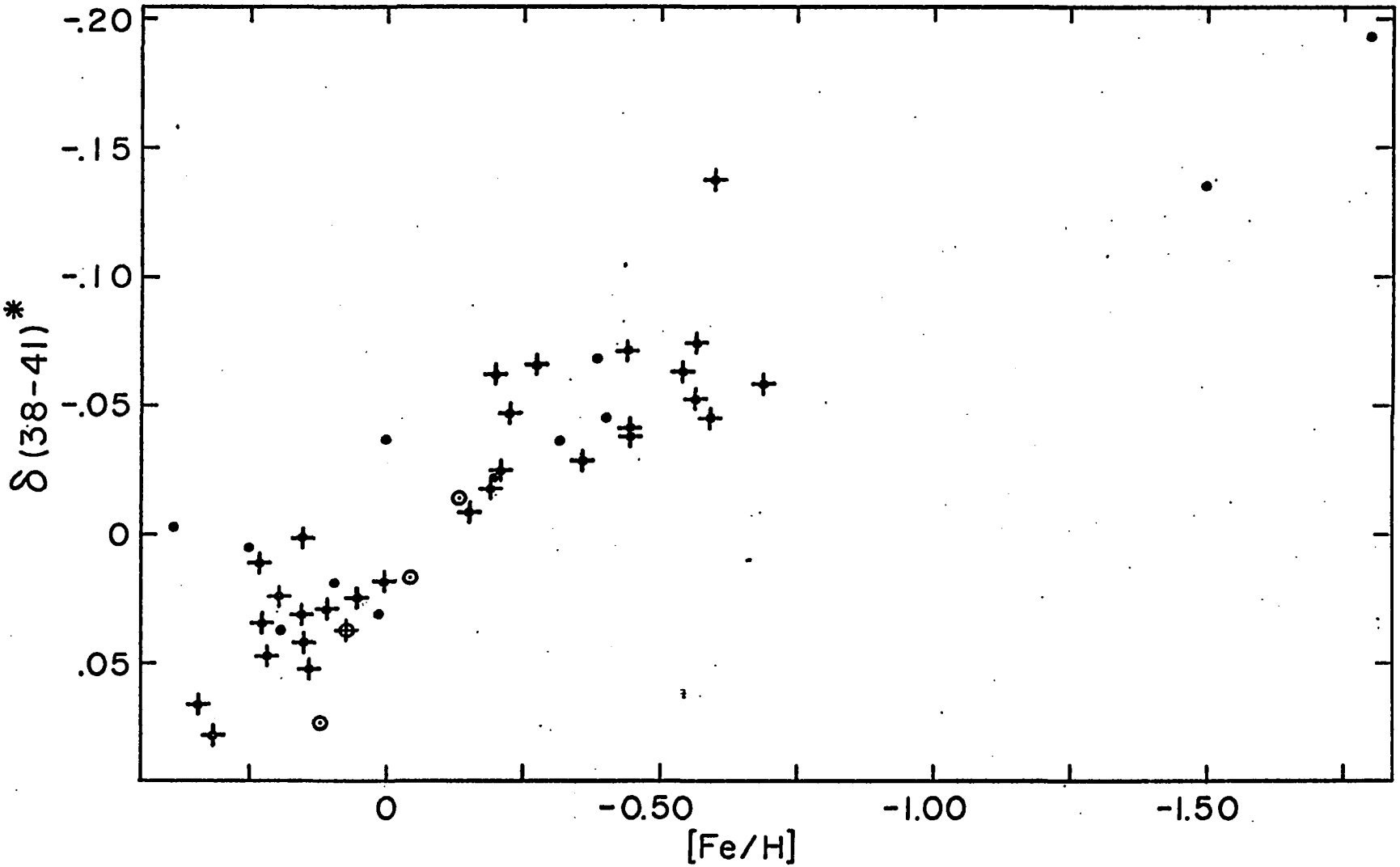

Fig. 8. The reddening-free UV excess $\delta(38\text{-}41)^*$ versus values of [Fe/H] from Table 5 for dwarf stars. Open circles represent stars of luminosity class IV. The crosses represent values of [Fe/H] measured by Wallerstein (1963).

the abundances for the G dwarfs shown in Table 5. The reddening-free ultraviolet excess $\delta(38\text{-}41)^*$ is closely correlated with [Fe/H]. The scatter becomes slightly smaller if only those stars with abundances determined by Wallerstein (1963) (crosses) are considered. Four stars of luminosity class IV (open circles) lie near the lower envelope enclosing the points. The systematically lower values of $\delta(38\text{-}41)^*$ for these stars may indicate a slight dependence of this quantity on surface gravity.

Using a technique similar to the method above, McClure (1970) has shown that in G and K giants, the CN index (41-42) is stronger in metal-rich stars. His analysis is of particular interest because the SMR stars invariably possess strong CN absorption. Hence, a plot of CN strength against conventionally measured values of [Fe/H] summarizes much of the currently available information concerning the composition of these stars. McClure's treatment is extended here to include most of the giants of known composition.

By means of the transformations given above between the DDO system and the system in the present paper, one can compute McClure's surface-gravity-independent CN index, $C_m(41\text{-}42)$, for all G and K giants in Table 4. A comparison between values of $C_m(41\text{-}42)$ measured here and those measured by McClure is shown in Figure 9 for stars in common. The fig-

Reproduced with permission of the copyright owner. Further reproduction prohibited without permission.

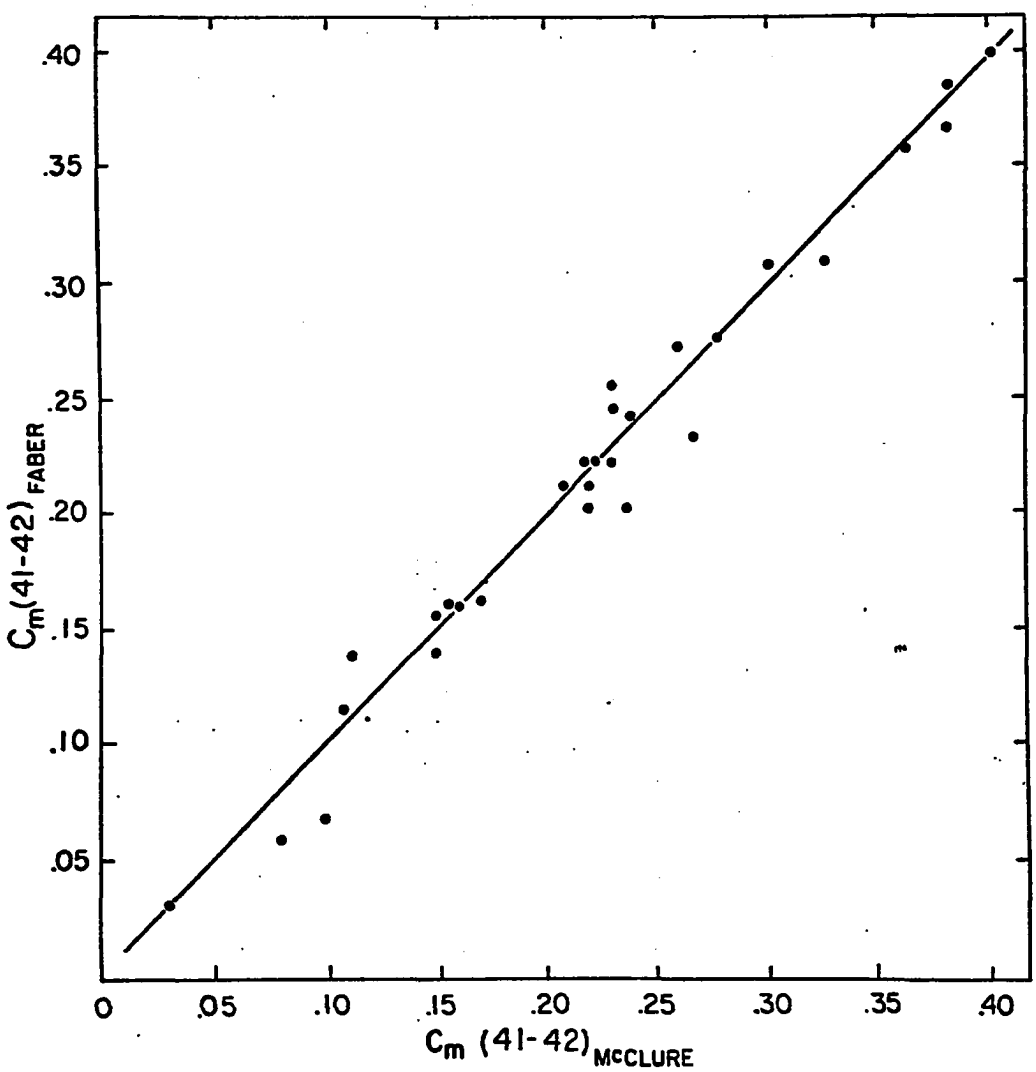

Fig. 9. Comparison between the values of the surface-gravity-independent CN index $C_m(41\text{-}42)$ measured in this paper with values measured by McClure.

Reproduced with permission of the copyright owner. Further reproduction prohibited without permission.

ure indicates that the mean error in $C_m(41-42)$ for stars in this paper is 0.014 magnitude.

Values of the cyanogen anomaly, $\delta C_m(41-42)$, computed by means of the mean relation between $C_m(41-42)$ and C (42-48) given by McClure, were corrected for reddening according to the technique of McClure and Racine (1969). These corrections were very small. Final values of $C_m(41-42)$ are plotted against [Fe/H] in Figure 10, where crosses represent abundances measured by Helfer, Wallerstein and their co-workers. The dashed line connects the two values of [Fe/H] for α Ser (HR 5854) found by Griffin (1969) and by Gratton (1953).

Knowing the composition of the SMR stars is equivalent to determining the slope of the correlation between $\delta C_m(41-42)$ and [Fe/H] at a value of [Fe/H] = 0.15 dex, corresponding to the position of the Hyades. With regard to this question, one may take several different points of view. If all the data points are accepted as they lie in the figure, the slope of the correlation at [Fe/H] = 0.15 is moderate and positive, leading to a mean overabundance of metals in strong CN stars ($\delta C_m(41-42)$ = 0.11) of approximately 2 with respect to the sun. This result, however, depends critically on the inclusion of two particular stars, μAql (HR 7429) and υ^2 Cnc (HR 3369). If these two points are excluded, the resulting correlation has nearly infinite slope at [Fe/H] = 0.15. We

Reproduced with permission of the copyright owner. Further reproduction prohibited without permission.

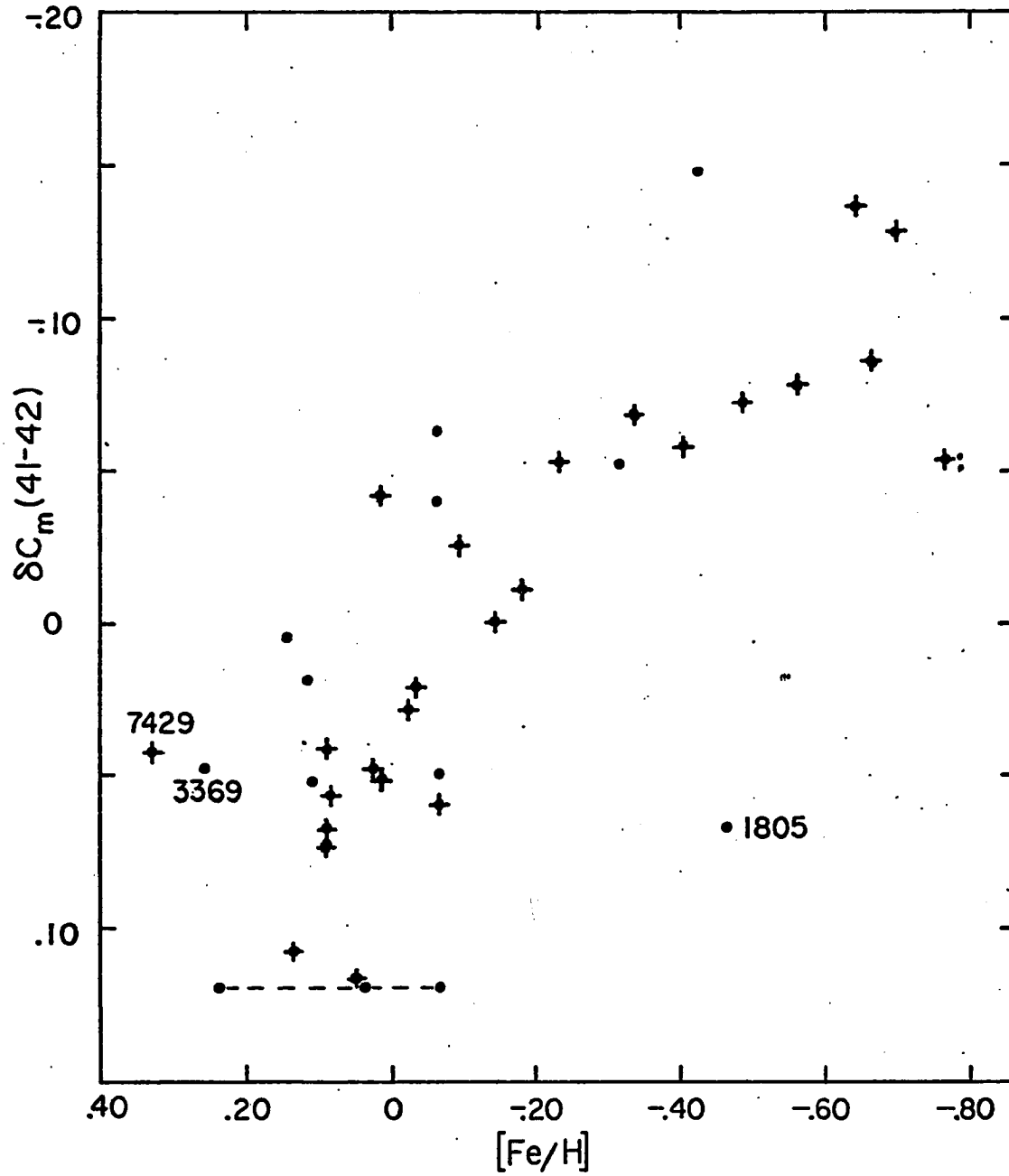

Fig. 10. The cyanogen anomaly, $\delta C_m(41-42)$, plotted versus values of [Fe/H] for G and K giant stars. Crosses represent values of [Fe/H] determined by Helfer, Wallerstein, and their co-workers. The dashed line connects the two available estimates of [Fe/H] for α Ser (HR 5854).

Reproduced with permission of the copyright owner. Further reproduction prohibited without permission.

would then conclude that the strong-cyanogen stars are at most slightly overabundant with respect to the Hyades.

On the other hand, it is possible that the measured abundances are systematically in error for some or all of the stars in Figure 10. Spinrad and Taylor (1971b) have suggested that model-atmosphere analyses yield abundances that are too low in stars of low temperature. In this connection, we note that three of the four stars with strongest CN have spectral types three-tenths of a spectral class later than those of the stars lying just above in Figure 10. Corrections to the systematic underestimates of the abundances for these stars would move the strong-CN stars to higher values of [Fe/H]. The correlation between $\delta C_m(41\text{-}42)$ and [Fe/H] would then again have positive slope.

Since the alternatives discussed here appear equally possible, the available data do not warrant a conclusion concerning the composition of the strong cyanogen stars. In any case the star ϕ Aur (HR 1805) seems distinctly peculiar. The physical properties of ϕ Aur may not be relevant to the question of super-metallicity.

VI. SUMMARY

This paper has presented measurements for 148 stars on a 10-color photometric system based on the absolute calibration for α Lyr by Oke and Schild (1970). The photometric

Reproduced with permission of the copyright owner. Further reproduction prohibited without permission.

system combines the 5-color David Dunlap Observatory system with six filters from Wood's 12-color system, both of which were intended for the study of stellar populations in old clusters and in galaxies. Transformations between the absolutely calibrated system in this paper and the DDO and Wood systems show that reliable transformations are possible for stars having B-V less than 1.30 magnitude.

A discussion of the reddening-free ultraviolet excess $\delta(38\text{-}41)^*$ shows that this index can be used to determine the iron-to-hydrogen ratio in G dwarfs. The accuracy of the abundance determination at values of [Fe/H] near the solar value is approximately ± 0.15 dex. New observations of McClure's (1970) parameter $\delta C_m(41\text{-}42)$ for G and K giants with measured abundances are also presented. These data emphasize the uncertainty in the correlation between the cyanogen anomaly and [Fe/H] for stars more metal-rich than the sun.

Reproduced with permission of the copyright owner. Further reproduction prohibited without permission.

CHAPTER II

Photometry of Elliptical Galaxies and Globular Clusters

I. INTRODUCTION

Most photometric studies of elliptical galaxies have emphasized that these objects form a fairly homogeneous family. Integrated color indices of ellipticals generally fall within restricted limits, and many investigators (see below) have noted that intrinsically faint ellipticals tend to be bluer than more luminous ones. The reddening-free metallicity index Q also varies as a function of luminosity (McClure and van den Bergh 1968b). These results imply that the stellar population of an elliptical galaxy depends upon its absolute magnitude.

However, closer inspection of these data reveals a considerable amount of scatter, larger than the quoted observational errors, within the color-color and color-magnitude diagrams published to date. Significant discrepancies also exist among the mean relations between color and absolute magnitude determined by various investigators. Specifically, the C-M diagram of Baum (1959) suggested an extremely rapid blueing trend for ellipticals with intrinsic visual luminosities less than -16 magnitude. Brighter than this limit, all galaxies seemed to have identical colors, and the scatter at all points in the relation was very small. De Vaucouleurs

Reproduced with permission of the copyright owner. Further reproduction prohibited without permission.

(1961) subsequently located the onset of this blueing trend, as measured with the integrated color index B-V , at -19, while Rood's (1969) diagram for the Coma and Virgo clusters indicated that in U-B, the blueing begins immediately at the highest luminosities. The data of Hodge (1963), Webb (1964), and Lasker (1970) showed a general change in color with magnitude for elliptical galaxies but were insufficient to delineate the relation precisely.

Recently, Tifft (1969) has presented a color-magnitude diagram for the Virgo cluster using his color index (1-3), which indicates an extremely close correlation between the colors and magnitudes of E galaxies brighter than -16 magnitude. The galaxies gradually become redder with increasing luminosity, and this relation extends with uniform slope to the brightest members of the cluster. In contrast to this result, Lasker found considerable deviations of over 0.10 magnitude from a mean color-luminosity relation. He concluded that these deviations were intrinsic to the galaxies and not due to observational errors. Tifft's galaxies were all members of one cluster and therefore might exhibit a tighter correlation than galaxies observed in many different regions of the sky. However, Lasker's analysis indicated that the scatter in colors within a cluster of galaxies equalled the scatter in the total population observed.

Reproduced with permission of the copyright owner. Further reproduction prohibited without permission.

Several factors might cause spurious differences among the color-magnitude diagrams of various investigators. The probable errors of observation in most of the studies cited above are fairly large, typically 0.05 magnitude for UBV photometry. Not all investigators present colors corresponding to a standard diameter defined in the same way for all galaxies independent of size or absolute magnitude. Color-magnitude relations might be different in different color systems. Inaccurate corrections for reddening in our own galaxy will also introduce additional scatter.

On the other hand, evidence of a somewhat different nature suggests that at least some of the scatter is real and that the the stellar content of elliptical galaxies cannot be completely specified with just one parameter, the luminosity. From his photographic photometry of double nebulae, Holmberg (1958) concluded that the stellar populations and surface brightnesses of the two components of a pair were similar. This result indicated that the mean colors and stellar populations of E galaxies in pairs depended upon the morphological type of the companion galaxy. Hodge (1963) found that the UBV colors of elliptical nebulae in two close, interacting pairs were abnormal. And Fish (1964) suggested that the mass-to-light (M/L) ratios of E galaxies with late-type galaxy companions were systematically lower than M/L ratios for ellipticals with early-type compan-

Reproduced with permission of the copyright owner. Further reproduction prohibited without permission.

ions, thus supporting Holmberg's contention that the properties of pair members are correlated. Lastly, a small number of peculiar dwarf ellipticals are known that are quite red and have unusually high surface brightness. These strange objects clearly do not fit into the sequence of normal ellipticals.

In the present study, integrated photometry in ten colors on 33 galaxies has been used to test whether elliptical galaxies form a one-parameter sequence. Expressed in another way, we ask whether at least some of the observed dispersion in elliptical colors is real and is correlated with the properties of the pairs or groups to which the ellipticals belong. The elliptical galaxies observed span a range in luminosity of almost 6 magnitudes. Nearly all are members of pairs or small groups. In some cases these groups are subsets of larger clusters, while in others the pair or small group is an isolated unit. Eleven galaxies are also listed in Arp's (1966) Atlas of Peculiar Galaxies, six of which interact visibly with their companions. Types of companions range from E to Irr I. In short, these elliptical galaxies are found under a wide variety of physical conditions. They are therefore suitable subjects to observe for a study of correlations between the photometric properties of ellipticals and aspects of their immediate environment.

Reproduced with permission of the copyright owner. Further reproduction prohibited without permission.

II. SELECTION OF PAIRS

Holmberg (1937) has described a criterion for selecting physical double galaxies from a population of galaxies randomly arranged on the sky. This criterion was adopted as a starting point in choosing candidates for observation in this study. Let D_1 and D_2 represent the diameters of two pair members and S the separation between them. Holmberg has shown that if the apparent photographic magnitudes of both galaxies are less than 15.7 magnitude and $S \leq 2(D_1 + D_2)$, then the probability that the pair is an optical double, that is, physically unrelated, is only 13 per cent. This result can be scaled easily to different limiting magnitudes. If the limiting magnitude is increased, corresponding to an increase in the volume of space searched for doubles, and if the number of galaxies tested for pair membership increases in proportion to the volume of space searched, the mean separation between galaxies decreases faster with distance than do their diameters. If r represents the mean radius of the volume of space searched, the mean separation varies inversely as $r^{3/2}$ while D_1 and D_2 vary inversely as r. Thus, as one looks further into space, the galaxies draw closer together on the celestial sphere faster than they become smaller. Therefore the contrast between optical and physical doubles can be increased by applying Holmberg's criterion to a set of galaxies with brighter limiting

Reproduced with permission of the copyright owner. Further reproduction prohibited without permission.

magnitude. In general, the limiting photographic magnitude of pair members in this study was 14.0. For this case, less than 6 per cent of the pairs chosen according to Holmberg's criterion are optical pairs. Since the analysis by Holmberg required that the galaxies be randomly arranged on the sky, his criterion has no validity in large clusters, where the probability of chance alignment is higher. Some of the objects considered here are members of large clusters and, except as noted, no claim is made for pair membership in these cases.

When the radial velocities available for both members of a possible pair were similar, it was felt that Holmberg's criterion could be relaxed by a factor of 2. Page's (1961) list of double galaxies with measured velocities indicates that true physical doubles sometimes have radial velocities that differ by as much as 650 km/sec. Accordingly, if two galaxies with $v \leq 650$ km/sec also had a separation $S \leq 4(D_1 + D_2)$, they were accepted as candidates for observation. In the case of groups with three or more members, the velocities and separations were measured relative to the brightest member of the group. With one exception, at least one radial velocity was required for each pair or group, since too large a velocity would shift important spectral features out of the bandpasses of the filters. This upper limit was set at 4000 km/sec. Only groups with at least one elliptical galaxy were considered.

Reproduced with permission of the copyright owner. Further reproduction prohibited without permission.

The great majority of pairs finally chosen satisfied both Holmberg's criterion and the velocity criterion and so are of high reliability. The principal sources consulted for double and multiple galaxies were Holmberg's (1937) catalog, Page's (1961) lists, and the notes to the Reference Catalogue of Bright Galaxies (RCBG) (de Vaucouleurs and de Vaucouleurs 1964).

Table 1 identifies the galaxies observed, together with information concerning their pair or group membership. Column 1 contains the NGC number of the object or its designation in the RCBG. Columns 2 and 3 give the corresponding numbers in the catalogs of Holmberg and Arp, if any. Column 4 lists all the members in the immediate group of which the object is a member, determined according to the criteria already set forth. Footnotes describe those few cases in which the criteria were not strictly obeyed. Column 5 indicates membership in a larger aggregate, if any. Morphological types according to de Vaucouleurs (from the RCBG) are found in column 6. Columns 7 and 8 contain the types of the earliest and latest companions in the immediate pair or group.

III. PHOTOMETRIC SYSTEM AND OBSERVATIONS

A photometric system designed to study small differences in the energy distributions among elliptical galaxies

Reproduced with permission of the copyright owner. Further reproduction prohibited without permission.

Reproduced with permission of the copyright owner. Further reproduction prohibited without permission.

TABLE 1

E GALAXIES FOR WHICH 10-COLOR PHOTOMETRY EXISTS

(1) Name	(2) Holmberg No.	(3) Arp No.	(4) Immediate Group Members	(5) Larger Aggregate	(6) E Galaxy	(7) Earliest Companion	(8) Latest Companion
NGC 205	17c		205,221,224	Local Group	E^+5p	E2	SA(s)b
221	17b	168	205,221,224	Local Group	E2	E^+5p	SA(s)b
584	45b		584,586,596	Ft. gal. in	E4	E0	SA(s:)a?
596			584,586,596	field	E0	E4	SA(s:)a?
1332			1331,1332, I324[1]	1315-1332 group[4]	SO^-:	E2:	E2:
1889		123	1888,1889		E0	SB(s)cp	SB(s)cp
2300		114	2276,2300	Ft. gal. in field	E^+2	SAB(rs)c	SAB(rs)c
2634			2634,2634A[2]	Probably in a group	E1:	SB(s):	SB(s):
2672	99a	167	2672,2673	Probably in group[4,8]	E1-2	E^+0:	E^+0:
2872	130a	307	2872,2874		E?	SB(s):	SB(s):
3073	156b		3073,3079		Ep?	SB(s)msp	SB(s)msp
3193	175b	316	3185,3187, 3190,3193	3193 Group[4,5]	E2	SA(s)ap(sp)	SB(s)cp
3226	187b	94	3226,3227		E^+2p:	SAB(s)ap	SAB(s)ap
3379	212a		3377,3379, 3384	Leo Group[4,5]	E^+1	SB(s:)0	SA(s)c
3605	240c		3605,3607, 3608	3607 Group[4]	E4-5	E2	$SA(s:)0^0$
3608	240b		3605,3607, 3608	3607 Group[4]	E2	E4-5	$SA(s:)0^0$
3613			3613,3619	3642 Group[5]	E^+6	(R?)SA(s:)0^+	(R?)SA(s:)0^0
4261			4260,4261, 4264	Group W-a[6]	E2-3	SB(rs)0^+	SB(s)a
4278	369a		4274,4278, 4283	4274 Group[5]	E1-2	E0	(R)SB(r)ab

Reproduced with permission of the copyright owner. Further reproduction prohibited without permission.

TABLE 1 continued

E GALAXIES FOR WHICH 10-COLOR PHOTOMETRY EXISTS

(1) Name	(2) Holmberg No.	(3) Arp No.	(4) Immediate Group Members	(5) Larger Aggregate	(6) E Galaxy	(7) Earliest Companion	(8) Latest Companion
NGC 4283	369b		4274,4278, 4283	4274 Group[5]	E0	E1-2	(R)SB(r)ab
4464				Virgo Cluster	E2		
4472	413a	134		Virgo Cluster	E2		
4478				Virgo Cluster	E2		
4486		152		Virgo Cluster	E0-1p		
4486B				Virgo Cluster	E0		
4627	442b	281	4627,4631, 4656-7	Canes Venatici Cluster[7]	E^+p	SB(s)d sp	SB(s)mp+Im
4649	448a	116	4647,4649[3]	Virgo Cluster	E2	SAB(rs)c	SAB(rs)c
5846	694a		5846,5846A, 5850	5846 Group[4,5]	E^+0-1	E2-3	SB(r)b
5846A	694b		5846,5846A, 5850	5846 Group[4,5]	E2-3	E^+0-1	SB(r)b
5982	719a		5981,5982, 5985		E3	SAB(r)b	SC?sp
6307	769a		6306,6307		E4:	S:	S:
7619				Peg I Cluster	E3		
7626				Peg I Cluster	E1		

Notes to Table 1:

1. NGC 1331 fainter than 14.0.
2. NGC 2634A fainter than 14.0. Velocity available only for NGC 2633.
3. Considered a pair even though in Virgo Cluster.
4. Notes, RCBG.
5. van den Bergh, Ap. J., 131, 215, 1960.
6. Vaucouleurs, Ap. J. Suppl., 5, 233, 1961.
7. van den Bergh, Ap. J., 131, 558, 1960.
8. NGC 2673 fainter than 14.0.

cannot be a wide-band system because wide-band filters are insensitive to changes in the strengths of absorption features. Comparison of published scans of elliptical galaxies (Oke and Sandage 1968; Schild and Oke 1971; Whitford 1971) with the bandpasses defining the 5-color David Dunlap Observatory (DDO) system (McClure and van den Bergh 1968a), designed for use with old stellar populations, shows that the DDO system monitors the major absorption features to the blue of 4600 Å and detectable with a resolution of 50 Å. The principal features to the red of 4600 Å are the Mg "b" plus Mg H feature near 5200 Å, the sodium D lines, and TiO bands near 6200 Å and 7100 Å. (All other features either are too narrow or lie to the red of 7500 Å and are out of the region accessible to an S-20 photocathode.) The 12-color photometric system of Wood (1966, 1969) has filters located at each of these absorption features. Therefore, a combination of the DDO and Wood filter systems offers a reasonably complete intermediate-bandpass filter set for elliptical galaxies and, at the same time, affords access to a considerable body of data already published on these two systems.

Because of the greater utility of the DDO filters at shorter wavelengths, Wood's v and b filters were omitted. The possibility that some of the sodium D absorption in galaxy spectra is of interstellar origin (Deutsch 1964; Spinrad and

Reproduced with permission of the copyright owner. Further reproduction prohibited without permission.

Peimbert 1972) renders the D filter in Wood's system of questionable value. Along with the D filter, Hα and the redundant TiO filter at 7100 Å were also omitted. The characteristics of the 10 filters ultimately adopted are presented in Table 2.

Because of the Doppler effect, relative motion between the source and observer results in a change in the effective wavelength of the observing passbands as measured in the rest-frame of the object. Published scans of elliptical galaxies (see above) show that, due to this cause, redshifts greater than 2000 km/sec will have a non-negligible effect on colors measured with six of the filters used in the present study. However, the number of elliptical galaxies satisfying the criteria described above and having velocities less than 2000 km/sec is too small to yield statistically significant results. Therefore, the effect of redshift was compensated for through the use of six additional filters, all of which were redshifted by approximately 1500 km/sec from the rest wavelengths of the original system. Table 2 indicates which bandpasses possessed filters at both rest and redshifted wavelengths. (Δv is the differential velocity in km/sec between the zero-velocity and redshifted members of the pair.) The methods used in reducing observations made with the redshifted set to the zero-velocity set are described below.

The observations were taken largely at the Cassegrain focus of the f/13.5 Number 2 36-inch reflector of the

Reproduced with permission of the copyright owner. Further reproduction prohibited without permission.

TABLE 2

PHOTOMETRIC SYSTEM IN THIS PAPER

Filter	Source	λ_{eff}	Half-width	Differential velocities, Δv	Spectral Feature Monitored
35	DDO, Wood	3450 Å	390 Å		Balmer discontinuity
38	DDO	3803 3818	140	1180 km/sec	Line-blanketing discontinuity
41	DDO	4167 4181	79	1070	CN absorption
42	DDO	4257 4275	82	1270	G-band
45	DDO	4517 4543	84	1730	
52	Wood	5162 5195	54	1910	MgH + Mg"b"
55	Wood	5545	214		Continuum
62	Wood	6222 6257	108	1690	TiO
67	Wood	6702	131		Continuum
74	Wood	7415	188		Continuum

Reproduced with permission of the copyright owner. Further reproduction prohibited without permission.

Kitt Peak National Observatory. The Observatory also provided all peripheral observing equipment. The UBV 3-channel photometer equipped with an extensive set of aperture diaphragms. was used in single-channel mode, together with an ITT FW-130 photomultiplier refrigerated with dry ice. The output of the photomultiplier was measured in the pulse-counting mode with a fast amplifier-discriminator and a digital counter. Coincidence corrections never exceeded 2 per cent of the measured counts. All observations of NGC 4464, 4627, 5982, 6307 and partial observations of certain other galaxies were taken with the f/9.0 61-inch Mt. Hopkins reflector of the Smithsonian Astrophysical Observatory. In addition, 10 globular clusters were measured with the Number 3 f/18.0 16-inch telescope at Kitt Peak National Observatory. In both cases the peripheral equipment was very similar to that on the 36-inch telescope.

Integrated colors of galaxies corresponding to a diameter D_o as listed in the RCBG were originally desired, but measurement of most objects with sufficiently large diaphragm sizes proved impossible for a number of reasons. The largest diaphragm available set an absolute upper limit to aperture size of approximately 65 arc sec. In several cases, observations with a diaphragm size D_o would have been contaminated by light from a nearby companion. Most important, however, was the fact that on a 36-inch telescope, measurements

Reproduced with permission of the copyright owner. Further reproduction prohibited without permission.

of fairly faint objects through relatively narrow filters are limited by the sky background. At apertures comparable to D_o, the sky counts in filter 35 overwhelm the galaxy signal. Consequently somewhat smaller aperture sizes were chosen that approximate the diameter of the object on the E plates of the Palomar Sky Survey when that diameter is less than or equal to 65 arc sec. A discussion of aperture effects below shows that this procedure has not introduced significant errors. During the course of the observing, a change of the primary mirror on the 36-inch telescope caused the scale to change from 16.5"/mm to 15.7"/mm. Because of this fact and because the aperture sizes available at Mt. Hopkins were somewhat different from the Kitt Peak apertures, it was impossible to observe many objects with an absolutely constant diaphragm size. Average diaphragm sizes A in seconds of arc, together with A/D_o, are given for all objects in Table 3, but the actual sizes used in some cases fluctuated about the mean value by as much as 15 per cent.

Galaxies were initially centered visually in the aperture, and an offset guider was used for subsequent guiding. Each observation represented an average of 30 minutes of integration time in all 10 filters, divided approximately equally between object and sky. The time interval between observations of sky and object in the same filter was never greater than

Reproduced with permission of the copyright owner. Further reproduction prohibited without permission.

5 minutes. Sky regions were inspected at the telescope to insure that they were free of visible stars, and on subsequent nights an effort was made to vary the sky region used for comparison in an attempt to obtain a sky subtraction that was statistically representative of the region. For a galaxy of average surface brightness, the ratio of galaxy signal to sky background was approximately 0.75 in the ultraviolet and 2 to 4 in the red. Except for the brightest galaxies, total integration times were two to four times longer in the blue region than in the red in order to equalize approximately the mean errors in all filters.

The magnitudes have been reduced to an absolute energy system through observations of standard stars published by Oke (1964) and Hayes (1970) and corrected to the revised calibration of α Lyr determined by Oke and Schild (1970). A magnitude on this system represents the mean incident energy in magnitudes per unit frequency over the passband of the filter, weighted by the total response function of the observing system. The methods employed in reducing the magnitudes to an absolute energy resembled those described by Wood (1969) (see also Chapter 1). Colors are formed on this system relative to filter 55.

Table 3 presents the average colors measured for all galaxies and globular clusters, together with the internal mean error in magnitudes associated with each color; n repre-

Reproduced with permission of the copyright owner. Further reproduction prohibited without permission.

Reproduced with permission of the copyright owner. Further reproduction prohibited without permission.

TABLE 3

ORIGINAL COLORS OF ELLIPTICAL GALAXIES AND GLOBULAR CLUSTERS

Name	Aperture Size A	Number of Observations	Filter Set	(35-55)	(38-55)	(41-55)	(42-55)	(45-55)
Galaxies:								
NGC 584	39".3[1]	4	1500 km/sec	$2^m.391$	$2^m.099$	$1^m.206$	$1^m.076$	$^m.608$
				.014	.010	.014	.018	.009
596	55.0	4	1500	2.291	1.963	1.104	1.027	.586
				.034	.021	.022	.014	.006
1332	47.1	6	0	2.560	2.229	1.324	1.190	.675
				.008	.006	.002	.010	.006
1889	15.5	6	1500	2.328	1.911	1.150	1.028	.604
				.017	.020	.024	.020	.024
2300	55.0	5	1500	2.675	2.318	1.411	1.233	.710
				.008	.017	.016	.008	.015
2634	31.4	5	1500	2.335	2.034	1.172	1.064	.589
				.018	.019	.005	.013	.009
2672	39.3	5	1500	2.526	2.112	1.225	1.150	.672
				.015	.022	.013	.012	.014
2872	31.4	3	1500	2.498	2.202	1.271	1.161	.637
				.012	.025	.048	.035	.017
3073	19.9	5	0	1.657	1.220	.552	.472	.305
				.021	.034	.024	.026	.014
3193	55.0	4	1500	2.319	2.028	1.159	1.061	.587
				.016	.003	.008	.010	.007
3226	55.0	4	1500	2.333	1.920	1.154	1.037	.605
				.022	.010	.018	.009	.010
3379	62.4	4	0	2.429	2.140	1.233	1.118	.619
				.012	.014	.014	.013	.009
3605	46.2	6	0	2.177	1.856	1.024	.977	.518
				.030	.036	.009	.021	.023
3608	62.9	4	0	2.342	2.030	1.141	1.071	.608
				.010	.012	.006	.008	.011
3613	54.6	5	1500	2.337	2.038	1.143	1.040	.558
				.006	.010	.006	.014	.010

Reproduced with permission of the copyright owner. Further reproduction prohibited without permission.

TABLE 3 continued

ORIGINAL COLORS OF ELLIPTICAL GALAXIES AND GLOBULAR CLUSTERS

Name	Aperture Size A	Number of Observations	Filter Set	(35-55)	(38-55)	(41-55)	(42-55)	(45-55)
				m	m	m	m	m
4261	66".6	4	1500 km/sec	2.460	2.205	1.277	1.132	.609
				.007	.010	.010	.004	.013
4278	62.4	4	0	2.411	2.039	1.212	1.126	.624
				.014	.009	.010	.012	.011
4283	39.9	7	0	2.337	2.016	1.156	1.087	.610
				.020	.018	.011	.009	.020
4464	27.0	7	0	2.295	2.013	1.158	1.085	.618
				.009	.016	.004	.006	.006
4472	65.3	4	0	2.524	2.213	1.290	1.167	.633
				.013	.007	.008	.001	.002
4478	15.2[1]	3	1500	2.339	2.031	1.144	1.063	.589
				.012	.005	.025	.005	.021
4486	65.6	3	1500	2.487	2.208	1.304	1.141	.615
				.021	.007	.016	.004	.010
4486B	13.7	5	0	2.502	2.197	1.265	1.140	.625
				.021	.026	.017	.016	.017
4627	54.6	6	1500	1.687	1.142	.516	.495	.307
				.016	.007	.027	.018	.018
4649	61.7	3	1500	2.559	2.275	1.320	1.149	.613
				.008	.026	.015	.010	.013
5846	55.0	3	1500	2.616	2.306	1.334	1.184	.663
				.011	.014	.009	.006	.001
5846A	15.2	4	1500	2.484	2.129	1.236	1.141	.638
				.022	.023	.021	.023	.016
5982	58.0	12	1500	2.339	2.033	1.165	1.045	.585
				.007	.010	.005	.004	.006
6307	39.4	4	1500	2.313	1.993	1.135	1.056	.611
				.007	.030	.006	.019	.024
7619	55.0	4	1500	2.627	2.231	1.344	1.230	.676
				.025	.011	.016	.021	.013
7626	55.0	3	1500	2.611	2.162	1.283	1.177	.656
				.032	.054	.010	.021	.013

Reproduced with permission of the copyright owner. Further reproduction prohibited without permission.

TABLE 3 continued

ORIGINAL COLORS OF ELLIPTICAL GALAXIES AND GLOBULAR CLUSTERS

Name	(52-55)	(62-55)	(67-55)	(74-55)	Name	(52-55)	(62-55)	(67-55)	(74-55)
Galaxies:									
NGC 584	m .349	m -.228	m -.401	m -.648	4261	m .359	m -.216	m -.406	m -.657
	.012	.005	.003	.009		.005	.006	.010	.015
596	.308	-.203	-.384	-.603	4278	.346	-.239	-.430	-.702
	.009	.020	.010	.014		.006	.005	.006	.003
1332	.351	-.233	-.428	-.680	4283	.282	-.195	-.402	-.655
	.009	.008	.006	.008		.012	.016	.008	.016
1889	.278	-.275	-.421	-.647	4464	.295	-.189	-.371	-.612
	.009	.018	.015	.018		.004	.003	.005	.011
2300	.391	-.280	-.474	-.773	4472	.360	-.228	-.416	-.687
	.012	.013	.009	.010		.006	.011	.015	.017
2634	.323	-.186	-.399	-.625	4478	.344	-.207	-.391	-.630
	.010	.013	.008	.005		.016	.026	.008	.003
2672	.309	-.266	-.432	-.654	4486	.405	-.212	-.427	-.692
	.005	.012	.012	.009		.013	.007	.002	.005
2872	.339	-.221	-.417	-.665	4486B	.358	-.218	-.404	-.648
	.018	.023	.015	.021		.006	.012	.001	.021
3073	.119	-.181	-.322	-.428	4627	.143			
	.014	.020	.015	.027		.010			
3193	.331	-.277	-.391	-.641	4649	.378	-.246	-.436	-.706
	.008	.011	.004	.006		.009	.014	.013	.003
3226	.311	-.234	-.424	-.674	5846	.406	-.232	-.436	-.712
	.014	.015	.015	.019		.005	.007	.008	.005
3379	.329	-.249	-.410	-.681	5846A	.356	-.244	-.431	-.676
	.017	.020	.008	.013		.018	.010	.009	.011
3605	.249	-.215	-.358	-.587	5982	.293			
	.022	.014	.024	.041		.014			
3608	.290	-.230	-.393	-.642	6307	.268	-.240	-.400	-.596
	.010	.012	.008	.017		.016	.017	.013	.011
3613	.307	-.225	-.394	-.612	7619	.333	-.306	-.470	-.700
	.010	.006	.009	.587		.005	.024	.007	.005
					7626	.319	-.274	-.469	-.701
						.017	.019	.017	.004

Reproduced with permission of the copyright owner. Further reproduction prohibited without permission.

TABLE 3 continued

ORIGINAL COLORS OF ELLIPTICAL GALAXIES AND GLOBULAR CLUSTERS

Name	Aperture Size A	Number of Observations	Filter Set	(35-55)	(38-55)	(41-55)	(42-55)	(45-55)
Clusters:								
NGC 5024	63".0	2	0	m 1.626	m 1.166	m .653	m .619	m .415
				.027	.026	.010	.004	.001
5272	63.0	3	0.	1.689	1.239	.684	.658	.430
				.010	.015	.010	.010	.005
5904	63.0	4	0	1.745	1.289	.720	.691	.441
				.021	.013	.008	.012	.010
6205	63.0	4	0	1.671	1.240	.695	.666	.439
				.020	.016	.013	.017	.011
6254	63.0	3	0	2.105	1.629	1.012	.965	.653
				.006	.010	.025	.030	.019
6341	63.0	5	0	1.583	1.095	.610	.577	.401
				.013	.005	.007	.010	.010
6356	63.0	4	0	2.636	2.266	1.386	1.298	.839
				.023	.010	.012	.015	.027
6779	63.0	5	0	2.079	1.469	.906	.857	.601
				.033	.016	.017	.016	.019
7078	63.0	3	0	1.665	1.156	.670	.629	.427
				.024	.022	.022	.022	.019
7089	63.0	3	0	1.674	1.211	.706	.662	.447
				.006	.006	.005	.029	.025

Reproduced with permission of the copyright owner. Further reproduction prohibited without permission.

TABLE 3 continued

ORIGINAL COLORS OF ELLIPTICAL GALAXIES AND GLOBULAR CLUSTERS

Name	(5.2-5.5)	(6.2-5.5)	(6.7-5.5)	(7.4-5.5)
Clusters:	m	m	m	m
NGC 5024	.135	-.181	-.285	-.411
	.019	.012	.007	.004
5272	.167	-.196	-.293	-.422
	.007	.008	.015	.004
5904	.190	-.200	-.317	-.448
	.007	.013	.011	.012
6205	.164	-.198	-.300	-.427
	.003	.007	.012	.013
6254	.275	-.264	-.481	-.698
	.006	.016	.021	.024
6341	.135	-.197	-.286	-.412
	.004	.012	.003	.002
6356	.397	-.275	-.538	-.836
	.013	.014	.006	.011
6779	.215	-.277	-.428	-.618
	.011	.007	.006	.009
7078	.123	-.211	-.319	-.461
	.014	.014	.015	.015
7089	.178	-.182	-.306	-.437
	.016	.012	.000	.006

Notes to Table 3:

1. Small diaphragm because of nearby star.

sents the number of separate observations made, and "filter set" refers to the zero-point velocity (in km/sec) of the filter set used for the observation. Thus, 1500 in this column indicates that the filter set redshifted by 1500 km/sec was used for the measurement, and 0 denotes the use of the unredshifted set.

IV. CORRECTIONS TO OBSERVED COLORS

Before the colors in Table 3 can be analyzed further, corrections for the effects of redshift and reddening should be made. The fact that a redshift z decreases the effective bandwidth of a filter by $1/(1+z)$ affects all magnitudes equally. Hence colors remain unchanged. Likewise, overall changes in the apparent bolometric luminosity of the source due to redshift (Hoyle 1962) do not alter the colors. Therefore, it is necessary to correct only for the shift of a different region of the spectrum into the passband of the system. Published scans of elliptical galaxies (Oke and Sandage 1968; Schild and Oke 1971; Whitford 1971) indicate that for filter 55, effects of redshift up to 4000 km/sec are negligible. For filters 67 and 74, the corrections depend on the fine structure in the scans, which differs somewhat in the three sources listed. In any case, the corrections are less than 0.01 magnitude for most galaxies and were ignored. For filter

Reproduced with permission of the copyright owner. Further reproduction prohibited without permission.

35, corrections were impossible to compute since the published scans do not extend to sufficiently short wavelengths, and the differences between the scans in different papers are considerable. If the continuum declines no more steeply shortward than longward of 3375 Å, where the published data stop, then the data of Oke and Sandage predict an upper limit of 0.02 magnitude to the redshift correction in the (35-55) index. Whitford's scan yields a correction of 0.04 magnitude. Because these numbers are small and because all but six of the galaxies observed have redshifts of less than 2500 km/sec, no corrections were applied to the (35-55) index.

The effects of redshift on the remaining six colors, each of which can be measured through either an unredshifted or redshifted filter, were estimated in two ways. Oke standard stars were used to calibrate both the shifted and unshifted sets of filters. Hence, magnitudes on both sets are measures of the mean energy per unit frequency in the galaxy continuum at both the zero-velocity and the red-shifted wavelengths. Four galaxies with velocities near 1500 km/sec, NGC 584, 4486, 4649, and 5846, were measured through both sets of filters, and the colors were compared. The average observed differences in the six colors appear in Table 4. The differences describe the errors incurred by measuring a galaxy with a redshift 1500 km/sec larger than the velocity of the filter set.

Reproduced with permission of the copyright owner. Further reproduction prohibited without permission.

TABLE 4

PHOTOMETRIC ERRORS CAUSED BY REDSHIFT WHEN $(V_g - V_f) = 1500$ km/sec

Photometric Index	Error Observed	Predicted
	m m	m
(36-55)	-.024 ± .005	-.040
(41-55)	+.007 ± .010	-.007
(42-55)	+.035 ± .008	+.020
(45-55)	+.035 ± .006	+.030
(52-55)	-.035 ± .007	-.040
(62-55)	-.007 ± .008	-.010

Reproduced with permission of the copyright owner. Further reproduction prohibited without permission.

Table 4 also includes the expected errors, estimated from published galaxy scans. The errors computed in the two different ways agree closely.

The observed errors were used to correct the galaxy colors in Table 3 under the assumption that the correction required is a linear function of $(v_g - v_f)$, where v_g is the galaxy velocity and v_f is the zero-point velocity of the filter set, either 0 or 1500 km/sec. Color corrections for galaxies with velocities greater than 3000 km/sec represent extrapolations past the measured point and are consequently somewhat more uncertain. There are only four such galaxies in Table 3, however. The globular cluster data were not corrected for redshift effects.

A cosecant law for galactic reddening was assumed in order to correct the galaxy colors for the effect of absorption and reddening occurring in the Milky Way. The corrections were of the form $K_{(x-55)} \csc b$, where b is the galactic latitude of the object. A coefficient of 0.05 magnitude in E_{B-V} for reddening at the galactic pole was adopted as suggested by de Vaucouleurs and Malik (1969) for use with bright galaxies. The consequences of assuming a different value for the reddening are discussed below. Comparison of stellar colors in B-V and in (45-55) indicates that a change of 0.05 magnitude in B-V corresponds to a change of 0.038 magnitude in (45-55). The effect in the other colors was derived from the

Reproduced with permission of the copyright owner. Further reproduction prohibited without permission.

Whitford (1958) reddening curve. The coefficients $K_{(x-55)}$ for all colors, corresponding to a reddening excess of 0.05 magnitude in B-V, are shown in Table 5. The galaxy colors corrected for both redshift and reddening are presented in Table 8. Colors in Table 8 will be denoted $(x-55)_o$ to distinguish them from the uncorrected data in Table 3.

Since color-magnitude diagrams have been published for all of the globular clusters listed in Table 3, reddening estimates exist for all of them. The values of E_{B-V} assumed in order to correct the colors for reddening, together with the sources of E_{B-V}, are shown in Table 6. Table 8 also contains corrected colors for the clusters. Since the reddening for NGC 6356 seemed quite uncertain, corrected colors are presented for two extreme values, E_{B-V} equal to 0.30 and 0.50 magnitude.

Table 7 presents the rms error of observation in each color computed from the internal mean errors for all the galaxies and globular clusters in Table 3. Mean errors for clusters and galaxies are similar. Figure 1 displays energy distributions representative of the elliptical galaxies and clusters measured in this study.

In order to make use of data already published on the DDO and Wood systems, it is important to establish that the set of filters used here actually does reproduce stellar

Reproduced with permission of the copyright owner. Further reproduction prohibited without permission.

TABLE 5

ASSUMED REDDENING AT THE GALACTIC POLE

$K_{(35-55)}$	$K_{(38-55)}$	$K_{(41-55)}$	$K_{(42-55)}$	$K_{(45-55)}$	$K_{(52-55)}$	K_{55}	$K_{(62-55)}$	$K_{(67-55)}$	$K_{(74-55)}$
$+^{m}.080$	$+^{m}.061$	$+^{m}.050$	$+^{m}.048$	$+^{m}.038$	$+^{m}.013$	$+^{m}.150$	$-^{m}.017$	$-^{m}.028$	$-^{m}.039$

Reproduced with permission of the copyright owner. Further reproduction prohibited without permission.

TABLE 6

REDDENING OF GLOBULAR CLUSTERS

Cluster	$E_{(B-V)}$	Source
NGC 5024	m .05	Hartwick (1968)
5272	.00	Sandage (1969), McClure and Racine (1969)
5904	.01	Arp (1962)
6205	.015	Sandage (1969), McClure and Racine (1969)
6254	.26	Sandage (1969)
6341	.02	Hartwick (1968)
6356	.50 .38	Sandage and Wallerstein (1960), Hartwick (1968)
6779	.27	Hartwick (1968)
7078	.12	Sandage (1969)
7089	.08	Hartwick (1968)

Reproduced with permission of the copyright owner. Further reproduction prohibited without permission.

TABLE 7

INTERNAL MEAN ERRORS OF GALAXY AND CLUSTER OBSERVATIONS

Index	Error	Index	Error
	m		m
(35-55)	.018	(74-55)	.014
(38-55)	.021	$(LB)_o$	.025
(41-55)	.017	$(CN)_o$	.016
(42-55)	.017	$(G)_o$	.016
(45-55)	.014	$(Mg)_o$	.013
(52-55)	.012	$(TiO)_o$	.016
(62-55)	.015	$(CN+Mg)_o$	.020
(67-55)	.011		

Reproduced with permission of the copyright owner. Further reproduction prohibited without permission.

Reproduced with permission of the copyright owner. Further reproduction prohibited without permission.

TABLE 8

GALAXY COLORS CORRECTED FOR REDDENING AND REDSHIFT AND CLUSTER COLORS CORRECTED FOR REDDENING

Name	A/D_o	$(35-55)_o$	$(38-55)_o$	$(41-55)_o$	$(42-55)_o$	$(45-55)_o$	$(52-55)_o$	$(62-55)_o$	$(67-55)_o$	$(74-55)_o$
		m	m	m	m	m	m	m	m	m
NGC 205	.13[1]	1.66	1.26	.63	.60	.37	.23	-.15	-.28	-.51
221	.21[1]	2.17	1.95	1.08	1.02	.53	.31	-.19	-.33	-.49
224	[2]	2.52	2.32	1.34	1.16	.60	.37	-.20	-.37	-.58
584	.31	2.304	2.037	1.149	1.015	.558	.341	-.207	-.370	-.605
596	.49	2.204	1.904	1.046	.961	.531	.305	-.181	-.353	-.560
1332	.27	2.459	2.177	1.253	1.098	.589	.371	-.203	-.392	-.631
1889	.57	2.131	1.776	1.022	.885	.486	.269	-.228	-.352	-.551
2300	.69	2.504	2.195	1.301	1.118	.617	.374	-.240	-.414	-.689
2634	.63	2.191	1.935	1.078	.961	.504	.315	-.151	-.348	-.555
2672	.53	2.386	2.048	1.124	1.002	.541	.349	-.222	-.383	-.586
2872	.47	2.373	2.130	1.185	1.050	.542	.352	-.187	-.373	-.604
3073	.34	1.550	1.157	.479	.380	.226	.128	-.152	-.284	-.376
3193	.57	2.221	1.950	1.097	1.005	.543	.311	-.206	-.356	-.593
3226	.59	2.236	1.843	1.092	.982	.562	.291	-.213	-.390	-.626
3379	.42	2.334	2.082	1.168	1.040	.553	.332	-.223	-.376	-.635
3605	.79	2.090	1.800	.965	.907	.459	.250	-.192	-.327	-.544
3608	.74	2.255	1.983	1.080	.989	.537	.303	-.205	-.362	-.599
3613	.46	2.240	1.972	1.079	.969	.499	.303	-.201	-.360	-.564
4261	.50	2.313	2.149	1.218	1.062	.550	.360	-.193	-.375	-.614
4278	.54	2.330	1.987	1.158	1.062	.570	.346	-.218	-.401	-.662
4283	.76	2.256	1.971	1.099	1.012	.545	.293	-.171	-.373	-.615
4464	.51	2.209	1.967	1.098	1.005	.549	.308	-.164	-.341	-.570
4472	.23	2.438	2.162	1.231	1.091	.568	.368	-.204	-.386	-.645
4478	.21	2.255	1.966	1.091	1.013	.549	.329	-.189	-.361	-.589
4486	.29	2.404	2.140	1.253	1.096	.580	.385	-.195	-.398	-.651
4486B	1.14	2.419	2.132	1.213	1.090	.585	.343	-.200	-.375	-.607
4627	.46	1.606	1.090	.462	.431	.253	.143	-.079	-.187	-.226
4649	.30	2.475	2.207	1.268	1.104	.578	.358	-.229	-.406	-.665
5846	.44	2.507	2.227	1.264	1.112	.604	.394	-.207	-.398	-.659
5846A	1.01	2.376	2.058	1.164	1.057	.567	.356	-.217	-.393	-.623
5982	.79	2.227	1.969	1.088	.946	.500	.305	-.171	-.330	-.505

Reproduced with permission of the copyright owner. Further reproduction prohibited without permission.

TABLE 8 continued

GALAXY COLORS CORRECTED FOR REDDENING AND REDSHIFT AND CLUSTER COLORS CORRECTED FOR REDDENING

	Name	A/D_o	$(35-55)_o$	$(38-55)_o$	$(41-55)_o$	$(42-55)_o$	$(45-55)_o$	$(52-55)_o$	$(62-55)_o$	$(67-55)_o$	$(74-55)_o$
NGC	6307	.55	$2^m.173$	$1^m.914$	$1^m.038$	$^m.930$	$^m.502$	$^m.286$	$-^m.201$	$-^m.351$	$-^m.528$
	7619	.78	2.519	2.184	1.264	1.112	.571	.367	-.272	-.432	-.647
	7626	.83	2.503	2.108	1.206	1.068	.560	.344	-.242	-.431	-.648
	5024		1.545	1.105	.603	.570	.375	.121	-.164	-.257	-.371
	5272		1.688	1.239	.684	.658	.430	.167	-.196	-.293	-.422
	5904		1.728	1.276	.709	.681	.433	.187	-.196	-.311	-.440
	6205		1.646	1.221	.679	.651	.427	.160	-.192	-.291	-.415
	6254		1.688	1.311	.751	.715	.455	.207	-.175	-.335	-.494
	6341		1.550	1.070	.589	.557	.385	.129	-.190	-.274	-.396
	6356[3]		1.835	1.655	.886	.817	.459	.267	-.105	-.258	-.446
	6356[4]		2.155	1.899	1.086	1.009	.611	.319	-.173	-.370	-.602
	6779		1.647	1.139	.636	.597	.395	.144	-.185	-.276	-.407
	7078		1.473	1.009	.550	.513	.335	.091	-.170	-.251	-.367
	7089		1.546	1.113	.626	.585	.386	.157	-.154	-.261	-.374

Reproduced with permission of the copyright owner. Further reproduction prohibited without permission.

TABLE 8 continued

GALAXY COLORS CORRECTED FOR REDDENING AND REDSHIFT AND CLUSTER COLORS CORRECTED FOR REDDENING

	Name	$(LB)_o$	$(CN)_o$	$(G)_o$	$(Mg)_o$	$(TiO)_o$	Name	$(LB)_o$	$(CN)_o$	$(G)_o$	$(Mg)_o$	$(TiO)_o$
		m	m	m	m	m		m	m	m	m	m
NGC	205	-.10	.03	.23	-.09	-.01	4649	-.326	.164	.526	-.142	-.008
	221	-.31	.06	.49	-.11	.00	5846	-.332	.152	.508	-.169	-.025
	224	-.38	.18	.56	-.15	-.01	5846A	-.278	.107	.490	-.144	-.012
	584	-.301	.134	.457	-.133	-.009	5982	-.302	.142	.446	-.119	-.022
	596	-.270	.085	.430	-.107	-.025	6307	-.299	.108	.428	-.099	-.004
	1332	-.311	.155	.509	-.151	-.026	7619	-.282	.152	.541	-.154	.020
	1889	-.191	.137	.399	-.088	.022	7626	-.243	.138	.508	-.135	-.010
	2300	-.283	.183	.501	-.144	-.002						
	2634	-.291	.117	.457	-.127	-.052						
	2672	-.283	.122	.461	-.147	-.002	5024	-.023	.032	.195	.019	.013
	2872	-.341	.135	.508	-.150	-.031	5272	-.044	.026	.228	-.006	.024
	3073	-.134	.099	.154	-.044	-.014	5904	-.049	.028	.248	-.025	.014
	3193	-.282	.092	.462	-.108	-.002	6205	-.051	.028	.224	-.001	.022
	3226	-.170	.110	.420	-.081	-.015	6254	-.084	.036	.260	-.037	-.021
	3379	-.322	.128	.487	-.126	.003	6341	-.007	.032	.172	.015	.030
	3605	-.263	.058	.448	-.079	.001	6356[3]	-.287	.068	.359	-.095	-.046
	3608	-.306	.091	.452	-.103	-.006	6356[4]	-.270	.077	.398	-.093	-.045
	3613	-.303	.110	.470	-.117	-.009	6779	.009	.038	.202	.003	.024
	4261	-.344	.156	.512	-.155	-.026	7078	.009	.036	.178	.034	.023
	4278	-.234	.096	.492	-.133	-.016	7089	-.021	.040	.199	-.013	.001
	4283	-.284	.087	.467	-.090	-.047						
	4464	-.305	.093	.456	-.103	-.035						
	4472	-.318	.140	.523	-.156	-.021						
	4478	-.284	.078	.464	-.124	-.022						
	4486	-.302	.157	.516	-.169	-.037						
	4486B	-.306	.123	.505	-.125	-.019						
	4627	-.047	.031	.178	-.049	-.030						

Notes to Table 8:

1. Assuming mean diaphragm size of 46". A = 40" (McClure and van den Bergh 1968a), 51" (Wood 1966).
2. A = 17" (McClure and van den Bergh 1968a), 18" (Wood).
3. $E_{(B-V)} = 0.50$.
4. $E_{(B-V)} = 0.30$

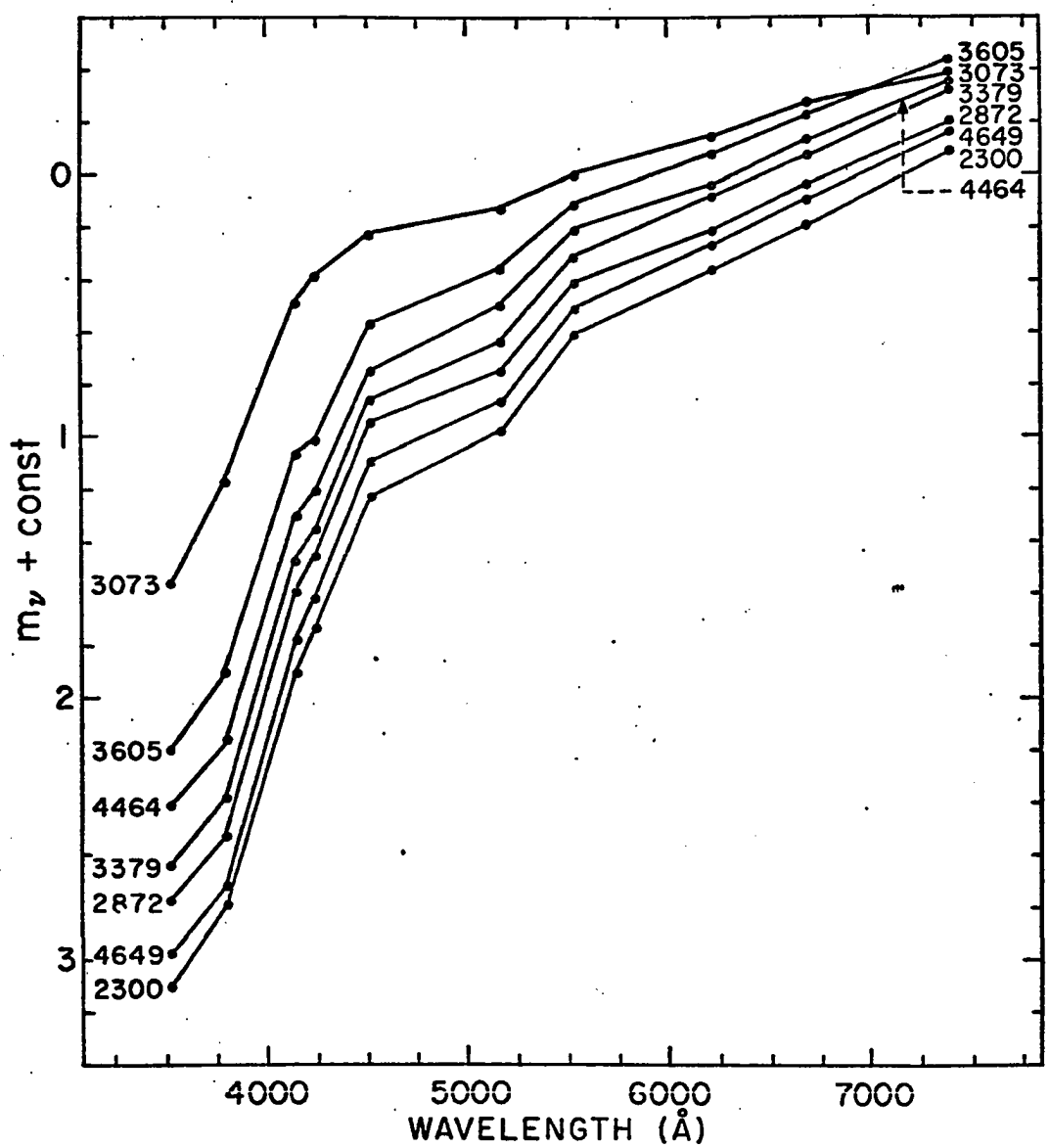

Fig. 1. Colors, approximately corrected for reddening, for a selection of elliptical galaxies observed in this study.

Reproduced with permission of the copyright owner. Further reproduction prohibited without permission.

and galaxy colors measured on these two systems. Transformations of stellar colors between the absolute energy system used in this paper and those of McClure and van den Bergh and Wood are quite accurate for stars bluer than +1.30 in B-V. These transformations are presented and discussed in another paper (Chapter 1). The colors for nine galaxies measured in common with McClure and van den Bergh (1968a) are consistent with the stellar transformations within the quoted mean errors, with the exception of filter 35 for NGC 5846. In the present investigation, the magnitude found in filter 35 for NGC 5846 is fainter by 0.20 magnitude than the value given by McClure and van den Bergh. The intensities at the other wavelengths in the spectrum of NGC 5846 are more in accord with the redder value given in this paper. None of the galaxies in Table 3 were observed by Wood, but the small errors in the stellar transformations to the Wood system for stars bluer than +1.30 in B-V suggest that the transformations for galaxies are quite accurate.

M 31 and its two companions, M 32 and NGC 205, form a group that meets all the criteria for group membership discussed above, and colors for all three on both the DDO and Wood systems have been published. Accordingly, colors were first transformed to the photometric system in this paper by means of the transformation equations derived from the stellar

Reproduced with permission of the copyright owner. Further reproduction prohibited without permission.

data, and were then corrected for reddening and redshift. The transformed colors for all three galaxies are less accurate than those for objects in Table 3 and have estimated mean errors of 0.05 magnitude in the blue and 0.10 magnitude in the red, where Wood's errors are large. In all plots, these objects are represented by crosses in order to distinguish them from the galaxies in Table 3.

In view of the large differences in widths and effective wavelengths between the 10-color filters and the UBV filters, the correlation between the present photometry and that on the UBV system should not be particularly close. Comparisons between the two systems are shown in Figures 2-4. In Figure 2, C_o from the RCBG, corrected for aperture effects, redshift, and galactic reddening, is plotted versus $(45-55)_o$. C_o for NGC 3605 was taken from Webb (1964), the RCBG value being of low weight and quite discrepant. Values of B-V given by van den Bergh (1967) and corrected in accordance with the color excesses in Table 6 have been used to locate globular clusters (triangles) in the diagram. Also shown is the relation between B-V and (45-55) for stellar data. The line does not represent the galaxy relation because the galaxy intensity distributions do not turn down as quickly at 4000 Å as do those of stars with comparable (45-55) indices.

Reproduced with permission of the copyright owner. Further reproduction prohibited without permission.

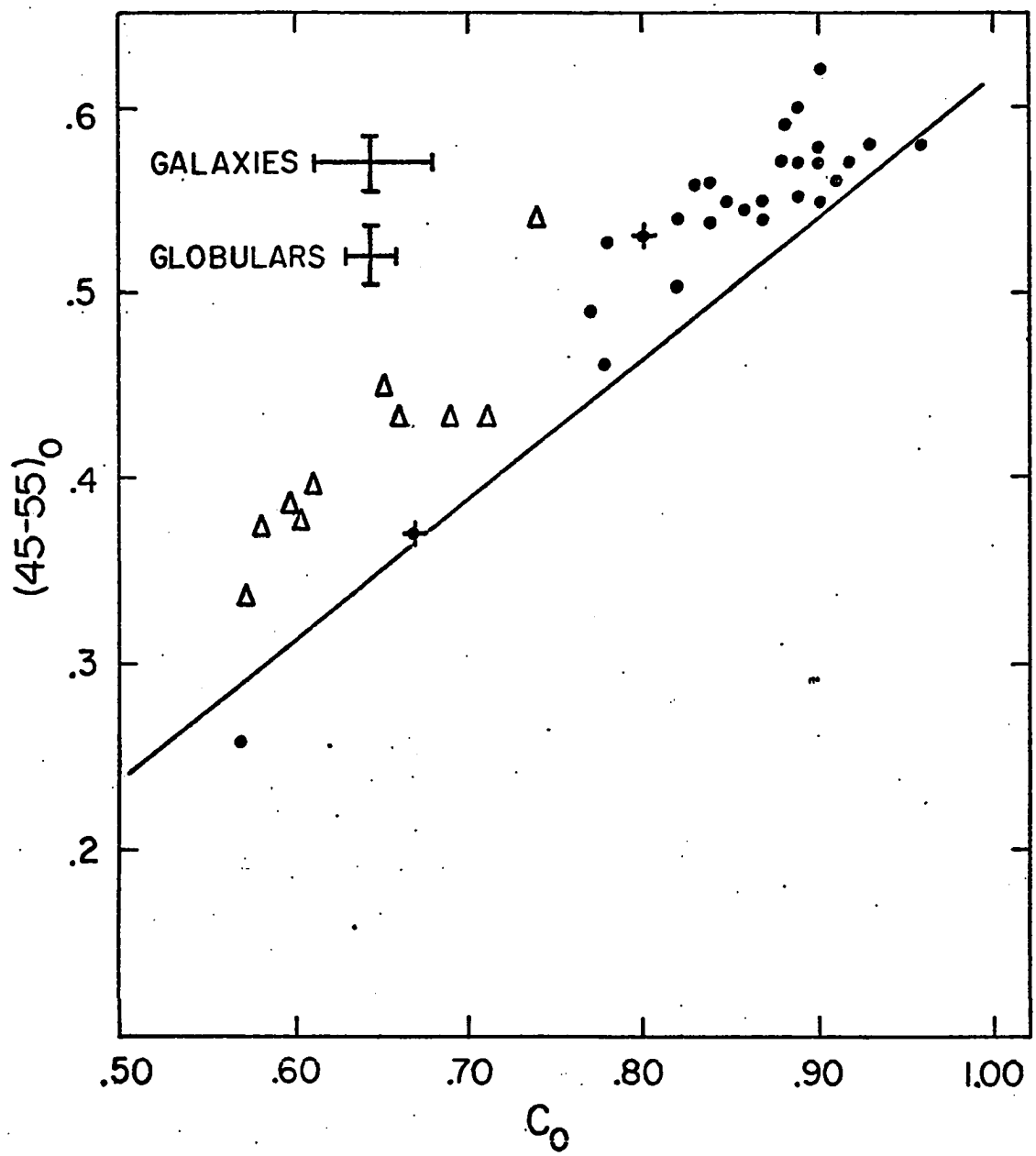

Fig. 2. Comparison between C_o, from the RCBG, and $(45-55)_o$ for elliptical galaxies (circles) and globular clusters (triangles). The solid line represents the transformation between B-V and $(45-55)_o$ determined from stellar observations. Crosses represent M 32 and NGC 205.

Reproduced with permission of the copyright owner. Further reproduction prohibited without permission.

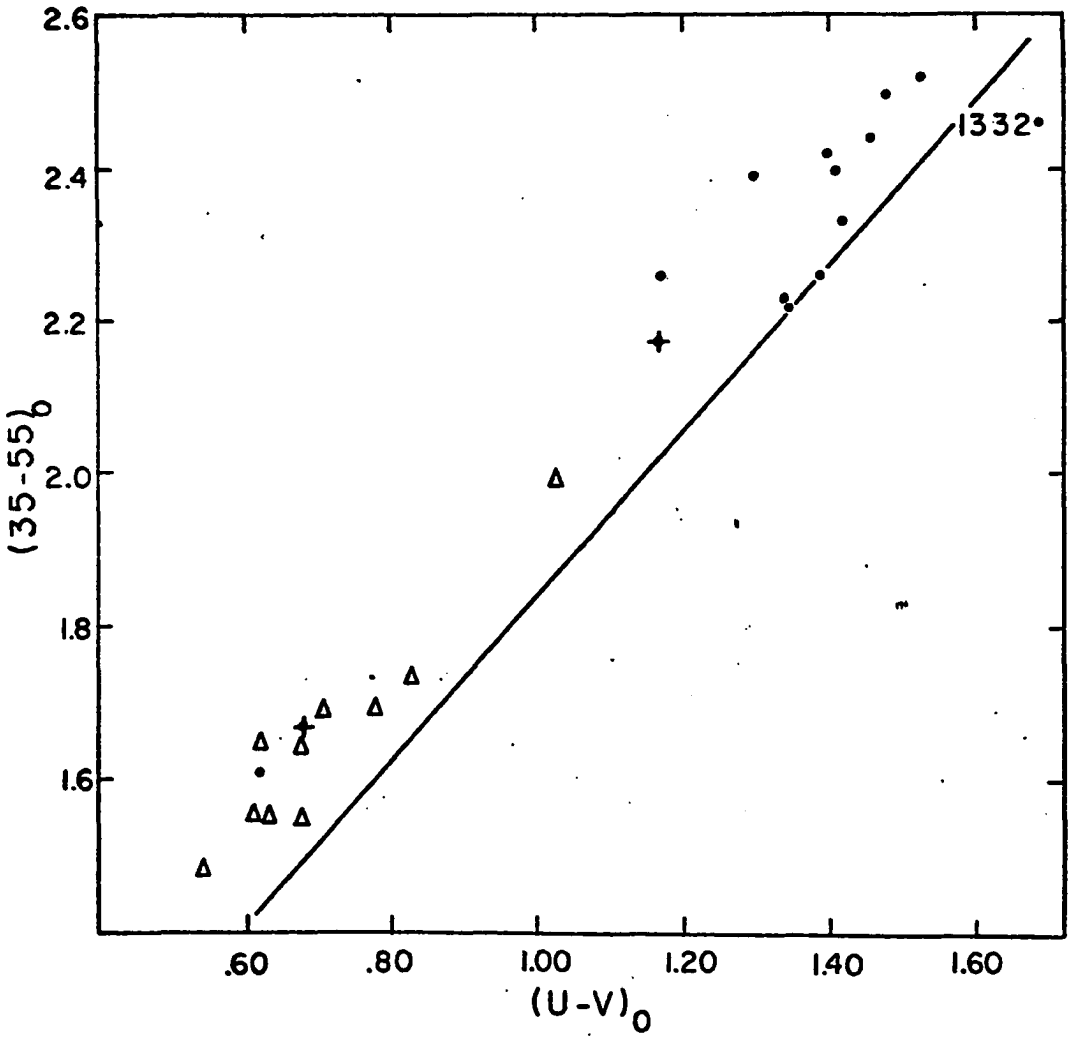

Fig. 3. Same as Figure 2 for $(U-V)_o$ versus $(35-55)_o$.

Reproduced with permission of the copyright owner. Further reproduction prohibited without permission.

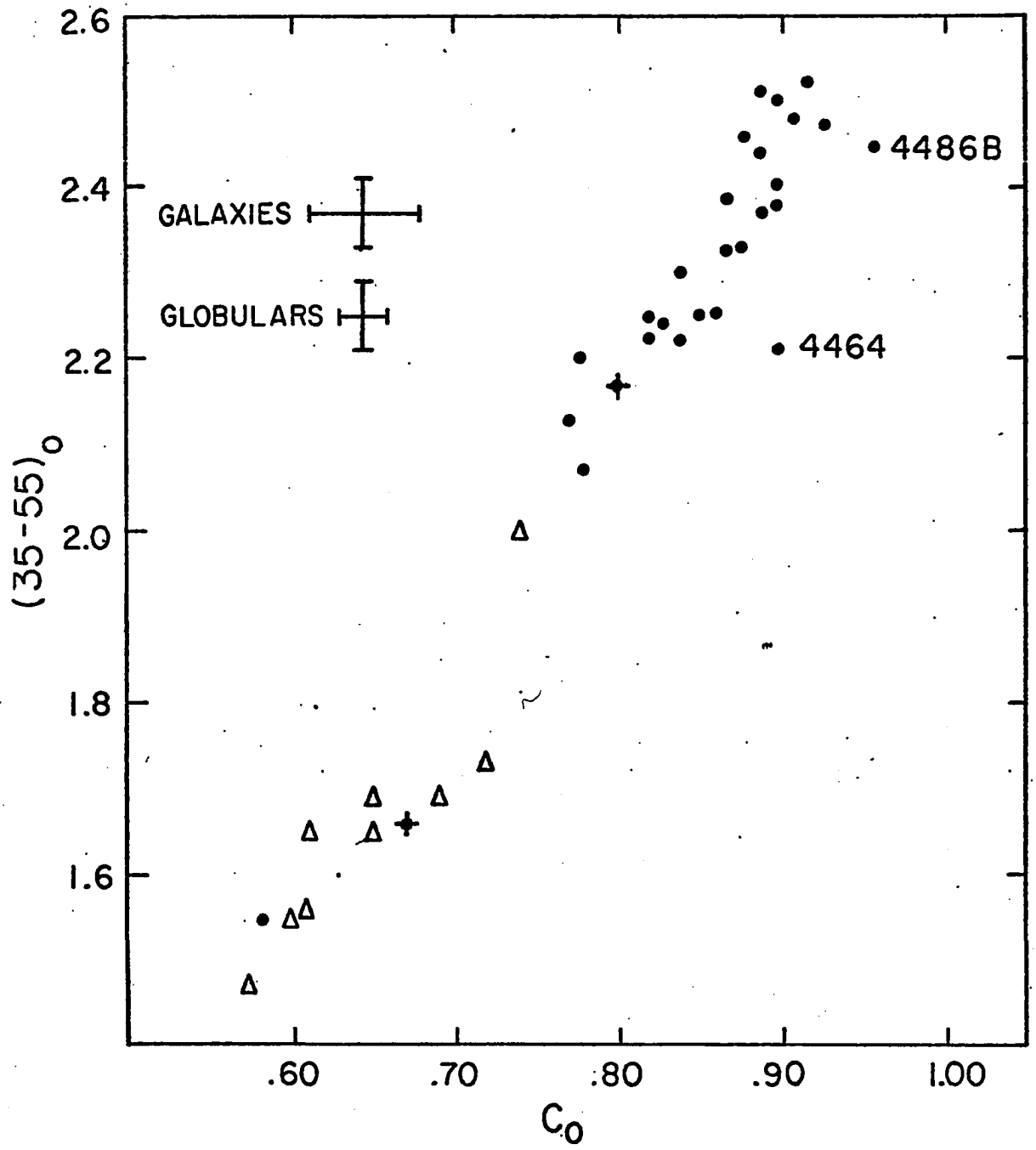

Fig. 4. $(35\text{-}55)_o$ versus C_o. The symbols have the same meanings as in Figures 2 and 3.

Reproduced with permission of the copyright owner. Further reproduction prohibited without permission.

Since the effective wavelengths of filter 35 and the U filter do not differ widely, we might expect the transformation between the colors U-V and (35-55) to be better defined. Figure 3 shows that this is indeed the case. $(U-V)_o$ from the RCBG, found from the sum of $(B-V)_o$ and $(U-B)_o$, both corrected only for galactic absorption and aperture effect, is plotted versus $(35-55)_o$, corrected for absorption only. U-B for globular clusters was again taken from van den Bergh (1967). The only discrepant point is NGC 1332, observed by Hodge (1963). The measure is of low weight, and Hodge has suggested that it might be in error. Since the other eight color indices appearing in Table 8 for NGC 1332 are inconsistent with an extremely large value of $(U-V)_o$, the discrepancy is due to an error in the measured $(U-V)_o$.

Figure 4 compares C_o with $(35-55)_o$. The graph demonstrates that changes in $(35-55)_o$ do indeed correspond to changes in the integrated B-V color of the objects observed, even though the measures generally were made with aperture sizes smaller than D_o.

V. COLOR-COLOR AND COLOR-MAGNITUDE DIAGRAMS

With the 10 magnitudes available for each galaxy on the present color system one can form five photometric indices that are useful indicators of the strengths of absorption

Reproduced with permission of the copyright owner. Further reproduction prohibited without permission.

due to CN, the G band, Mg "b" plus MgH, TiO, and metallic-line blanketing near 3800 Å (denoted by $(LB)_o$). Following McClure and van den Bergh (1968a), we have taken the CN index as (41-42) and G as (42-45). The other three indices correspond to the difference between the magnitude measured in the absorption feature and the magnitude computed by interpolating the magnitude measured at neighboring "continuum" points. Figure 5 describes the geometry of the procedure. The indices are therefore as follows:

$$(CN)_o = (41-42)_o$$

$$(G)_o = (42-45)_o$$

$$(LB)_o = (35-55)_o + 0.492[(41-55)_o-(35-55)_o]-(38-55)_o$$

$$(Mg)_o = 0.373(45-55)_o-(52-55)_o$$

$$(TiO)_o = 0.584(67-55)_o-(62-55)_o$$

The values of these indices for all objects are given in Table 8, and Table 7 presents the mean error of observation associated with each index. $(CN)_o$ and $(G)_o$ increase with increasing line absorption, while the other three indices decrease.

Figure 6 presents values of the line indices along with the three continuum colors $(45-55)_o$, $(67-55)_o$, and $(74-55)_o$, plotted against $(35-55)_o$. (Globulars are again represented by triangles.) NGC 6356 has been plotted twice in accordance with the two values of the reddening excess used to correct the colors. Hence the line connecting the two points for NGC 6356

Reproduced with permission of the copyright owner. Further reproduction prohibited without permission.

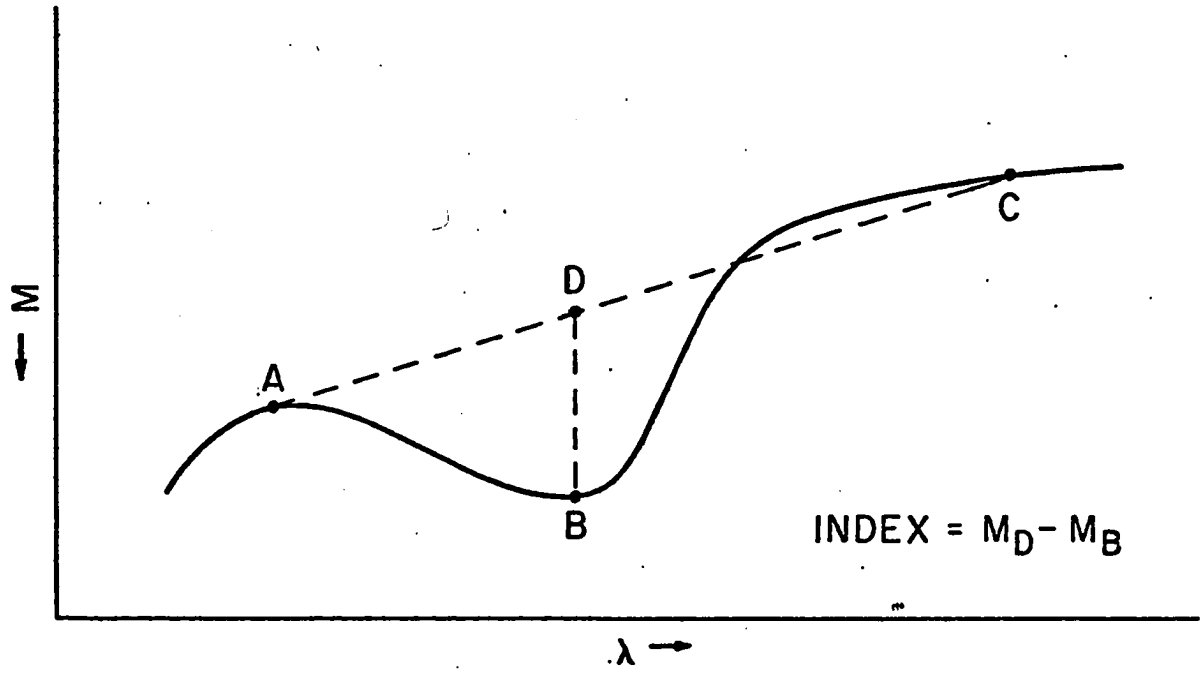

Fig. 5. An idealized section of a galaxy spectrum showing a broad absorption feature. The indices $(LB)_o$, $(Mg)_o$, and $(TiO)_o$ (defined in the text) correspond to the difference in magnitudes between points D and B.

Reproduced with permission of the copyright owner. Further reproduction prohibited without permission.

Reproduced with permission of the copyright owner. Further reproduction prohibited without permission.

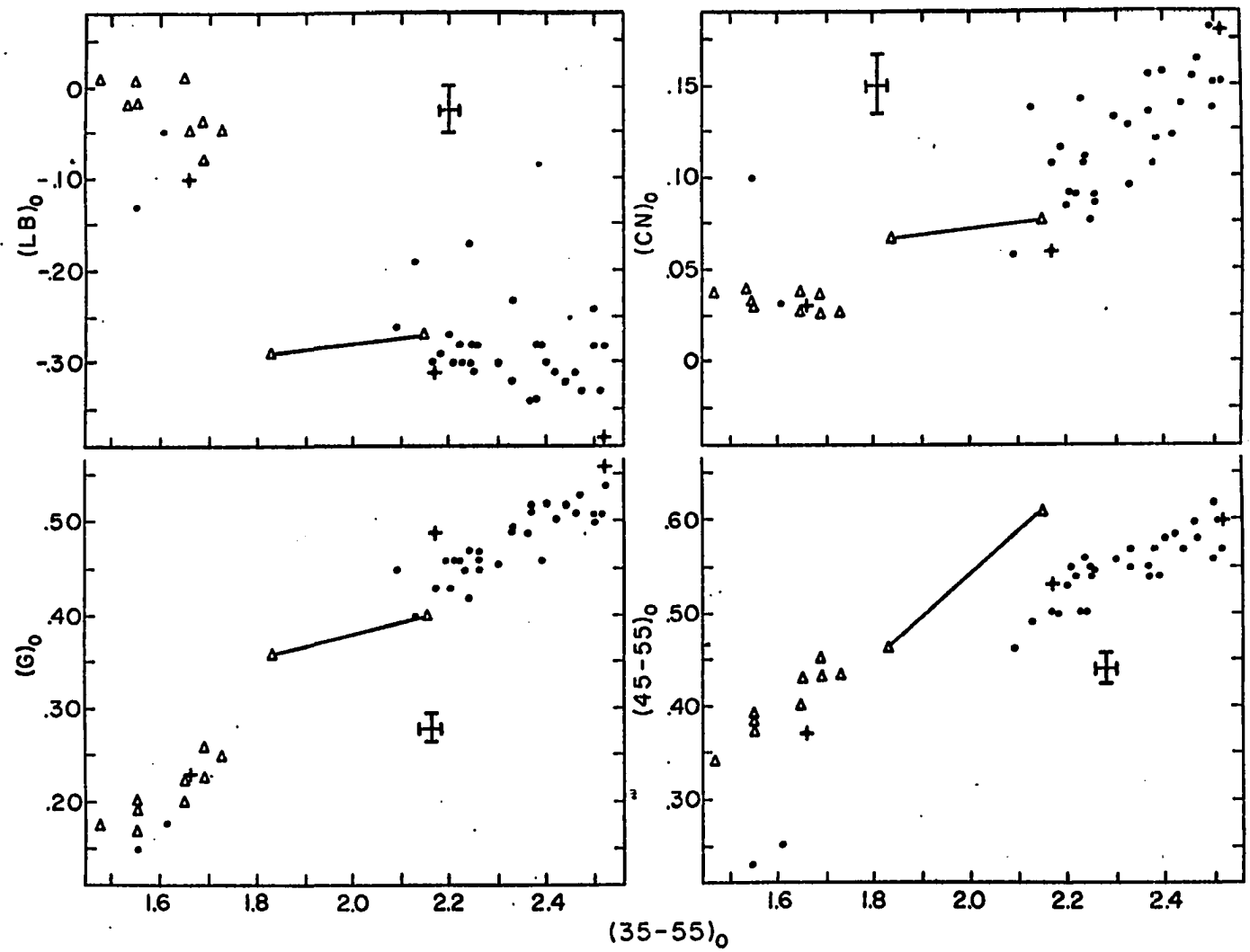

Fig. 6. Line indices and continuum colors plotted against $(35\text{-}55)_o$ for elliptical galaxies (circles) and globular clusters (triangles). Crosses represent M 31, M 32, and NGC 205. NGC 6356 is plotted twice according to the two values assumed for the reddening excess, E_{B-V} =0.30 and 0.50 magnitude.

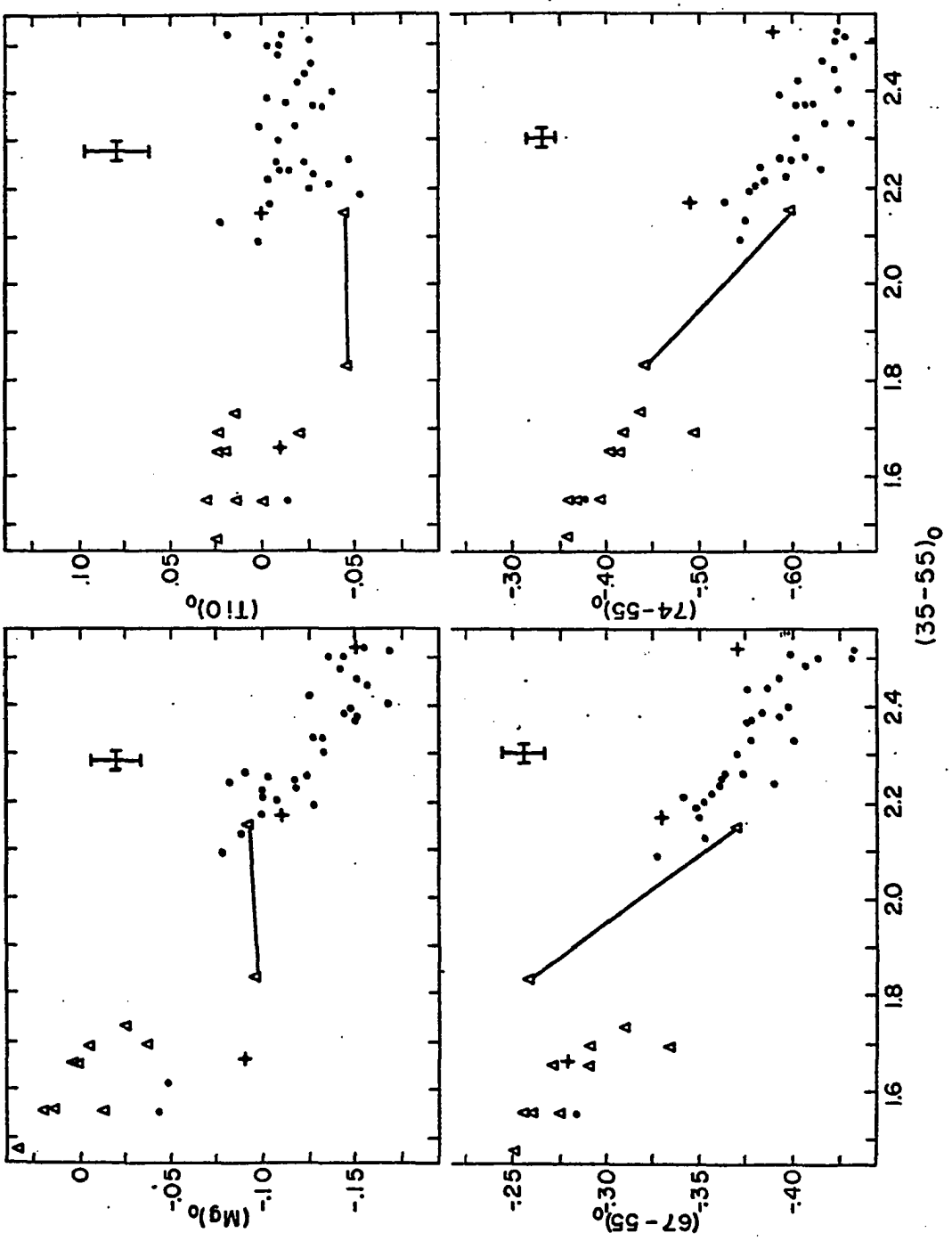

Fig. 6 (continued).

Reproduced with permission of the copyright owner. Further reproduction prohibited without permission.

represents a reddening vector with length 0.20 magnitude in E_{B-V}. The figure demonstrates that the colors of elliptical galaxies redder than $(35-55)_o = 2.1$ are definitely not all alike. The variations in continuum color are real and closely correlated with line strengths. Indeed, the line strengths increase monotonically with increasing continuum color.

Figure 7a presents a color-magnitude diagram for these elliptical galaxies. The ordinate is $(35-55)_o$. The absolute visual magnitude, M_v, was determined from the apparent magnitude, m_v, in the RCBG and corrected for galactic absorption. An absorption of 0.15 magnitude in V at the galactic pole was assumed. Mean group radial velocities, together with a Hubble constant equal to 95 km/sec/Mpc (van den Bergh 1970), yielded the distance moduli. van den Bergh (1960) has suggested that the pair of galaxies NGC 4627, 4631 are members of the Canes Venatici cluster. If so, the distance modulus should be calculated with the mean velocity of the cluster, 437 km/sec, rather than the mean velocity of the immediate pair members, 715 km/sec. Since these two velocities differ considerably, NCG 4627 is plotted twice according to the two resultant values of the distance. This is the only case for which the mean velocity of the immediate subgroup and the velocity of the larger cluster differ significantly. The absolute magnitudes of NGC 205 and M 32 correspond to a distance modu-

Reproduced with permission of the copyright owner. Further reproduction prohibited without permission.

Reproduced with permission of the copyright owner. Further reproduction prohibited without permission.

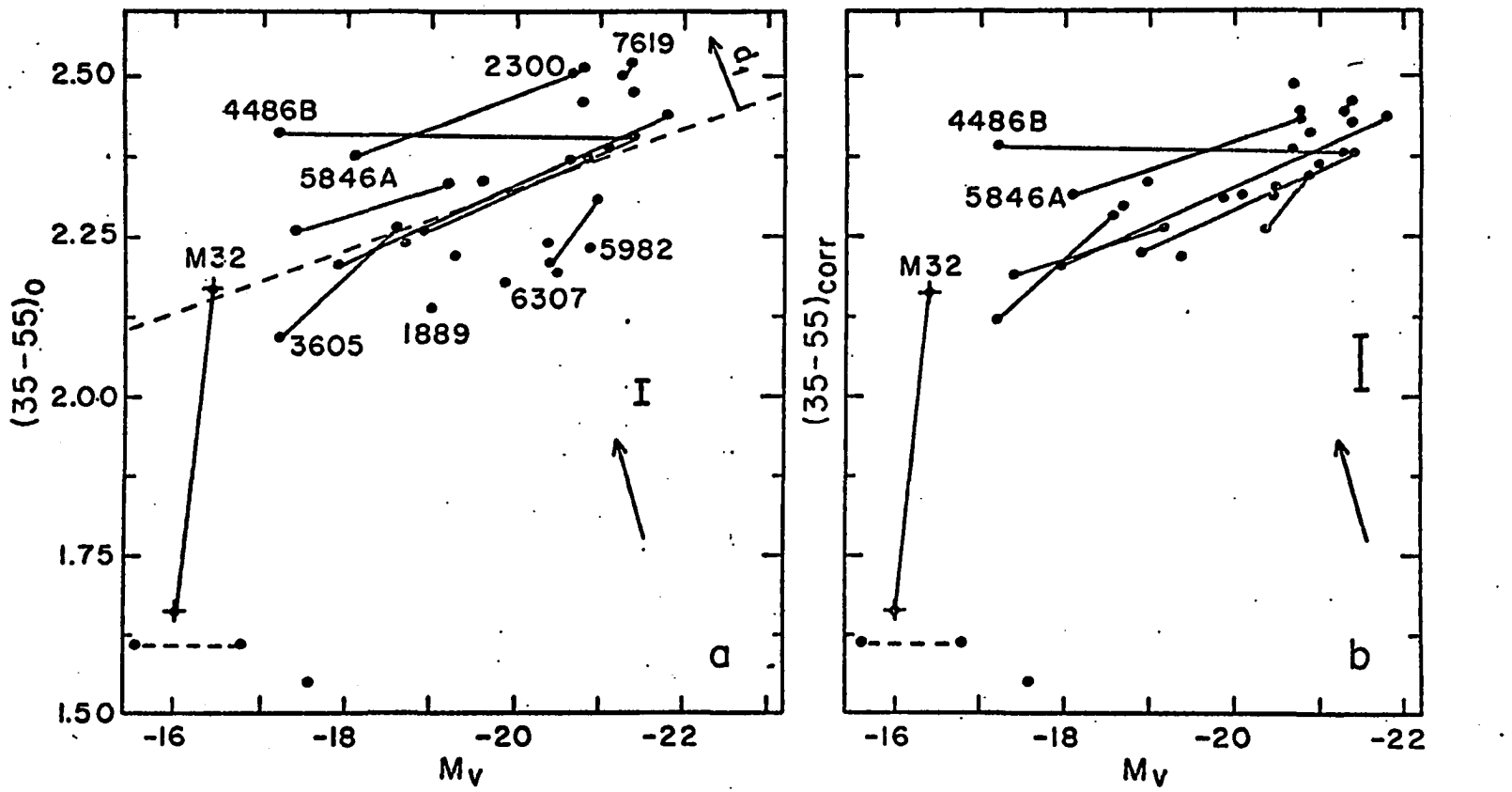

Fig. 7a. Color-magnitude diagram for elliptical galaxies. The ordinates are values of $(35-55)_o$ from Table 8. Straight lines connect members of the same pair. The long dashed line represents the linear least-squares relation for the upper group of points. NGC 4627 has been plotted twice (points connected by dashed line) according to two different values of the distance modulus (see text). Crosses represent M 32 and NGC 205. The arrow is a reddening vector of length 0.10 in E_{B-V}.

Fig. 7b. Same as Figure 7a except $(35-55)_{corr}$, corrected for residual reddening errors, is used as ordinate.

lus of 24.50 (van den Bergh 1970). With the exception of the latter two galaxies a change in the Hubble constant does not affect the relative spacing of the remaining points in the diagram. Table 11 contains the adopted values of the group recessional velocities and M_V for each elliptical galaxy.

Figure 7a shows a rapid decline in the $(35-55)_o$ index between -16 and -17 in absolute magnitude. In this regard, the diagram resembles that of Baum (1959). However, beyond the point $M_V = -17$, the color index continues to increase as a function of absolute magnitude. Although substantiated by the data as a whole, this trend is most clearly delineated by the slopes of lines joining members of the same pair. The slopes are unaffected by errors in the galactic reddening corrections and by errors in M_V caused by scatter about the redshift distance relation. For the purpose of determining the slope in Figure 7a, it is legitimate to consider the objects in large clusters as pairs, and they have been grouped as follows: NGC 4464 with NGC 4472, NGC 4478 and 4486B with NGC 4486, and NGC 7619 with NGC 7626. NGC 4486B stands out as clearly abnormal, being too red for its absolute magnitude. It is discussed further below.

Reproduced with permission of the copyright owner. Further reproduction prohibited without permission.

VI. ANALYSIS INTO PRINCIPAL COMPONENTS: GALAXIES

Although these diagrams indicate that colors and absolute magnitudes of elliptical galaxies are highly correlated, the scatter in many of these plots exceeds the scatter to be expected from observational errors alone. Therefore, some physical parameter (or parameters) in addition to absolute magnitude may be required in order to specify precisely the colors and line strengths of an elliptical galaxy. Principal component analysis is a statistical technique that can explore this question in a systematic way. Deeming (1964) has used it to classify 5-color photometry for late-type giant stars, and Martin and Bingham (1970) have applied it to Wood's 12-color measures on galaxies. The reader is referred to these papers and to Kendall and Stuart's (1966) Advanced Theory of Statistics for a fundamental discussion of the method. A qualitative description is given here.

A 10-color photometric system provides 9 independent color indices for each object observed. Each object can be represented as a point in a 9-dimensional space. We wish to find the number of dimensions in the subspace occupied by the elliptical galaxies in Table 8. The number of dimensions in this subspace equals the number of independent parameters necessary to specify exactly the colors of a given elliptical galaxy. For example, if the ellipticals in Table 8 actually

Reproduced with permission of the copyright owner. Further reproduction prohibited without permission.

lie along a line in this 9-dimensional space, each elliptical galaxy can be uniquely and completely described by specifying its position along that line. If the galaxies lie in a plane, two linearly independent parameters corresponding to the two dimensions of the plane will be necessary, and so on.

Because of observational errors alone, the galaxies in Table 8 actually fill a 9-dimensional volume. But the width of the space in certain directions may be due purely to observational scatter, in which case this variation would not signify the need for an additional independent descriptive parameter. In other words, in order to be useful, a method that yields the number of dimensions in the subspace should also indicate whether the width in certain directions has statistical significance, given the observational errors in the original quantities. We also require expressions for the linearly independent parameters needed to specify uniquely the position of an object in the space. In the case of the elliptical galaxies, for example, the discussion above suggests that at least one of these parameters might be related to the absolute magnitude.

The method of principal component analysis meets all these requirements, provided that the correlations among the original variables are linear. Generally the original

Reproduced with permission of the copyright owner. Further reproduction prohibited without permission.

variables are transformed to ones having zero mean and unit variance. After this transformation, the subspace spanned by the points representing the objects is centered on the origin of the coordinate system and has unit variance in all directions parallel to the axes of the coordinate system. In general, it is possible to choose a vector attached to the origin along which the variance of the distribution of points is a maximum. Let n be the number of dimensions in the original space, and let $\underset{\sim}{x}_j$ be the vector representing object j in this n-dimensional space. If $\underset{\sim}{y}_1$ is a unit vector along which the variance is maximized, let K_{1j} be the scalar parameter associated with $\underset{\sim}{y}_1$. This parameter K_{1j} is just the projected distance of a point from the origin along the vector $\underset{\sim}{y}_1$. Hence $K_{1j} = \underset{\sim}{y}_1 \cdot \underset{\sim}{x}_j$. Furthermore, the variance λ_1 along the line parallel to $\underset{\sim}{y}_1$ is $\sum_j (\underset{\sim}{y}_1 \cdot \underset{\sim}{x}_j)^2/N$, where N is the total number of objects. Thus $\lambda_1 = \sum_j K_{1j}^2/N$, and λ_1 is the variance associated with the parameter K_{1j}. We then seek the direction orthogonal to $\underset{\sim}{y}_1$ along which the remaining variance is a maximum. Associated with this second vector $\underset{\sim}{y}_2$ would be a second parameter K_{2j} and variance λ_2. In an n-dimensional space, the process would continue until no orthogonal vectors (actually eigenvectors of the correlation matrix of the set of points $\underset{\sim}{x}_j$) were found.

Reproduced with permission of the copyright owner. Further reproduction prohibited without permission.

If the subspace spanned by the points $\underset{\sim}{x}_j$ has fewer dimension than n, say n', after n' orthogonal eigenvectors have been found, all subsequent variances (actually eigenvalues of the correlation matrix of the set of points $\underset{\sim}{x}_j$) will be 0. In this way, the number of dimensions in the subspace is determined. In the case of the elliptical galaxies studied here, the variances will never be exactly 0 because of the scatter due to observational errors. Since λ_i is the variance associated with the parameter K_{ij} and since K_{ij} is a function of the quantities $\underset{\sim}{x}_j$, we can compute the expected variance in K_{ij} due to errors in the original quantities $\underset{\sim}{x}_j$. Let the mean errors associated with each coordinate m be δx_m. If Q_i is the expected variance in K_{ij} due to errors alone, and $v_i = (v_{i1}, v_{i2}, \ldots v_{i3}, \ldots v_{in})$, then

$$Q_i = \sum_m (v_{im})^2 (\delta x_m)^2.$$

If λ_i is much larger than Q_i, the variance along $\underset{\sim}{y}_i$ is much larger than can be explained by errors alone and must have physical significance. According to Deeming (1964) the quantity λ_i/Q_i follows the F distribution with (N-1) degrees of freedom. This fact provides a convenient statistical test that can be applied to λ_i/Q_i in order to estimate the significance of λ_i.

The galaxy and cluster colors in Table 8 were analyzed into principal components in two separate solutions. The

Reproduced with permission of the copyright owner. Further reproduction prohibited without permission.

first of these utilized all the galaxy colors, while the second solution combined colors for both galaxies and clusters. Instead of using the nine independent color indices of the form $(x-55)_o$ as the quantities x_{jm}, the solutions utilized the four continuum color indices plus the five line indices, suitably translated to the origin and normalized to unit variance as described above. These variables were assigned to the coordinate axes as described in Table 9. For example, x_{j3} indicates the $(CN)_o$ index, translated and normalized, for the j^{th} object in Table 8.

Table 10 presents the values of the variances λ_i, the expected variances Q_i, the ratio λ_i/Q_i, and the components of the vectors χ_i for the first solution for galaxies only. The expression for Q_i given above is valid only if the observational errors, δx_m, are uncorrelated. This is not true for the galaxy color indices since in most cases the measurement through a particular filter has been used to form more than one color index. The correlation will cause some of the variances to be artificially large and others to be artificially small. Thus, any parameter K_{ij} with variance only slightly larger than that expected due to random errors must be scrutinized carefully to insure that the excess variance associated with this parameter does not result from correlated errors of observation. In spite of this difficulty, Q_i is still the

Reproduced with permission of the copyright owner. Further reproduction prohibited without permission.

Reproduced with permission of the copyright owner. Further reproduction prohibited without permission.

TABLE 9

ORIGINAL COORDINATES FOR THE ANALYSIS INTO PRINCIPAL COMPONENTS

Coordinate	x_{j1}	x_{j2}	x_{j3}	x_{j4}	x_{j5}	x_{j6}	x_{j7}	x_{j8}	x_{j9}
Index	$(35-55)_o$	$(LB)_o$	$(CN)_o$	$(G)_o$	$(45-55)_o$	$(Mg)_o$	$(TiO)_o$	$(67-55)_o$	$(74-55)_o$

Reproduced with permission of the copyright owner. Further reproduction prohibited without permission.

TABLE 10

ANALYSIS INTO PRINCIPAL COMPONENTS: ALL GALAXIES

i	λ_i	Q_i	λ_i/Q_i	V_{i1}	V_{i2}	V_{i3}	V_{i4}	V_{i5}	V_{i6}	V_{i7}	V_{i8}	V_{i9}
1	6.560	.072	91.1	.383	-.327	.301	.374	.372	-.344	.021	-.361	-.355
2	.515	.146	3.53	-.018	.088	.849	-.231	-.306	-.250	-.023	.058	.237
3	.434	.170	2.55	-.028	.692	.028	-.244	.044	.005	-.280	-.408	-.460
4	.011	.021	.52	-.754	.070	.100	.319	.343	-.082	-.006	-.313	.301
5	.022	.040	.55	.156	-.220	-.113	-.695	.396	-.048	.008	-.362	.373
6	.215	.190	1.13	.008	-.223	.345	.031	.067	.878	-.141	-.162	-.086
7	1.064	1.030	1.03	.009	.200	.064	-.044	-.024	.139	.945	-.174	-.095
8	.060	.049	1.22	-.211	.014	.188	-.257	.585	-.013	.069	.617	-.351
9	.122	.056	2.12	.461	.512	.067	.303	.376	.135	-.032	.177	.484

most useful quantity against which the actual variances can be compared.

The parameters K_{1j}, K_{2j}, K_{3j} for each galaxy appear in Table 11. Tables of percentage points for the F distribution show that λ_1 and λ_2 are significantly greater than Q_1 and Q_2 to the 0.1 per cent confidence level. The significance level for λ_3 is 1 per cent. The remaining variances are not significant.

The mathematical interpretation of the parameters K_{1j} and K_{2j} is straightforward. Because the strength of the absorption lines increases with increasing color index $(35\text{-}55)_o$, the variance λ_1 can be maximized if the continuum colors are added to the line absorption indices, provided that the signs of the latter are properly adjusted. This parameter might be described as the sum of the line absorption indices and the continuum colors. The parameter K_{1j} has just these properties. Inspection of the components of the associated vector χ_1 shows that every term but one in the sum $K_{ij} = \sum_m v_{im}x_{jm}$ increases positively with increasing continuum color $(35\text{-}55)_o$. The exception is the term containing the TiO absorption index, which has a small range in values and a very small coefficient v_{17} compared to the other terms in the expression for K_{ij}. On the other hand, the signs of the components in vector χ_2 are all opposite to those in χ_1, except for the absorption indices

Reproduced with permission of the copyright owner. Further reproduction prohibited without permission.

TABLE 11

INDEPENDENT PARAMETERS: ALL GALAXIES

Name	V	M_V	K_1	K_2	K_3	$\Delta(35-55)_{ap}$
NGC 205		-16.0	-5.27	- .48	1.05	
221		-16.4	- .94	-1.20	-1.52	.00
224			2.48	.93	-1.21	
584	1991 km/sec	-21.0	.76	.25	- .17	.05
596	1991	-20.4	- .77	- .67	.08	.01
1332	1401	-20.8	2.03	.52	.23	.06
1889	2364	-19.0	-1.37	.63	.08	.01
2300	2392	-20.7	2.63	.82	.64	.00
2634	2302[1]	-20.5	- .32	.26	.20	.00
2672	3784	-21.1	.85	.19	- .14	.01
2872	3123	-20.7	1.39	.31	- .32	.01
3073	1240	-17.6	-6.74	1.70	.33	
3193	1229[2]	-19.3	- .25	- .77	- .33	.01
3226	1118	-18.7	- .61	- .52	1.62	.01
3379	676[2]	-19.6	1.07	- .13	- .47	.02
3605	852	-17.2	-1.98	-1.23	- .72	.00
3608	852	-18.6	- .16	- .84	- .38	.00
3613	1872[2]	-20.4	- .14	- .11	- .56	.03
4261	1960	-20.9	1.73	.74	- .35	.01
4278	825[2]	-19.2	.85	- .82	1.08	.01
4283	825[2]	-17.4	- .24	-1.07	.68	.00
4464	1175[3]	-17.9	- .46	- .69	- .20	.01
4472	1175[3]	-21.8	1.94	.23	.05	.00
4478	1175[3]	-18.9	- .09	- .95	.01	.08:
4486	1175[3]	-21.4	2.21	.69	.66	.00
4486B	1175[3]	-17.2	1.14	- .29	- .12	.00
4627	437[4], 715	-16.8	-8.71	.73	- .27	
		-15.6				
4649	1175[3]	-21.4	2.38	.50	.03	.05
5846	1808[2]	-20.8	2.59	.43	.22	.02
5846A	1808[2]	-18.1	1.11	- .42	.30	.00
5982	2872	-20.9	- .48	.89	- .82	.00
6307	3418	-19.9	- .85	- .09	- .76	.01
7619	3803[5]	-21.4	2.48	.34	.05	.00
7626	3803[5]	-21.3	1.73	.09	1.03	.00

Notes to Table 11:

1. Velocity is for N2633.
2. Group velocity as given by van den Bergh, Ap. J., 131, 215, 1960.
3. Mean velocity of Virgo cluster, van den Bergh, Nature, 225, 203, 1970.
4. Mean velocity of Canes Venatici cluster, van den Bergh, Ap. J., 131, 558, 1960.
5. Mean of N 7611, 7617, 7619, 7623, 7626.
6. Assuming (m-M) = 24.50, van den Bergh, Nature, 225, 203, 1970.

Reproduced with permission of the copyright owner. Further reproduction prohibited without permission.

$(CN)_o$ and $(Mg)_o$. Hence, the parameter K_{2j} represents the difference between the two principal line absorption indices and the overall continuum color.

In Figure 8 K_{2j} is plotted versus K_{1j} for all galaxies in Table 8. Aside from the 3 bluest galaxies, NGC 205, 3073, and 4627, the remainder of the points fill a cigar-shaped region in the diagram. In order to distinguish them from the three blue dwarfs, this group of galaxies, with the omission of M 31, will henceforth be referred to as the "redder" group. A few of the points on the outer edge of the cigar have been labeled. Comparison of Figures 7a and 8 shows that points that lie on the outer edges of the distribution in Figure 8 also do so in Figure 7a. To display this correlation graphically, the distance (d_1) of objects from the least-squares line drawn in Figure 7a has been plotted versus their distance from the line drawn in Figure 8 (d_2). The line in Figure 8 was drawn by eye to correspond as closely as possible to the least-squares line in Figure 7a. Figure 9 displays the correlation between d_1 and d_2, both measured in arbitrary units. As noted before, since K_{1j} and K_{2j} are functions of the magnitudes in filters 35 and 55, errors in K_{1j} and K_{2j} will not be independent of errors in $(35-55)_o$, the ordinate in Figure 7a. The relation between d_1 and d_2 may therefore be simply a relation between the observational errors in $(35-55)_o$ and those in

Reproduced with permission of the copyright owner. Further reproduction prohibited without permission.

Reproduced with permission of the copyright owner. Further reproduction prohibited without permission.

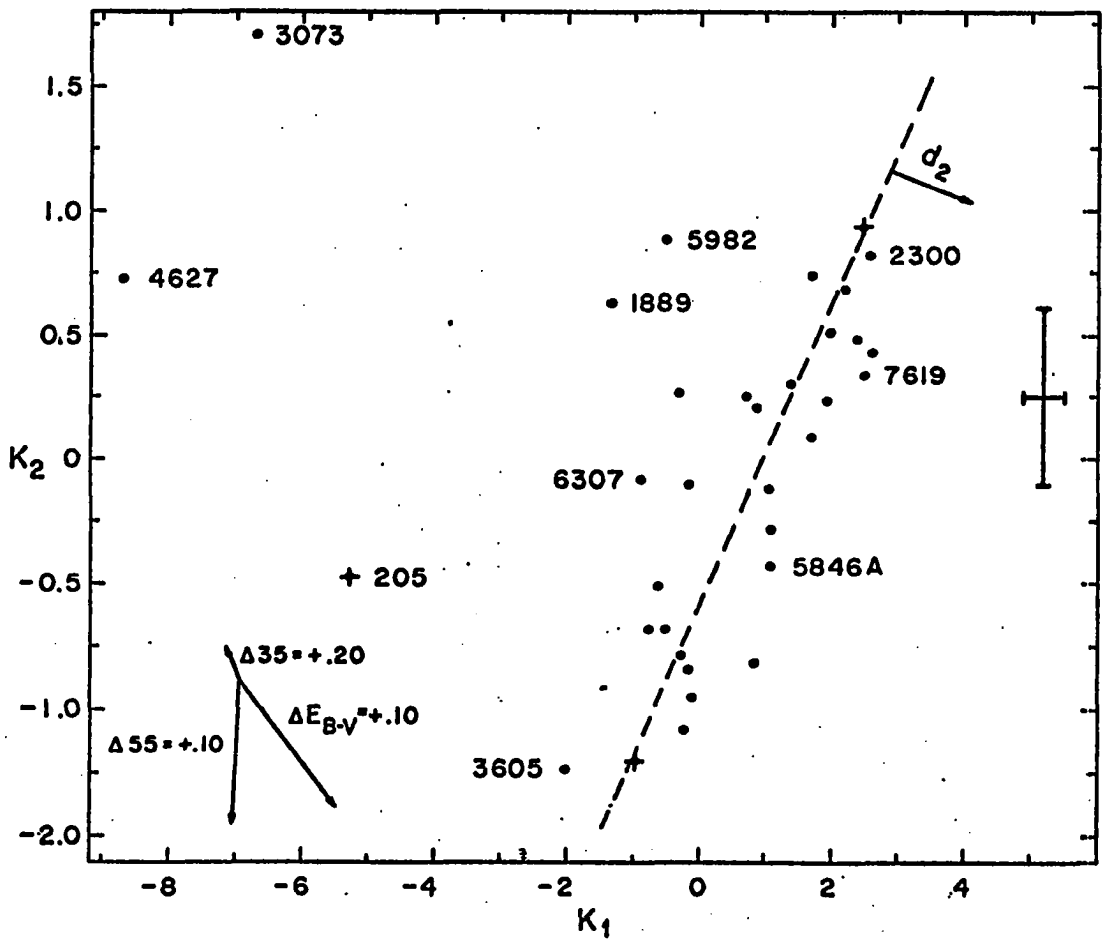

Fig. 8. The independent parameter K_2 plotted against the independent parameter K_1. The dashed line corresponds to the dashed line in Figure 7a. The vectors indicate changes in the positions of the points resulting from changes in the magnitudes through filters 35 and 55 and changes in the assumed reddening. Crosses represent M 31, M 32, and NGC 205.

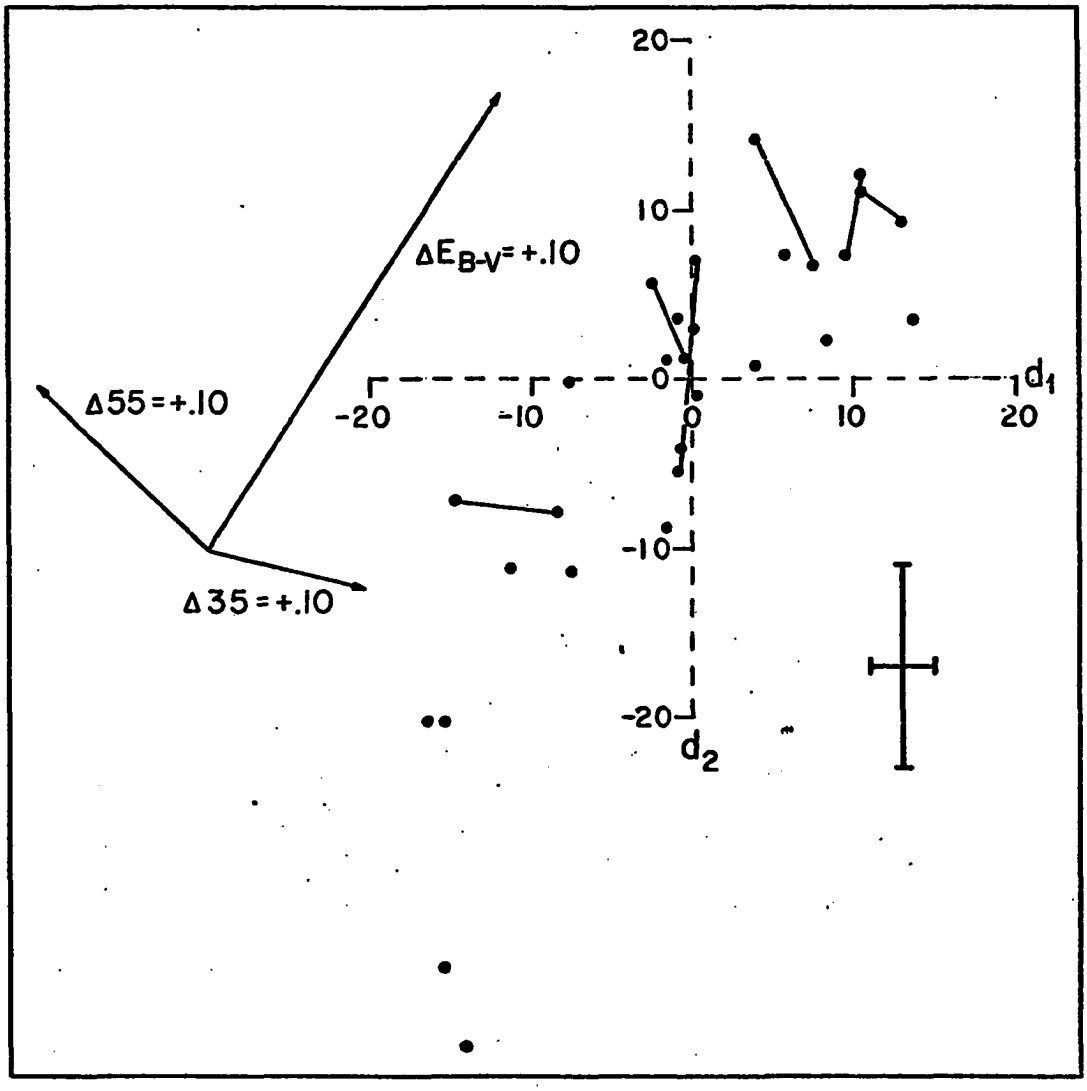

Fig. 9. The distance d_2, shown in Figure 8, versus the distance d_1, shown in Figure 7a. Straight lines connect members of the same pair. The vectors indicate changes in the positions of the points resulting from changes in the magnitudes through filters 35 and 55 and changes in the assumed reddening.

Reproduced with permission of the copyright owner. Further reproduction prohibited without permission.

K_{1j} and K_{2j}. The vectors in Figures 8 and 9 representing the effects on K_{1j}, K_{2j}, d_1, and d_2 of errors in 35 and 55 demonstrate that this is not the case. Moreover, a much more likely explanation is readily available. Errors of less than 0.10 magnitude in the reddening estimates E_{B-V} are sufficient to cause most of the scatter in Figure 9, as can be seen by noting the length and angle of the reddening vector shown in that diagram. Deviations from the mean lines in Figures 7a and 8 are generally parallel to the reddening vectors in those diagrams also.

Further insight into the cause of the scatter in these figures is provided by Figure 10, in which the sum of the $(CN)_o$ and $(Mg)_o$ indices (actually $(CN)_o$-$(Mg)_o$) is plotted versus absolute magnitude for the elliptical galaxies. As before, NGC 4627 is plotted twice. The figure shows that, aside from the points M 32, NGC 4486B, and NGC 5846A, which will be discussed below, the integrated line strength of elliptical galaxies in the $(CN)_o$ and $(Mg)_o$ indices is a monotonically increasing function of absolute magnitude. The scatter in the diagram is no larger than one would expect from observational errors alone, which suggests that the relation might be even closer than shown here. This index is totally unaffected by errors in the reddening correction. Therefore for these elliptical galaxies, $(CN+Mg)_o$ is a reliable indicator of

Reproduced with permission of the copyright owner. Further reproduction prohibited without permission.

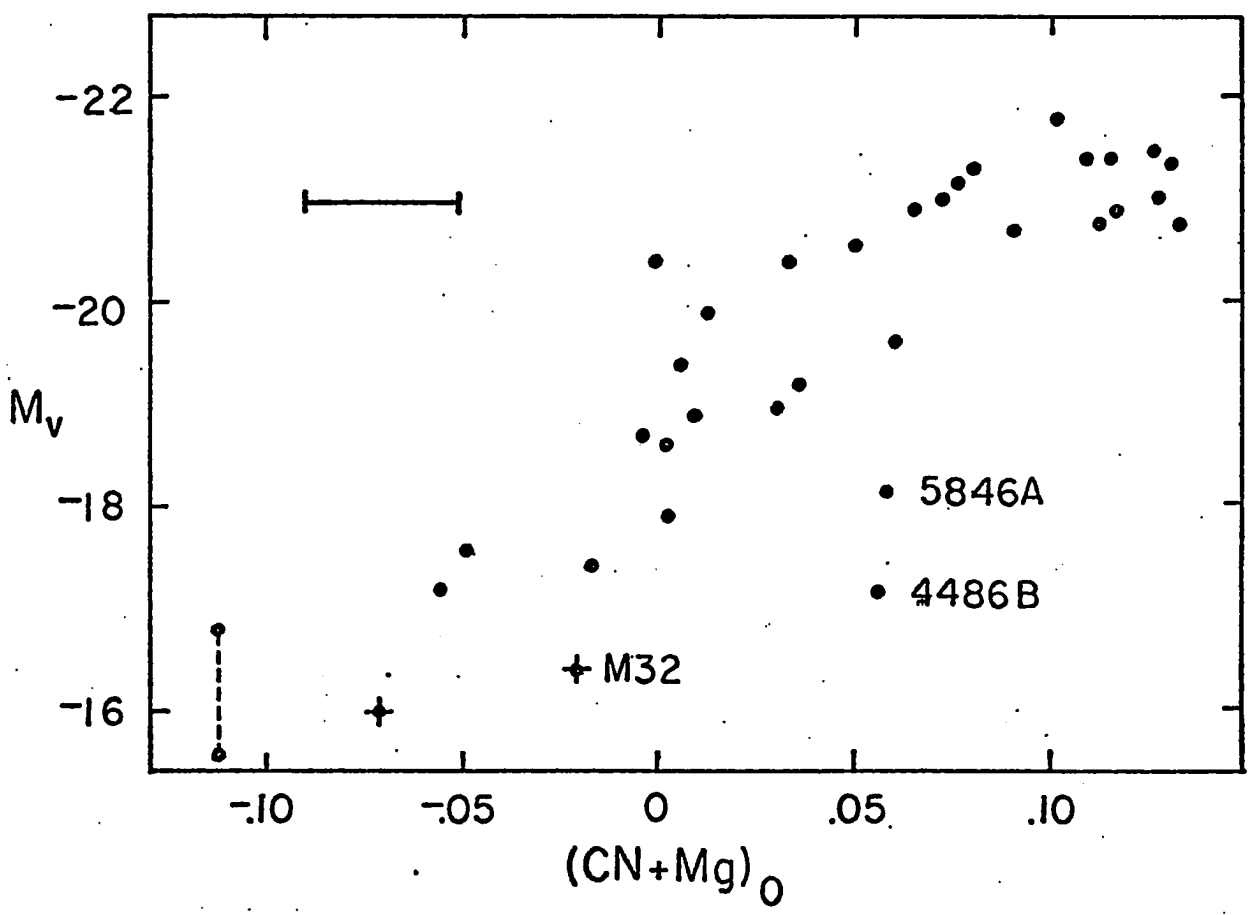

Fig. 10. The line index $(CN+Mg)_o$ versus absolute magnitude, M_V, for elliptical galaxies. NGC 4627 is plotted twice (two points connected by dashed line). The three labeled points are discussed in the text. Crosses represent M 32 and NGC 205.

Reproduced with permission of the copyright owner. Further reproduction prohibited without permission.

absolute magnitude, allowing one to estimate M_V with an error of slightly over 0.5 magnitude. The sense of the correlation is in accord with the suggestion by McClure and van den Bergh (1968a) that CN is weaker in dwarf elliptical galaxies. The increase in line strength with increasing luminosities found here also agrees with their result (McClure and van den Bergh 1968b) that the metallicity index Q increases with luminosity. However, the index $(CN+Mg)_o$ appears to be approximately twice as accurate as Q in predicting M_V.

This result further supports the idea that errors in the reddening correction are the cause of the scatter in Figures 7a and 8. To see this, we note that a galaxy that lies to the left of the line in Figure 8 has continuum colors that are bluer than those of the average galaxy with lines of the same strength. The same galaxy will also lie below the mean line in Figure 7a, since d_1 and d_2 are correlated. It will therefore also be bluer than the average galaxy of the same absolute magnitude. Yet Figure 10 shows that its line strength is closely related to its absolute magnitude. If reddening is rejected as the cause of scatter in Figures 7a and 8, and the deviations in the figures therefore represent features intrinsic to the spectra of these galaxies, we reach the implausible conclusion that the line strengths of elliptical galaxies are very closely correlated with absolute magnitude while continuum colors are much less

Reproduced with permission of the copyright owner. Further reproduction prohibited without permission.

closely correlated. Reddening errors provide a much more attractive explanation, and in the ensuing discussion, reddening will be accepted as the cause of scatter.

Approximate corrections to $(35-55)_o$ for each galaxy can then be derived if the distance of the points from the line drawn in Figure 8 is taken as a measure of the error in reddening associated with each object. In no case, however, should a "dereddening" correction be used that exceeds the original correction applied. The galaxy would then be redder than originally observed. Only two objects, NGC 1889 and 5982, encountered this limit. The colors of the three bluest galaxies of course cannot be treated in this way and have not been altered. Figures 7b and 11 show that, for the redder galaxies, plots of M_V and $(CN+Mg)_o$ versus this corrected index do indeed have considerably less scatter than before.

Thus far, the location of the reddening medium has not been discussed. Calculating the reddening vectors in Figures 7-9 required only the assumption that the absorption with wavelength obeys the Whitford law. If the reddening variations are intrinsic to our galaxy or to entire groups of galaxies, however, the deviations d_1 and d_2 should be similar for members of the same pair. Figure 9 suggests that this is true. In this diagram, pair members, connected by straight lines, tend to lie within similar regions of the sequence.

Reproduced with permission of the copyright owner. Further reproduction prohibited without permission.

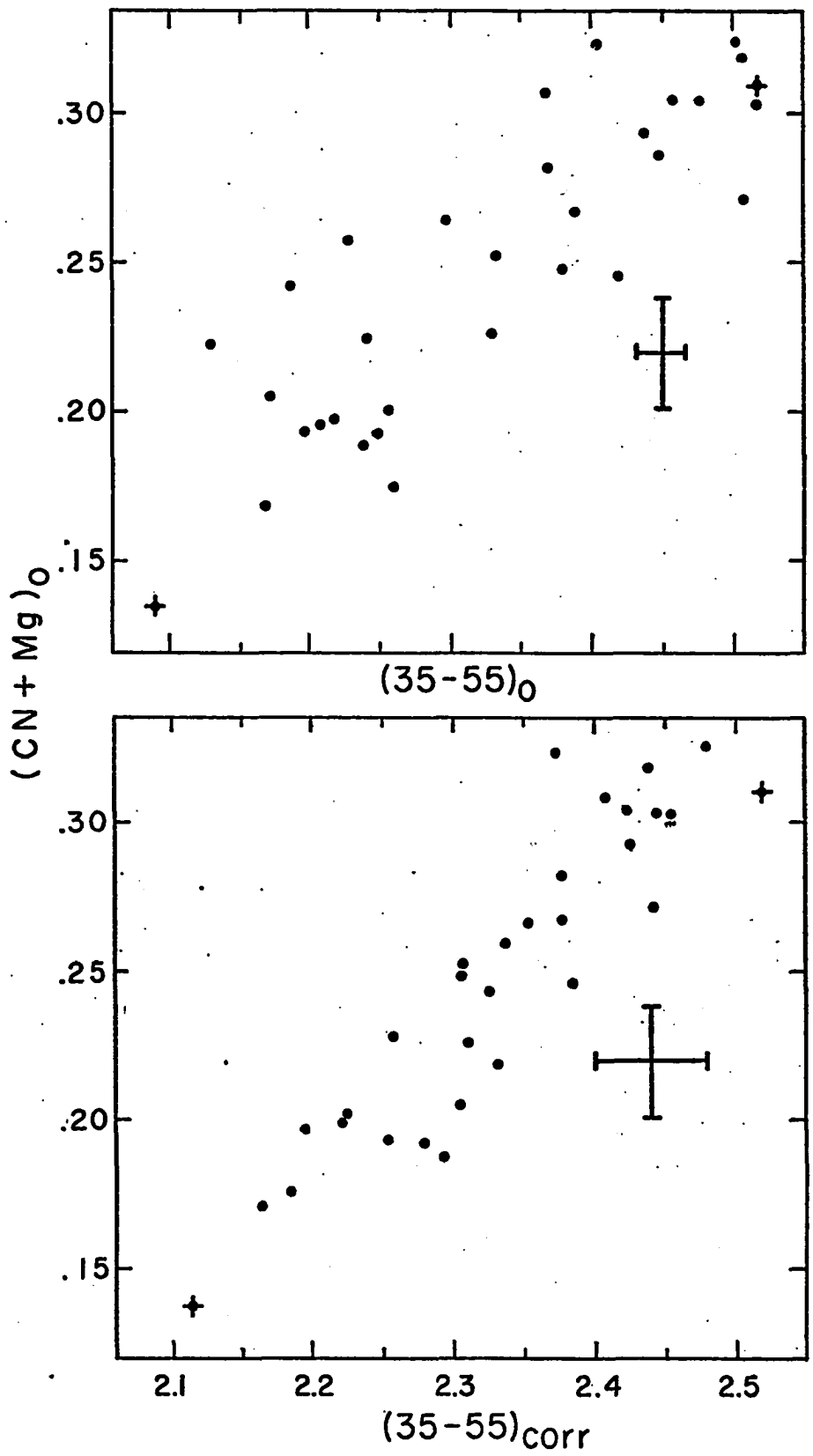

Fig. 11. The line index $(CN+Mg)_o$ versus the values of $(35-55)_o$ in Table 8 and versus $(35-55)_{corr}$, corrected for residual reddening errors. Only the galaxies in the redder group, plus the nucleus of M 31, are shown. Crosses represent M 31 and M 32.

Reproduced with permission of the copyright owner. Further reproduction prohibited without permission.

This result suggests that within the accuracy attained in the present study, reddening errors for pair members are equal. Hence, reddening intrinsic to individual ellipticals is small.

Since the galaxy colors were originally corrected for reddening by means of the cosecant law, the presence of residual reddening errors indicates that the cosecant law may be inaccurate in some cases. By plotting the reddening corrections $\Delta(35\text{-}55)_o$ for each object versus the absolute value of the galactic latitude, one can investigate whether the reddening variations are due to systematic inaccuracies in the cosecant law. The result is shown in Figure 12. A positive correction indicates that the original cosecant correction made the galaxy too blue. Therefore, the absorption in that direction is less than that predicted by the cosecant law. Since the number of objects in the sample is fairly small, the deviation of the mean level of the correction from 0 is not significant, nor is there any obvious dependence on galactic latitude. Taken at face value, this result suggests that no mean correction to a cosecant law with a coefficient of 0.05 magnitude in E_{B-V} is required.

This conclusion, however, results principally from the way the least-squares line was drawn in Figure 7a. We might have decided at that point, for example, that all the galaxies had been undercorrected for reddening and were too

Reproduced with permission of the copyright owner. Further reproduction prohibited without permission.

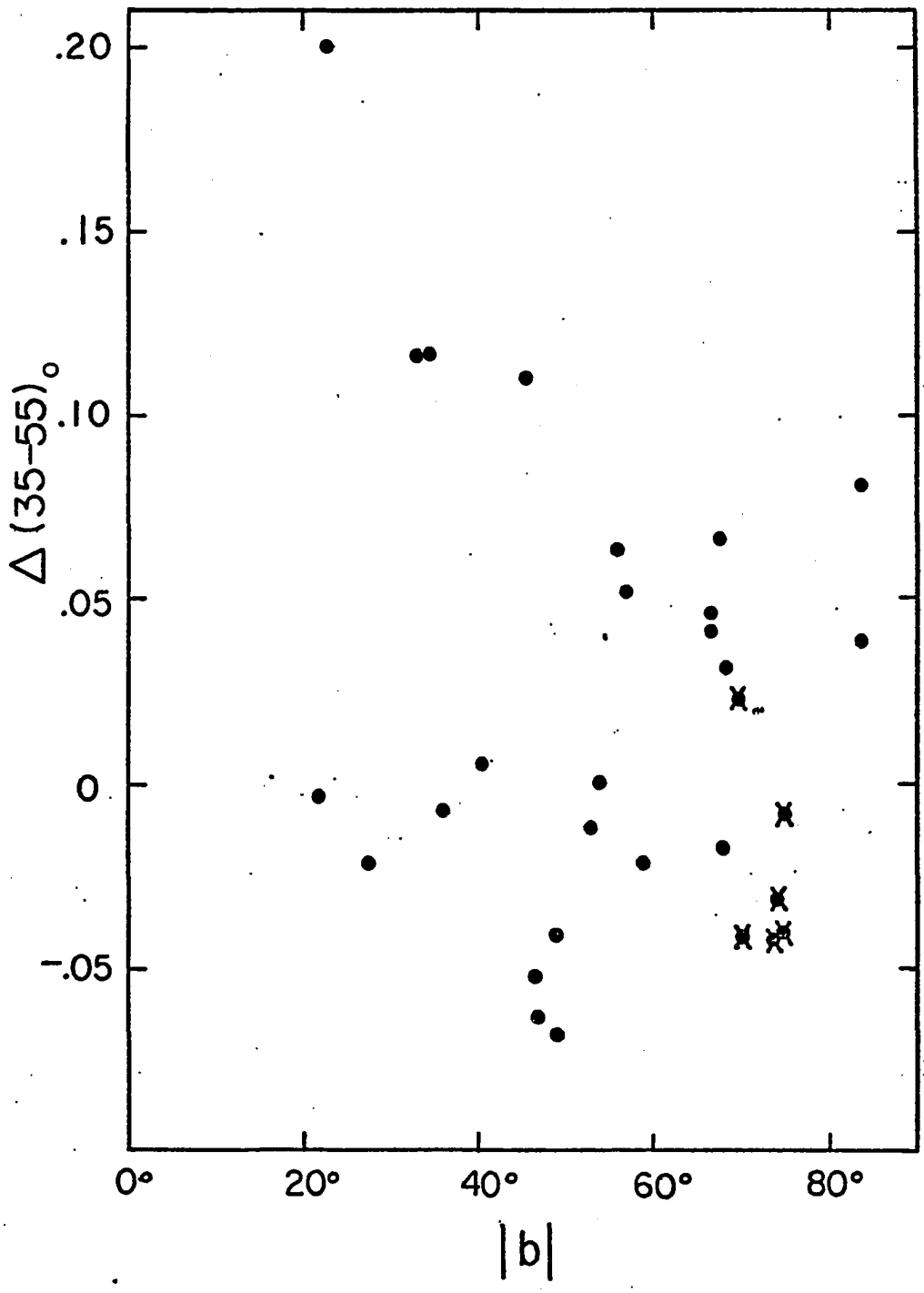

Fig. 12. Residual reddening corrections, $\Delta(35-55)$, versus the absolute value of the galactic latitude. Crosses represent members of the Virgo Cluster.

Reproduced with permission of the copyright owner. Further reproduction prohibited without permission.

red. In that case, the line, supposedly representing the intrinsic colors of elliptical galaxies, would have been drawn below the actual line in Figure 7a. The analogous line in Figure 8 would have lain to the left of its present position, and all reddening corrections would have been large and negative. A diagram corresponding to Figure 12 would then indicate that the coefficient in the cosecant law should be greater than 0.05 magnitude. But this result would reflect only the initial assumptions concerning the true color of elliptical galaxies and nothing about galactic reddening.

In any case, it seems clear from Figure 12 that local variations about a mean reddening law are considerable. The largest deviations are positive, indicating that negative fluctuations in the absorption, that is, clear windows, may be stronger than positive fluctuations, or dense clouds. The present data suggest that elliptical galaxies can be a useful tool in mapping absorption as a function of position in our galaxy and along the line of sight in intergalactic space. Uniformity of absorption in clusters of galaxies can be studied, for example, as well as the reddening excess in the direction of clusters out of the plane of our own galaxy. The ultimate accuracy of the method depends only on how closely correlated the integrated continuum colors and line strengths in elliptical galaxies actually are. As discussed below, within

Reproduced with permission of the copyright owner. Further reproduction prohibited without permission.

the accuracy of the present data they appear to be precisely correlated, but such a bold conclusion should await further study of more objects with greater accuracy. The error bar associated with the points in Figure 9 indicates that with the photometric accuracy available in the present study, the reddening can be determined to within 0.02 magnitude in E_{B-V}.

Except for NGC 3073, in which the $(CN)_o$ index is abnormally strong, the $(Mg)_o$ and $(CN)_o$ indices are closely correlated, as shown in Figure 13. Since Spinrad (1966), Wood (1969), McClure and van den Bergh (1968a), and many others have shown that Mg is stronger in dwarf stars while CN is stronger in giants, the change in the line index $(CN+Mg)_o$ cannot be explained as a change in the dwarf-giant ratio of the mean stellar population. The close correlation between Mg and CN in the integrated light of ellipticals contrasts with the differing behavior of CN and Mg found in the central bulge of M 31 by Spinrad et al. (1971). In M 31, the CN strength declines quickly at small distances from the nucleus, while Mg remains almost constant out to 2'. The reason for this difference between the integrated light of elliptical galaxies and the bulge of M 31 is not known.

It is important to verify that the correlations among absolute magnitude, $(CN+Mg)_o$, and continuum color do not result from systematic error. Since $(35-55)_o$ was not corrected

Reproduced with permission of the copyright owner. Further reproduction prohibited without permission.

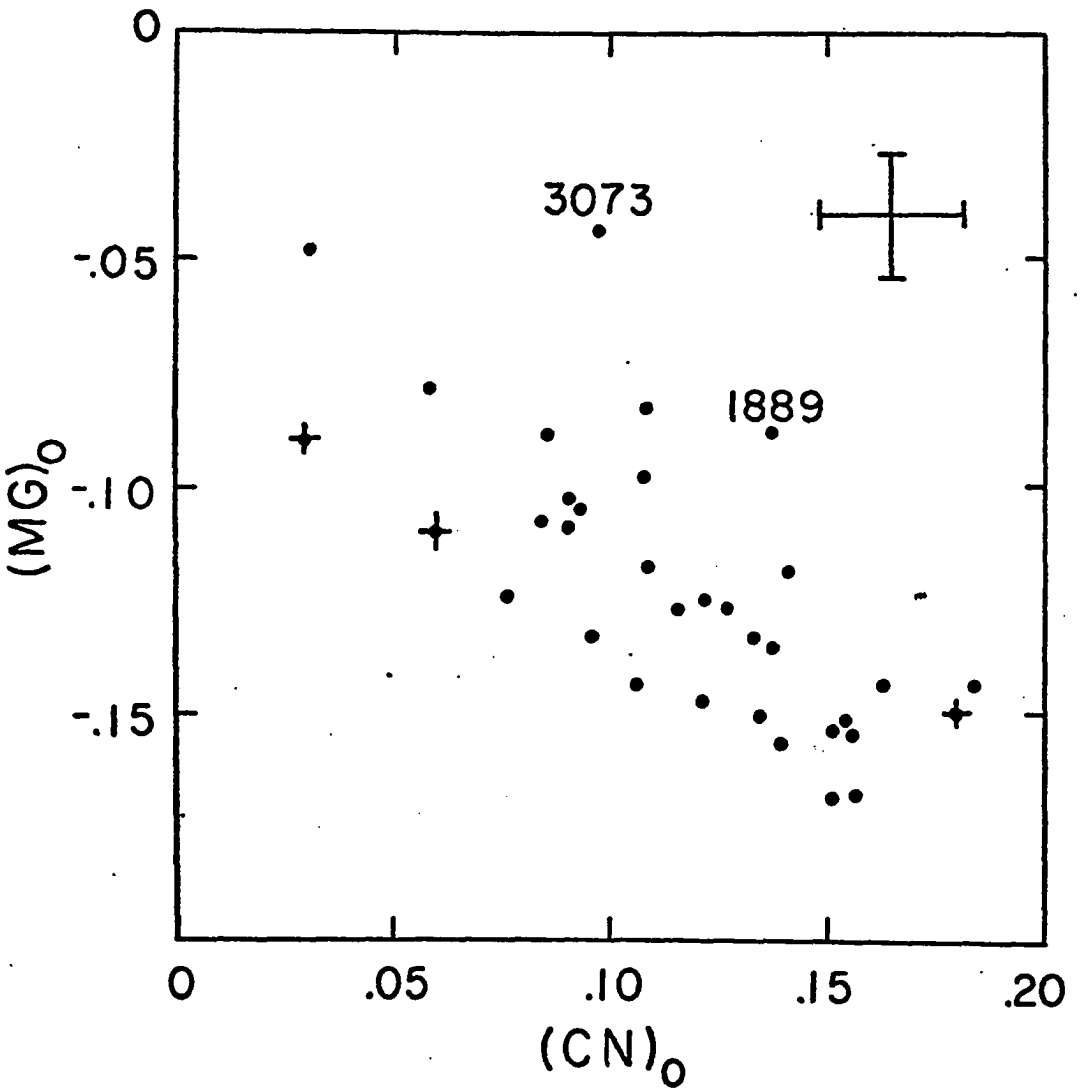

Fig. 13. The line index $(Mg)_o$ versus the line index $(CN)_o$. Crosses represent M 31, M 32, and NGC 205. The colors for NGC 1889 have larger-than-average associated errors.

Reproduced with permission of the copyright owner. Further reproduction prohibited without permission.

for redshift, the $(35-55)_o$ index of the more distant galaxies may be systematically increased owing to the redshift effect. Since these galaxies are also in general intrinsically brighter than those nearby, this effect would preferentially increase the color indices of the most luminous objects, producing the observed reddening with increasing magnitude. However, only the four galaxies with velocities greater than 3000 km/sec should be markedly affected, and estimates above of the size of the shift expected, only 0.02 to 0.04 magnitude, indicate an amount much too small to explain the observed range of color of over 0.30 magnitude among the redder galaxies.

A more serious problem is that of aperture effect. In normal elliptical galaxies, the continuum reddens (de Vaucouleurs 1961; Tifft 1963; 1969; and others) and CN strengthens (McClure and van den Bergh 1968 ; Spinrad et al. 1971) towards the center. If the more luminous objects were measured at generally smaller values of A/D_o, they would appear redder and have stronger CN than fainter galaxies. The apparent correlations between color, line absorption index, and absolute magnitude might arise in this way. A plot of color index $(35-55)_o$ from Table 8 versus A/D_o, Figure 14 displays no strong correlation between $(35-55)_o$ and A/D_o, but there is a suggestion in the large, central group of points that A/D_o is in fact smaller for the reddest galaxies. Therefore aper-

Reproduced with permission of the copyright owner. Further reproduction prohibited without permission.

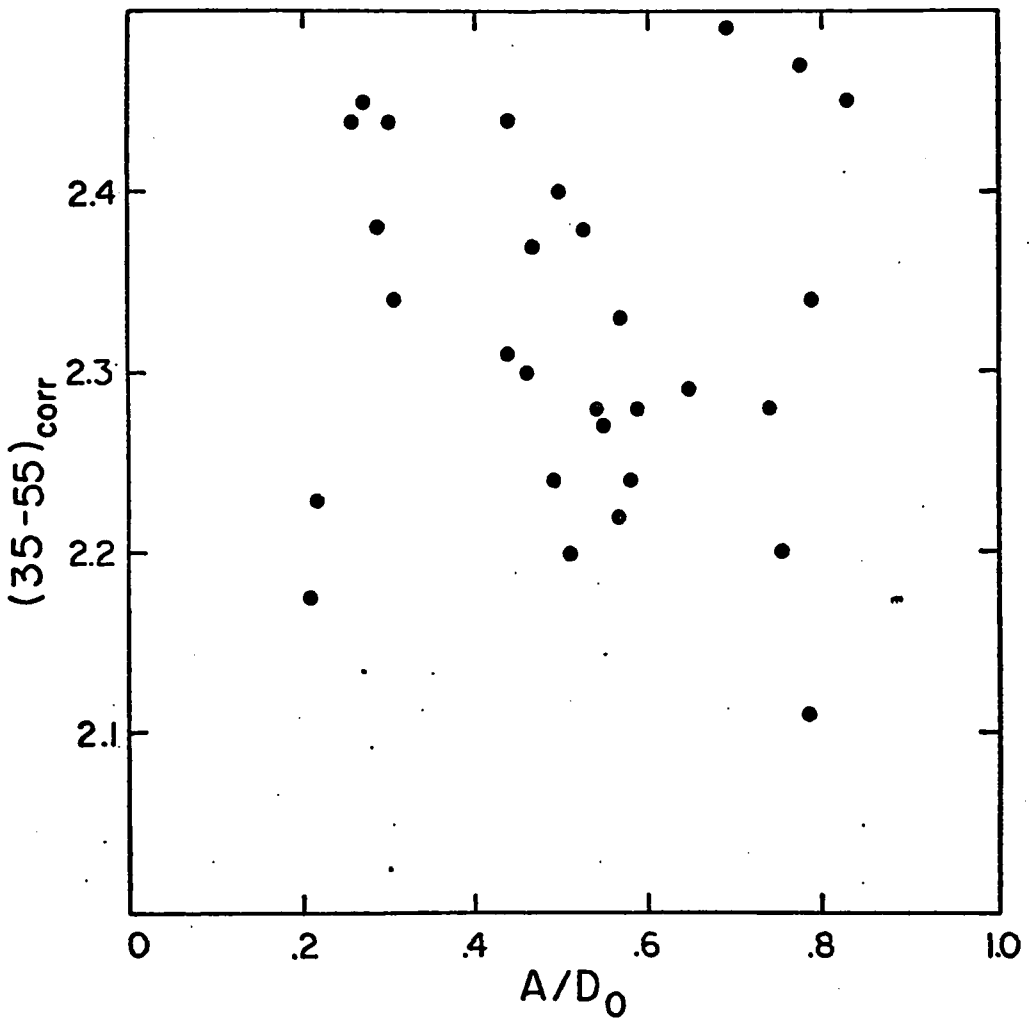

Fig. 14. $(35-55)_{corr}$, corrected for residual reddening errors, versus the ratio of observing aperture to RCBG diameter D_o.

Reproduced with permission of the copyright owner. Further reproduction prohibited without permission.

ture corrections necessary to reduce measured $(35-55)_o$ indices for the redder galaxies to a standard value of A/D_o equal to 1.0 were computed by means of Tifft's (1963) aperture-color data for normal ellipticals. When the galaxy has actually been measured by Tifft (1969), the more recent aperture-color curves were used. In the Notes to the RCBG, B-V for M 32 is said to be independent of aperture. Hence, no correction was computed for this galaxy. These corrections, called $\Delta(35-55)_{ap}$, appear in Table 11. Since the effect for most galaxies is very small, the correlation between $(35-55)_o$ and M_V for the redder galaxies remains unaffected. Figure 4 also demonstrates that the values of $(35-55)_o$ measured in this paper correlate well with integrated values of C_o. This fact is further evidence that the change in $(35-55)_o$ with absolute magnitude reflects a change in the integrated properties of the galaxies as a function of luminosity.

Data adequate to compute aperture corrections to the line indices are unavailable. However, Whitford's (1971) mean scans of five giant elliptical galaxies with apertures A/D_o of 0.2 and 0.6 show no change in the strength of CN and Mg absorption between these two diameters. Furthermore, if the close relationship between $(35-55)_o$ and $(CN+Mg)_o$ that holds for the integrated light of elliptical galaxies also

Reproduced with permission of the copyright owner. Further reproduction prohibited without permission.

applies to their interior regions, the corrections to the line indices will be negligible.

For all these reasons, the colors of elliptical galaxies presented here should be closely comparable to the colors one would measure with an aperture equal to D_o. For utmost accuracy, however, future investigations that seek to utilize or calibrate the absolute magnitude effects discussed in this paper should make sure that the colors obtained for individual galaxies are measured through standardized diaphragm sizes.

The correlation between $(35-55)_o$ and M_v found here is not as steep as that measured by Tifft (1969) for members of the Virgo cluster through a constant aperture size of 64". The slope of +0.09 mag/mag in his color index (1-3) corresponds to a slope of +0.12 mag/mag in Figures 7a and 7b, approximately twice the value of 0.065 actually found. Tifft's larger value might be caused in part by comparison of colors measured through a constant aperture size for objects of different intrinsic sizes and luminosities.

The significance level associated with the eigenvalue λ_3 in Table 10 is 1 per cent, which indicates that possibly a third parameter, K_{3j}, is also required to specify completely the colors of an elliptical galaxy. K_{3j} is plotted against K_{1j} in Figure 15, where pairs are again joined by straight lines.

Reproduced with permission of the copyright owner. Further reproduction prohibited without permission.

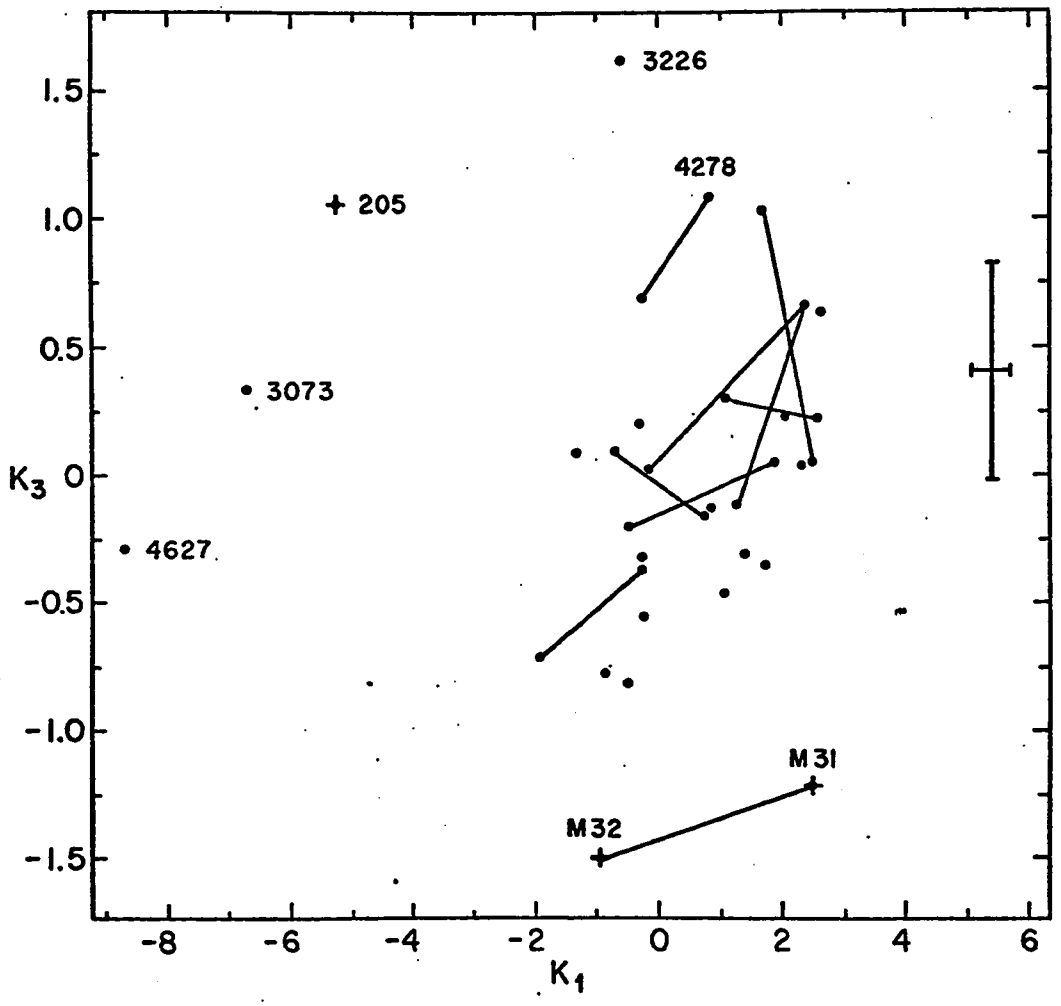

Fig. 15. The independent parameter K_3 versus the independent parameter K_1. Straight lines connect members of the same pair. Crosses represent M 31, M 32, and NGC 205.

Reproduced with permission of the copyright owner. Further reproduction prohibited without permission.

The major contributor to the parameter K_{3j} is the index $(LB)_o$, for which the observational errors are largest. The large negative values of K_{3j} for M 31 and M 32 might be due to errors in transforming the photometry of Wood and McClure and van den Bergh. However, the deviation of NGC 3226, and perhaps 4278, can certainly not be explained on those grounds. Both galaxies have the λ3727 line of [OII] in their spectra, 4278 strongly and 3226 weakly. Since the high value of K_{3j} might be produced by too high a measured intensity through filter 38, the extra flux contributed by the λ3727 line was estimated with the data on the intensity and spatial extent of the emission in NGC 4278 given by Osterbrock (1960). The computed effect on the measurement through filter 38 is only 0.02 magnitude for NGC 4278, and the effect for NGC 3226 should be smaller still. This added flux is much less than the amount required (0.11 magnitude for 4278, 0.16 magnitude for 3226) to produce the large values of K_{3j} in Figure 15.

K_{3j} is not correlated with any physical properties of the galaxies that were tested. K_{3j} was compared with radial velocity and velocity relative to the zero-velocity of the set of filters used, either 0 or 1500 km/sec. Since no relation was found, systematic errors in the radial velocity corrections to the photometry do not cause the scatter in K_{3j}. The positions of the galaxies in Figure 15 are also not asso-

Reproduced with permission of the copyright owner. Further reproduction prohibited without permission.

ciated with A/D_o, the time of year at which observations were made, the presence of emission lines (aside from the two objects mentioned), radio emission (see Table 12), number of galaxies in the same group, or the morphological types of the earliest and latest companion galaxies. Objects labeled "peculiar" in the RCBG, and those seemingly interacting with companions as shown in the Atlas of Peculiar Galaxies (Arp 1964), lie at random positions in Figure 15, although there is a slight suggestion that members of the same pair tend to have equal values of K_{3j}. However, in an analysis into principal components that excluded M 31 and M 32, the corresponding eigenvalue was not significant to the 10 per cent level.

With the exception of the clearly deviant object NGC 3226, we conclude that the available evidence for a third parameter needed to completely characterize elliptical galaxies is weak. Certainly the major differences in 10-color indices among elliptical galaxies can be accounted for by the use of only two parameters, which can in turn be used to obtain the intrinsic colors and reddening between the source and observer. The present study also indicates that the ellipticals brighter than -21 in absolute magnitude form a homogeneous set of objects. These data therefore support their use as standard sources in observational tests of cosmological theories, provided due allowance is made for changes in the energy distributions due to evolutionary effects.

Reproduced with permission of the copyright owner. Further reproduction prohibited without permission.

TABLE 12

GALAXIES HAVING RADIO SOURCES AND EMISSION LINES

Name	Emission		Reference(s)
	Radio	λ3727	
NGC 584	Ident. uncertain		Mills, Slee, Hill (1958) Minkowski (1961) Heeschen and Wade (1964) Rogstad and Ekers (1969)
3226	---	yes	Burbidge and Burbidge (1965)
4261	yes		Minkowski (1961)
4278	yes	yes	Osterbrock (1962) Heeshcen and Wade (1964) Rogstad and Ekers (1969)
4472	yes		Heeschen and Wade (1964)
4486	Virgo A	yes	Humason, Mayall, Sandage (1956)
5846		yes	Humason, Mayall, Sandage (1956)
7626	yes		Heeschen and Wade (1964)

Reproduced with permission of the copyright owner. Further reproduction prohibited without permission.

VII. ANALYSIS INTO PRINCIPAL COMPONENTS: GALAXIES AND GLOBULAR CLUSTERS

An analysis into principal components was also performed for galaxy and cluster colors taken together. The results were similar to the preceding except that the variance associated with K_{3j} had no significance, which further suggests that K_{3j} is not a physically meaningful parameter. Values of K_{2j}, the index measuring the difference between continuum color and line index strength, were systematically negative for the clusters, equaling -0.23 ± 0.12 for the globulars and $+0.10 \pm 0.10$ for the galaxies. Applying the reasoning of the previous discussion, we find that either the reddening errors for the globulars differ systematically from those of the elliptical galaxies by 0.06 magnitude in E_{B-V} or globular clusters differ from dwarf elliptical galaxies of the same color in having weaker absorption lines. Figure 16 compares the energy distributions of the three dwarf ellipticals measured here with those of globulars having similar $(35\text{-}55)_o$ indices. The absorption lines in the galaxies are definitely stronger, and the overall shape of the continua also differ. Of the three ellipticals, NGC 205 seems most similar to the clusters. Because several of the globulars lie in unobscured regions and have extremely small reddening excesses, it is virtually impossible that the reddening correction for these could be in error by 0.06 magnitude. Moreover, reddening corrections

Reproduced with permission of the copyright owner. Further reproduction prohibited without permission.

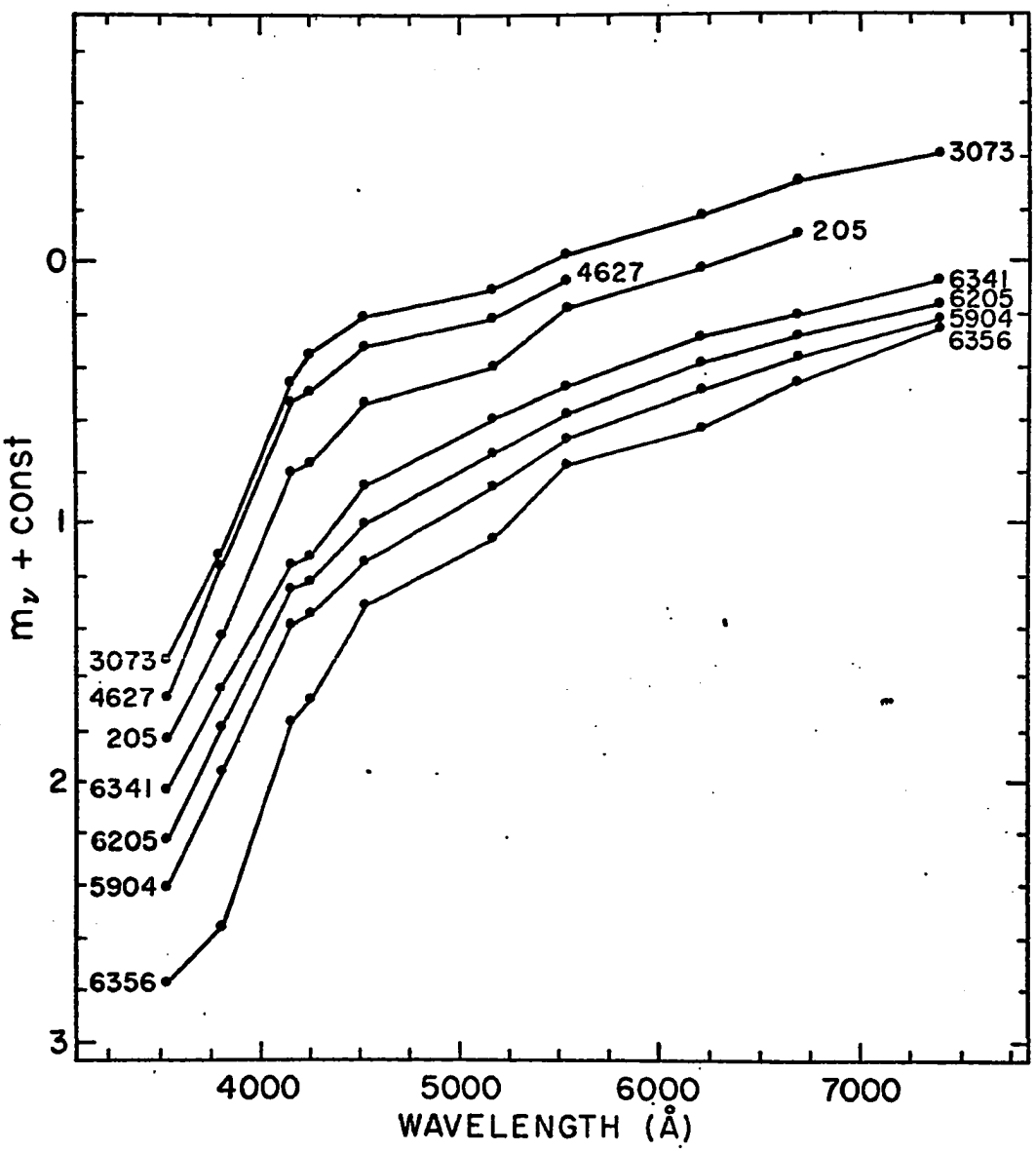

Fig. 16. Comparison of 10-color photometry for dwarf elliptical galaxies (upper group) with photometry for globular clusters (lower group).

Reproduced with permission of the copyright owner. Further reproduction prohibited without permission.

cannot alter the shoulder shortward of 4000 Å, which is present in the ellipticals but not in the clusters.

We conclude that the two classes of objects are similar in having blue continua and weak absorption lines. To this extent, these results support the findings of McClure and van den Bergh (1968a), Hodge (1971), and others, who have noted the similarities between dwarf ellipticals and globular clusters. However, the colors of these three galaxies indicate that the continuum distributions and line strengths of at least some dwarf galaxies differ significantly from those of globular clusters with similar values of $(35-55)_o$. Furthermore the dwarf ellipticals differ appreciably among themselves. In particular, the rather strong $(CN)_o$ index in NGC 3073, which cannot be due to observational errors, contrasts markedly with the weak $(Mg)_o$ index in the same object and with the weak $(CN)_o$ indices in the other two dwarfs.

VIII. DWARF ELLIPTICALS OF HIGH SURFACE BRIGHTNESS

NGC 4486B, 5846A, and possibly M 32 deviate systematically from the relation between absolute magnitude and line strength defined by normal galaxies in Figure 10. In all cases, the lines in these dwarf elliptical galaxies are too strong for their absolute magnitudes. Reference to Figure 7b shows that these galaxies also tend to be too red for

Reproduced with permission of the copyright owner. Further reproduction prohibited without permission.

their absolute magnitudes, although the deviation in this case is extreme only for NGC 4486B. However, their positions in all color-color or color-line strength diagrams are normal. A plot of color index $(35-55)_o$ versus surface brightness in visual magnitude V, computed from the data from the RCBG corrected for absorption in our galaxy, demonstrates (Figure 17) that these three objects also have much higher surface brightness than the average elliptical galaxy studied.

Several investigators (de Vaucouleurs 1961; Minkowski 1961; Tifft 1963; Zwicky 1964) have noted that NGC 4486B is unusual. Tifft and de Vaucouleurs remarked on its resemblance to M 32, de Vaucouleurs also describing NGC 1510 as similar. King (private communication) has noted the similar appearance of NGC 4486B and NGC 5846A on direct photographs. No other objects in the Notes to the RCBG have comparable descriptions. Unfortunately, no photometry or radial velocity is available for NGC 1510.

On the celestial sphere all four of these galaxies lie close to bright galaxies, at least three of which (NGC 4486, 5846, M 31) are massive objects. If at some time in the past, a normal elliptical of intermediate luminosity lost a considerable fraction of its outer material in a close tidal encounter with a more massive primary, the surviving remnant would resemble these dwarf galaxies in three respects. Because the surface brightness, line strengths, and continuum

Reproduced with permission of the copyright owner. Further reproduction prohibited without permission.

Reproduced with permission of the copyright owner. Further reproduction prohibited without permission.

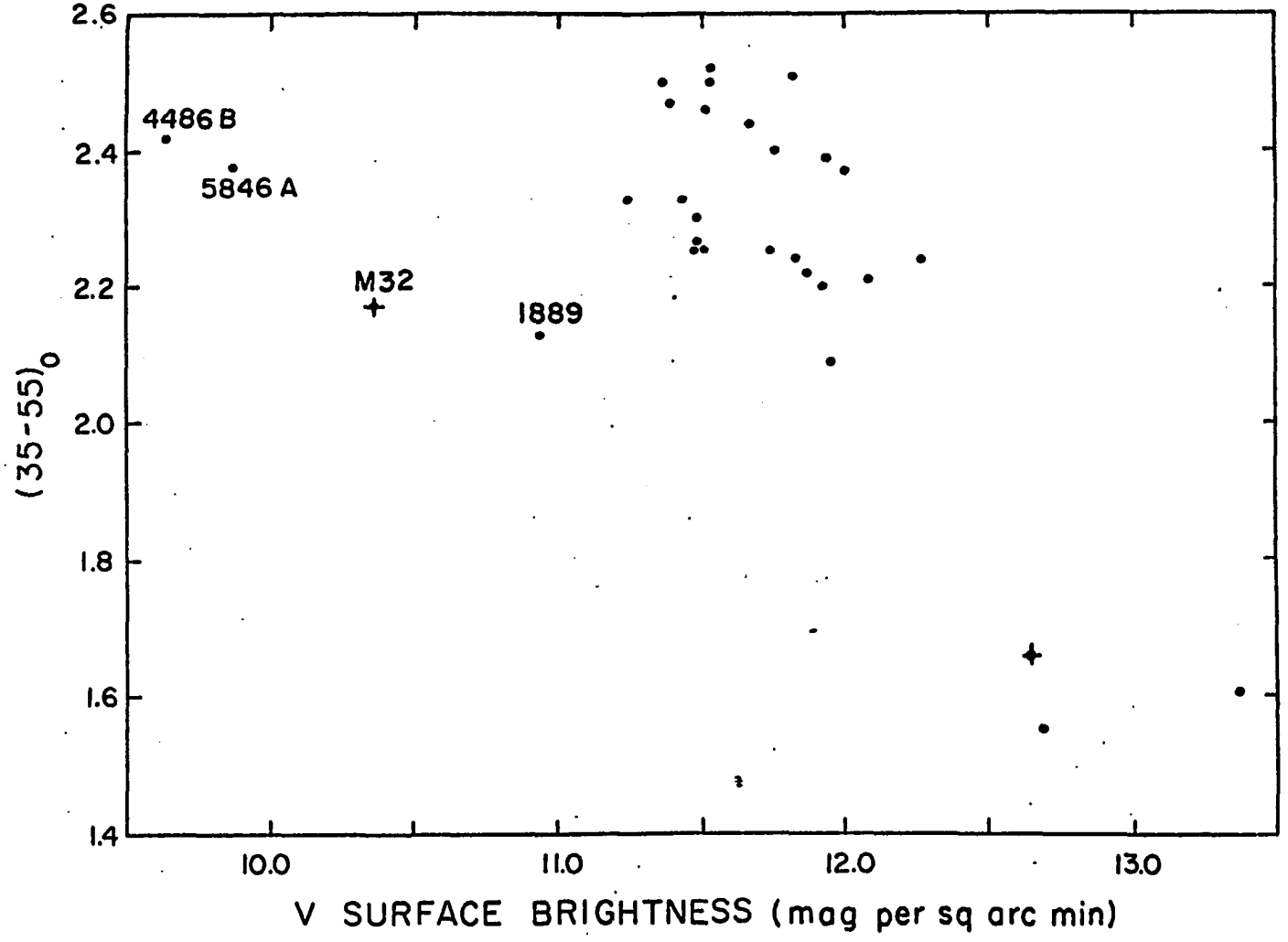

Fig. 17. $(35-55)_o$ versus surface brightness in V magnitudes per square minute of arc for elliptical galaxies. Crosses represent M 32 and NGC 205.

color indices in a normal elliptical galaxy increase toward the nucleus, the remnant would have a higher surface brightness, stronger lines, and a redder continuum than its absolute magnitude would indicate. Furthermore, King (1962) has stated that the luminosity profile of M 32 is consistent with the interpretation that M 32 is a tidally-limited system. Direct photographs of M 32 (Arp 1966) also show a disturbance on the side away from M 31 which may represent a tidal plume.

Although the surface brightnesses of these dwarf elliptical galaxies are high, they are no higher than the central surface brightnesses of normal elliptical galaxies. This fact can be seen through a comparison of the dwarf surface brightnesses with Tifft's (1969) measurements of the surface brightnesses of the inner regions of Virgo cluster elliptical galaxies. M 32 closely resembles NGC 4486B in linear dimensions (see Table 14), while NGC 5846A is approximately twice as large. Since the angular diameter of NGC 4486B is 12", one can compare the surface brightnesses of these three objects with Tifft's measurements in the Virgo cluster through diaphragms of 10" and 16" (see Table 13). The table shows that the dwarf surface brightnesses are no higher than would be expected under the hypothesis of tidal origin.

Using the available values of masses for the primary and dwarf galaxies, one can estimate the distances of

Reproduced with permission of the copyright owner. Further reproduction prohibited without permission.

TABLE 13

A COMPARISON OF SURFACE BRIGHTNESSES OF RED DWARF ELLIPTICALS WITH CENTERS OF NORMAL ELLIPTICALS

	Diameter[1] D	Surface Brightness	Absolute Magnitude, M_V
Dwarf Ellipticals:			
M 32	.78 Kpc	$10^m.36$[2]	
4486B	.76	9.63[2]	
5846A	1.38	9.87[2]	
Centers of Virgo Ellipticals:			
4374	.61 Kpc	$8^m.41$[3]	-20.9
	1.02	8.85[3]	
4429	.61	9.26[3]	-20.3
	1.02	9.77[3]	
4179	.61	8.95[3]	-19.4
	1.02	9.53[3]	

Notes to Table 13:

1. Diameter over which mean surface brightness is averaged.
2. In units of V magnitude/sq. minute of arc.
3. In units of '3' magnitude/sq. minute of arc (Tifft 1969).

Reproduced with permission of the copyright owner. Further reproduction prohibited without permission.

Reproduced with permission of the copyright owner. Further reproduction prohibited without permission.

TABLE 14

ORBITAL CHARACTERISTICS OF RED DWARF ELLIPTICALS

Name	Angular radius r	Linear radius R	Primary Mass M_1	Dwarf Mass M_2	Tidal distance T	Present projected separation S	Minimum distance at pericenter S'
M 32	11!2 1!82	2.4 Kpc .39	$1.8\times10^{11} M_\odot$ [1]	$3\times10^{9} M_\odot$ [2]	14.0 Kpc 2.3	5.5 Kpc	.08 Kpc
NGC 4486B	6".0	.38	2.6×10^{12} [2]	5.1×10^{10} [4]	2.1	28,0	1.9
NGC 5846A	7".5	.69	1.5×10^{12} [3]	3×10^{9} [5] 5.1×10^{10} [5]	10.0 3.8	3.9	.35

Notes to Table 14:

1. Rubin and Ford, Ap. J., 159, 379, 1970.
2. Fish, Ap. J., 139, 284, 1964.
3. Computed using M/L for NGC 4486.
4. Zwicky, Ap. J., 140, 1476, 1964.
5. M_2 assumed equal to masses of M 32 and NGC 5846A in two separate cases.

closest approach, T , necessary to reduce the dwarf galaxies to their present radii. Table 14 presents the results. Two calculations are shown for M 32, the first using the value of the tidally-limited radius derived by King (1962) from surface photometry of M 32 and the second using the standard diameter D_o from the RCBG. Sources of the other entries in Table 14 appear in the notes. The columns are as follows: r is the angular radius of the dwarf, R the linear radius of the dwarf in kiloparsecs, M_1 the primary mass in solar masses, M_2 the dwarf mass in solar masses, T the distance of closest approach in kiloparsecs, and S the present projected separation in kiloparsecs. The distances T were calculated with the formula of von Hoerner (1957) as modified by King(1962),

$$T = R(3.5M_1/M_2)^{1/3}.$$

One can also calculate the distance of closest approach possible given the observed differences in radial velocities between primary and companion. These are called S' in Table 14. The fact that S' is less than or equal to T in all cases shows that tidal interactions could have occurred, according to the best available estimates of the masses and distances of these systems.

Reproduced with permission of the copyright owner. Further reproduction prohibited without permission.

IX. DISCUSSION

The present data suggest that, to a high degree of accuracy, the integrated colors and line strengths of a normal elliptical galaxy are determined by its absolute magnitude. However, in an effort to examine whether pair membership, cluster membership, and line or radio emission correlate with elliptical galaxy colors, a search was made for relationships between these parameters, galaxy luminosity and isolated color anomalies. The following paragraph summarizes the results of this search.

Galaxies in this study having line or radio emission have colors that are completely normal for their absolute magnitudes. This conclusion accords with King's (1971) opinion that the stellar content of galaxies is unaffected by nuclear activity. The only definitely abnormal object, NGC 3226 (through filter 38), is also the only elliptical observed that is a companion of a Seyfert galaxy. Clearly, from a sample of one object, no conclusions can be drawn concerning the possible relation between the components of the pair. All of the other interacting systems (NGC 221, 1889, 2672, 3193, and 4627) have normal positions in all color-color and color-line strength diagrams. Furthermore, neither the colors nor the absolute magnitudes of the galaxies are related to the morphological types or number of companions. The colors of

Reproduced with permission of the copyright owner. Further reproduction prohibited without permission.

elliptical galaxies inside large clusters are identical to those of the same absolute magnitude in much smaller aggregates. Fish (1964) suggested that the mass-to-light ratio of elliptical galaxies with Sb or Sc companions was systematically low. No evidence was found from the colors of NGC 221, 2300, 3379, and 4649, the four galaxies cited by him, that M/L for these objects is anomalous. However, photometric indices shortward of 8000 Å are not particularly sensitive to the mass-to-light ratio.

Models of the stellar populations necessary to produce the integrated colors of these elliptical galaxies will be presented elsewhere (Chapter 3). In brief, it was found that, for the redder group of galaxies, an increase in the number of strong-lined stars and red stars, together with a decrease in the light contributions from metal-poor objects, was necessary to duplicate the increase in redness and line-strength with absolute magnitude. The mass-to-light ratios of the models were indeterminate. Even though a few giants indicated by Spinrad and Taylor (1969) as super-metal-rich (SMR) were available for the synthesis, the line strengths in the computed models for the brightest galaxies were much too weak. Furthermore, the integrated line strengths in $(CN)_o$ and $(Mg)_o$ over the central 2.5-4.5 kpc of the brightest ellipticals in this survey are comparable to the

Reproduced with permission of the copyright owner. Further reproduction prohibited without permission.

line strengths in M 31 over the innermost 60 pc. As Spinrad (1970) has noted, this fact implies that the nuclei of these galaxies possess extremely strong lines. Observations with the necessary spatial resolution have not yet been made to test this conclusion.

Considerable uncertainty still exists concerning the metal abundance of SMR stars in our own galaxy (see King 1971 for a discussion). This fact renders difficult an interpretation of the change in continuum colors and line strengths with magnitude found in these elliptical galaxies. Taken at face value, however, the data support Spinrad's (1970) conjecture that the number (or degree of extremity) of SMR stars produced in elliptical galaxies is an increasing function of galaxy luminosity.

X. SUMMARY

The colors of normal elliptical galaxies can be specified to a high degree of accuracy with only two independent parameters, which in turn may be utilized to determine both the intrinsic colors and the reddening between the galaxy and the observer. The intrinsic colors and line strengths are closely correlated with absolute magnitude at all luminosities. Elliptical galaxies form a sufficiently homogeneous group that they can be used to study galactic and intergalactic absorption as a function of direction and distance.

Reproduced with permission of the copyright owner. Further reproduction prohibited without permission.

The three blue dwarf elliptical galaxies with available 10-color photometry are generally similar to globular clusters in having blue continua and weak absorption lines. However, they have continuum distributions and line strengths that differ significantly from those of globular clusters having similar overall color. The hypothesis that red dwarf ellipticals once lost a considerable fraction of their outer mass in a tidal encounter with a massive primary seems possible, given the available data on the masses and orbital characteristics of these objects. This hypothesis also explains in a qualitative way the high surface brightnesses, anomalously strong lines, and red continua of these galaxies.

Reproduced with permission of the copyright owner. Further reproduction prohibited without permission.

CHAPTER III

Quadratic Programming Applied to the Problem of Population Synthesis

I. INTRODUCTION

Although several investigators (most recently Wood (1966), McClure and van den Bergh (1968a),Moore (1968), and Spinrad and Taylor (1971a) have utilized population synthesis as a method for studying the stellar content of galaxies, all such extensive studies have employed a trial-and-error method for fitting computed model colors to the observed galaxy indices. Automatic, objective methods of fitting were apparently tested by some of these authors but were rejected on the grounds that the resultant models were either physically impossible because they contained negative numbers of certain types of stars, or had astrophysically unreasonable H-R diagrams. However, there exists a mathematical procedure for solving minimization problems subject to constraints applied to the unknown variables. These constraints can be introduced in such a way as to ensure that the solution be both physically and astrophysically acceptable. Moore first suggested that such a technique, namely linear programming, might be applied successfuly to the population synthesis problem. Lasker (1970) actually used a close relative of the method, quadratic programming, to construct crude models for elliptical galaxy populations. This paper reports on an application of quadratic

Reproduced with permission of the copyright owner. Further reproduction prohibited without permission.

programming to the synthesis of population models using the most extensive body of photometric data yet available on galaxies, that found in Spinrad and Taylor (ST) (1971a). Results obtained by using a 10-color photometric system for elliptical galaxies are also presented.

II. THE SYNTHESIS PROBLEM

Before selecting a method for objective synthesis, one must adopt a criterion of best fit. In this study we chose to minimize the weighted sum of the per cent residuals squared in all photometric passbands. If L_j is the luminosity of the galaxy in filter j, x_k is the number of stars present of type k, ℓ_{kj} is the luminosity of type k stars in filter j, and J is the total number of filters, we minimize

$$Q = \sum_{j=1}^{J} W_j \left(1 - \frac{\sum_k x_k \ell_{kj}}{L_j}\right)^2 .$$

Here W_j is an arbitrary weight ≥ 0 that may be varied at one's convenience. The values of x_k that yield the absolute minimum of this quadratic function will in general not be acceptable for the reasons described above. Hence, the value of Q can be examined for a minimum only on a restricted subset of the space spanned by the x_k. The nature of these restrictions has been discussed at length by Spinrad and Taylor and will be briefly summarized here.

Reproduced with permission of the copyright owner. Further reproduction prohibited without permission.

Most important is the requirement that all unknowns x_k be greater than or equal to zero in the final solution, since negative numbers of stars are physically impossible. Second, if one assumes for simplicity that only one generation of stars is present, then the relative numbers of certain groups of stars must be close to those predicted either by empirical observations of cluster luminosity functions or by our theoretical knowledge of stellar evolution. In particular, the absence of a given kind of star implies the absence of its immediate evolutionary precursors. Lastly, the number of stars present must vary smoothly from group to group along the main sequence. In addition to imposing these constraints on the solution, the investigator may also find two other constraints useful in examining the properties of the model. The first is the requirement that a particular stellar group provide a certain percentage of the model luminosity in a given filter. The second is the requirement that the mass-to-light ratio (M/L) of the model population lie between certain limits.

Fortunately all of these restrictions can be imposed by minimizing Q subject to linear equalities or inequalities relating the unknowns x_k. The problem therefore may be solved by the method of quadratic programming. Let C_1, C_2, C_3, C_4, R_1 and R_2 be constants ≥ 0 chosen by the investigator. The restrictions discussed above can then be expressed as follows:

Reproduced with permission of the copyright owner. Further reproduction prohibited without permission.

$$\text{I. Group ratios: } C_1 \leq \frac{x_n}{x_{n'}} \leq C_2$$

$$\text{II. Light contributions in filter j: } C_3 \leq \frac{x_n \ell_{nj}}{\sum_k x_k \ell_{kj}} \leq C_4$$

$$\text{III. M/L in filter j: } R_1 \leq \frac{\sum_k x_k m_k / m_\odot}{\sum_k x_k \ell_{kj} / \ell_{\odot j}}$$

Here m_k is the mass of stellar group k, and $m_\odot$ and $l_{\odot j}$ are the solar mass and luminosity in filter j. In addition, the option of setting certain groups initially to zero was included.

Let us assume that galaxy and stellar observations are available in J passbands and that at most N of the vectors $\underset{\sim}{\ell}_k$, formed by taking the J components ℓ_{kj}, are linearly independent. If $J \geq N$, the space spanned by the solution set that minimizes Q has 0 dimensions, that is, it is a unique point. When $J < N$, the dimension of this space is N-J, so that the solution is no longer unique. In fact, Q is identically 0 everywhere on the solution set. If there is a total of K stellar groups, let $\underset{\sim}{x}$ represent the vector formed by taking the K components x_k. Let $\underset{\sim}{x}'$ be the transpose of $\underset{\sim}{x}$. It is possible to rewrite Q as the quadratic form

$$Q = 1/2[\underset{\sim}{x}'B\underset{\sim}{x}] - \underset{\sim}{a}\cdot\underset{\sim}{x},$$

where the matrix B and vector $\underset{\sim}{a}$ are functions of W_j, ℓ_{kj}, and L_j. If Q vanishes on a set with dimension greater than 0, the matrix B is positive semi-definite rather than positive definite. Therefore a method for minimizing Q must be used

Reproduced with permission of the copyright owner. Further reproduction prohibited without permission.

that does not require B^{-1}, since B^{-1} does not exist.

The most suitable algorithm for minimizing semi-definite forms is Dantzig's algorithm as described by Boot (1964). This method will give at least one point where Q is 0. In actual practice, even for solutions using just the 10-color data with over thirty possible stellar groups, this problem of uniqueness never arose since no part of the multi-dimensional set minimizing Q lay within a quadrant where more than ten unknowns were positive simultaneously. Hence the solutions were indeed unique even though many fewer filters than stellar groups were used.

The disadvantages of the trial-and-error method of population synthesis are considerable. Since one cannot test every possible combination of stars at hand, there may remain an undiscovered formula that is a better fit but has not been tried. Consequently if a fit is performed on two different occasions even by the same investigator, there is no quantitative measure available that can predict the extent to which the two solutions will agree or disagree. Moreover, the assumptions underlying a given model that influence the investigator's choice of allowable models on successive trials are never clearly expressed in quantitative form. Thus the effect of these assumptions on the resultant synthesis cannot be examined.

Reproduced with permission of the copyright owner. Further reproduction prohibited without permission.

The method of solution described above circumvents most of these difficulties. Identical assumptions, entered in the form of initial constraints, obviously result in identical models. Moreover the assumptions inherent in each synthesis are clearly expressed in the inputs, and hence it is immediately evident what sets of solutions have been explored. Perhaps even more important, it is possible to examine the sensitivity of the solution to observational errors in the input data and perturbations in the constraints. One may also delete or alter the input data in order to determine which aspects of the intensity distribution are responsible for particular features of the resultant models. The method also allows comparison of stellar populations in galaxies with similar but not identical intensity distributions. Such a comparison is not reliably possible with the trial-and-error method because there is little assurance that the uncertainty in the fits is smaller than the variations in stellar content implied by the differences in galaxy colors.

However, because the investigator still must choose the constraints to be supplied, population synthesis with quadratic programming is still far from the ultimate and totally objective method one might desire. The difficulty lies in the degree to which the final model is constrained. Overly weak constraints will result in a model that has been adjusted to fit the observational errors in the data. On the other hand

Reproduced with permission of the copyright owner. Further reproduction prohibited without permission.

overly strong constraints may be unrepresentative of the real population producing the integrated light. It is of course a matter of judgment as to when a proper balance has been reached.

III. MODELS FOR M 31

The data provided by Spinrad and Taylor on M 31, M 32, and M 81 provide an excellent test of the method, being the most accurate and by far the most extensive available. Using these data one may examine what currently can be achieved both with the technique of population synthesis in general and with the present method of solution in particular. The data have been adopted as published, with the addition of one more stellar group designated "horizontal branch." Because ST observed no field horizontal branch stars, the intensities for 32 Per (A3V) were adopted as an approximation to true horizontal-branch colors. Mean U-B and B-V corrected for reddening for the three horizontal branch stars HD 86986, 109995, and 161817 are +.10 and +.07 magnitude while U-B and B-V for 32 Per are +.07 and +.07 magnitude. Since the horizontal-branch group played no significant role in any of the better models for M 31, M 32, or M 81, the errors introduced by this approximation are very small.

The constraints for all models using ST's data are shown in Table 1, while the models for M 31 appear in Table 2.

Reproduced with permission of the copyright owner. Further reproduction prohibited without permission.

Reproduced with permission of the copyright owner. Further reproduction prohibited without permission.

TABLE 1

MODEL CONSTRAINTS FOR M 31, M 32, M 81

	Synthesis Groups set to zero		Light Contributors	Group A	Group B	Ratio A/B	M/L
M 31, 38 filters:							
Model 1:	35 36 37		None Specified				None Specified
Model 2:	1	33	None Specified	7	8	0.00-1.00	
	2	34		8	9	0.67-0.69	
	3	35		9	10	1.30-1.32	
	4	36		10	11	0.37-0.39	
	5	37		11	12	0.32-0.34	
	6	38		12	13	0.56-0.58	
	24			13	14	0.36-0.38	
				14	15	0.47-0.49	
				15	16	0.43-0.45	
				18	8	0.66-0.68	
				19	18	0.72-0.74	
				21	20	0.99-1.01	
				22	21	0.28-0.30	
				23	22	0.32-0.34	
				25	26	0.99-1.01	
				27	25	0.28-0.30	
				28	27	0.32-0.34	
Model 3:	2	33	8% at 3300 Å from Group 1	Same as Model 2			None Specified
	3	34					
	4	35					
	5	36					
	6	37					
	24						

Reproduced with permission of the copyright owner. Further reproduction prohibited without permission.

TABLE 1 continued

	Synthesis Groups set to zero		Light Contributors	Group A	Group B	Ratio A/B	M/L
M 31, M 32, M 81, 36 filters:							
Model A:	1	33	None	5	6	0.00-1.00	
	2	34	Specified	6	7	0.00-1.00	
	3	35		7	8	0.00-1.00	
	4	36		8	9	0.00-1.00	
	24	37		9	10	0.00-1.00	
		38		10	11	0.00-1.00	
				11	12	0.00-1.00	
				12	13	0.00-1.00	
				13	14	0.00-1.00	
				14	15	0.00-1.00	
				15	16	0.00-1.00	
				18	8	0.36-0.38	
				19	18	0.72-0.74	
				21	20	0.99-1.01	
				22	21	0.28-0.30	
				23	22	0.32-0.34	
				25	26	0.99-1.01	
				27	25	0.28-0.30	
				28	27	0.32-0.34	
				29	23	0.00-1.00	
				30	29	0.00-1.00	
				31	30	0.00-1.00	
				32	31	0.00-1.00	

Reproduced with permission of the copyright owner. Further reproduction prohibited without permission.

TABLE 1 continued

	Synthesis Groups set to zero	Light Contributors	Group A B	Ratio A/B	M/L
M 31, M 32, M 81, 36 filters:					
Model B:	1 32 2 33 3 34 4 35 24 36 30 37 31 38	None Specified	Same as Model B with constraints for Groups 30-32 omitted.		None Specified

Reproduced with permission of the copyright owner. Further reproduction prohibited without permission.

TABLE 2

M 31 MODELS

		Spinrad and Taylor's Model			Model 1		
Gr. No.	Group Name	No. Stars	Mass (%)	V Light (%)	No. Stars	Mass (%)	V Light (%)
1	O-B Dwarf						
2	Late B Dwarf				.432 E 01	.000	.214
3	Early A Dwarf				.119 E 01	.002	1.507
4	Late A Dwarf						
5	Early F Dwarf				.102 E 01	.001	.185
6	Middle F Dwarf						
7	Late F Dwarf	.159 E 02	.016	1.000	.393 E 02	.043	3.030
8	Early G Dwarf	.175 E 03	.148	6.460			
9	G5V-K0V	.289 E 03	.219	4.280	.182 E 04	1.481	32.979
10	K1V-K2V	.427 E 03	.252	4.250			
11	K3V-K4V	.501 E 03	.275	3.150	.114 E 04	.670	8.776
12	K5V-K7V	.912 E 03	.461	1.480			
13	M0V-M2V	.321 E 04	1.080	1.180			
14	M3V-M4V	.152 E 05	3.843	1.180	.384 E 05	10.426	3.656
15	M5V-M6V	.748 E 05	12.605	1.180			
16	M7V	.108 E 06	13.668	1.000			
17	M8V	.796 E 06	67.079	.500	.958 E 06	86.746	.738
18	Early G Subgt.	.118 E 03	.120	11.790			
19	Late G Subgt.	.965 E 02	.098	9.610			
20	SMR K0-K1IV	.878 E 02	.089	13.850			
21	SMR K2III-IV	.288 E 02	.029	18.120			
22	SMR K3III	.155 E 02	.016	16.030	.198 E 02	.021	25.036
23	SMR K4-5III	.313 E 01	.003	4.940			
24	Hyades G8III				.164 E 02	.030	20.729
25	Normal G8-K0III						
26	Normal K0-K1IV						
27	K1III-K3III						
28	K4III-K5III						
29	M0III-M2III				.765 E 00	.001	2.413

Reproduced with permission of the copyright owner. Further reproduction prohibited without permission.

TABLE 2 continued

M 31 MODELS

		Spinrad and Taylor's Model			Model 1		
Gr. No.	Group Name	No. Stars	Mass (%)	V Light (%)	No. Stars	Mass (%)	V Light (%)
30	M3III-M4III						
31	M5III-M6III						
32	M8III-M9III						
33	Carbon Star				.203 E 00	.000	.641
34	WD A				.708 E 03	.577	.096
35	M15+M92						
36	M3+M5						
37	NGC 6356						
38	Hor. Branch						
	M/L	43.690			49.882		
	$\Sigma\sigma^2$	324			198		

Reproduced with permission of the copyright owner. Further reproduction prohibited without permission.

TABLE 2 continued

M 31 Models

Model 2

Gr. No.	Group Name	No. Stars	Mass (%)	Light at 3300 Å (%)	V Light (%)	Light at 3.4μ (%)
1	O-B Dwarf					
2	Late B Dwarf					
3	Early A Dwarf					
4	Late A Dwarf					
5	Early F Dwarf					
6	Middle F Dwarf					
7	Late F Dwarf	.149 E 01	.002	.370	.136	.022
8	Early G Dwarf	.149 E 03	.140	17.379	7.961	1.467
9	G5V-K0V	.222 E 03	.189	7.470	4.774	1.170
10	K1V-K2V	.169 E 03	.111	2.918	2.434	.698
11	K3V-K4V	.432 E 03	.264	3.007	3.938	1.806
12	K5V-K7V	.127 E 04	.718	1.110	2.991	2.194
13	M0V-M2V	.227 E 04	.855	.313	1.212	2.427
14	M3V-M4V	.630 E 04	1.781	.130	.710	2.683
15	M5V-M6V	.129 E 05	2.423	.054	.294	2.200
16	M7V	.286 E 05	4.038	.000	.384	4.030
17	M8V	.947 E 06	89.212	.000	.863	43.416
18	Early G Subgt.	.984 E 02	.111	31.473	14.206	2.618
19	Late G Subgt.	.728 E 02	.082	16.167	10.513	3.335
20	SMR K0-K1IV	.277 E 02	.031	4.527	6.330	2.697
21	SMR K2III-IV	.274 E 02	.031	10.867	24.949	12.897
22	SMR K3III	.767 E 01	.009	3.212	11.487	8.122
23	SMR K4-5III	.245 E 01	.003	.876	5.615	6.177
24	Hyades G8II					
25	Normal G8-K0III					
26	Normal K0-K1IV					
27	K1III-K3III					
28	K4III-K5III					
29	M0III-M2III	.323 E 00	.000	1.129	1.204	2.042

Reproduced with permission of the copyright owner. Further reproduction prohibited without permission.

TABLE 2 continued

M 31 Models

		Model 2				
Gr. No.	Group Name	No. Stars	Mass (%)	Light at 3300 Å (%)	V Light (%)	Light at 3.4μ (%)
30	M3III-M4III					
31	M5III-M6III					
32	M8III-M9III					
33	Carbon Star					
34	WD A					
35	M5+M92					
36	M3+M5					
37	NGC 6356					
38	Hor. Branch					
	M/L	56.726				
	$\Sigma\sigma^2$	251				

Reproduced with permission of the copyright owner. Further reproduction prohibited without permission.

TABLE 2 continued

M 31 MODELS

Model 3

Gr. No.	Group Name	No. Stars	Mass (%)	Light at 3300 Å (%)	V Light (%)
1	O-B Dwarf	.329 E-02	.000	8.000	.442
2	Late B Dwarf				
3	Early A Dwarf				
4	Late A Dwarf				
5	Early F Dwarf				
6	Middle F Dwarf				
7	Late F Dwarf				
8	Early G Dwarf	.127 E 03	.120	14.720	6.869
9	G5V-K0V	.190 E 03	.162	6.327	4.119
10	K1V-K2V	.146 E 03	.097	2.510	2.133
11	K3V-K4V	.374 E 03	.230	2.586	3.450
12	K5V-K7V	.110 E 04	.628	.958	2.629
13	M0V-M2V	.197 E 04	.747	.270	1.066
14	M3V-M4V	.548 E 04	1.557	.112	.624
15	M5V-M6V	.117 E 05	2.209	.048	.270
16	M7V	.271 E 05	3.852	.000	.368
17	M8V	.952 E 06	90.148	.000	.877
18	Early G Subgt.	.839 E 02	.095	26.659	12.259
19	Late G Subgt.	.621 E 02	.071	13.699	9.072
20	SMR K0-K1IV	.311 E 02	.035	5.055	7.201
21	SMR K2III-IV	.308 E 02	.035	12.133	28.380
22	SMR K3III	.862 E 01	.010	3.586	13.067
23	SMR K4-5III	.276 E 01	.003	.978	6.387
24	Hyades G8III				
25	Normal G8-K0III				
26	Normal K0-K1IV				
27	K1III-K3III				
28	K4III-K5III				

TABLE 2 continued

M 31 MODELS

Model 3

Gr. No.	Group Name	No. Stars	Mass (%)	Light at 3300 Å (%)	V Light (%)
29	M0III-M2III				
30	M3III-M4III				
31	M5III-M6III				
32	M8III-M9III				
33	Carbon star				
34	WD A				
35	M15+M92				
36	M3+M5				
37	NGC 6356				
38	Hor. Branch	.278 E 00	.000	2.364	.787
	M/L	57.041			
	$\Sigma\sigma^2$	267			

Reproduced with permission of the copyright owner. Further reproduction prohibited without permission.

In Table 1, the entries in the column headed "Ratio" are the limits between which the number of stars in Group A relative to the number in Group B was constrained to lie. The numbers of stars presented have been normalized to a total of 10^6 stars per model. By applying sufficiently narrow constraints, it is possible to reproduce quite accurately any model already specified, and a version quite close to ST's best compromise model for M 31 is shown for comparison in Table 2. All models presented in this paper were computed with weights W_j equal to 1.0 in each filter unless otherwise specified.

As described above, the approach adopted involved beginning with few constraints, proceeding towards progressively well-determined models and observing at each step the effect on the solution. Interestingly, however, the very first model calculated for M 31 with no constraints whatever (Model 1) possesses all the characteristics of the final solution though the numbers of stars do not vary smoothly from group to group. Globular clusters were omitted from the solution because no far-infrared colors are available for them. This solution has a large number of M8 dwarfs, even more than are present in the ST model. These stars supply 87 per cent of the mass and virtually all the M star contribution in the infrared, some 38 per cent of the total flux at 3.4μ. Because of the large number of M8 dwarfs, M/L is almost 50. (All values of M/L in this paper represent the ratio of mass

Reproduced with permission of the copyright owner. Further reproduction prohibited without permission.

to visual light.) The largest single contributors to the visible light are super-metal-rich (SMR) giants. The upper main sequence contribution is negligible. Lastly, the galaxy appears to require a fairly strong ultraviolet continuum, to which the most important contributor after the G5V-K0V stars is the Hyades giant group. In fact, the required ratio of Hyades giants to main sequence precursors in this model is greater than 10.

The residuals σ, in the sense (model - observed), for all the M 31 models including ST's are presented in Figure 1. Comparison of the ST model with Model 1 shows that the run of the largest residuals is similar. Therefore these largest residuals represent intensities in the present photometry that cannot be duplicated by any physically possible combination of the available stellar groups. Whether these represent photometric errors, unknown sources of absorption or emission, or simply the presence in M 31 of stars unlike those in the stellar groups used in the synthesis is not known. It is of interest to compare $\Sigma\sigma^2$ (shown in Table 2) for the ST model and Model 1 with the sum expected from observational errors alone. The error in the computed flux due to errors in the stellar photometry is small and to a first approximation may be neglected. The expected sum due to errors in the galaxy colors depends crucially on whether the K and L filters are included, since the errors for these two quantities are 0.04 and 0.17

Reproduced with permission of the copyright owner. Further reproduction prohibited without permission.

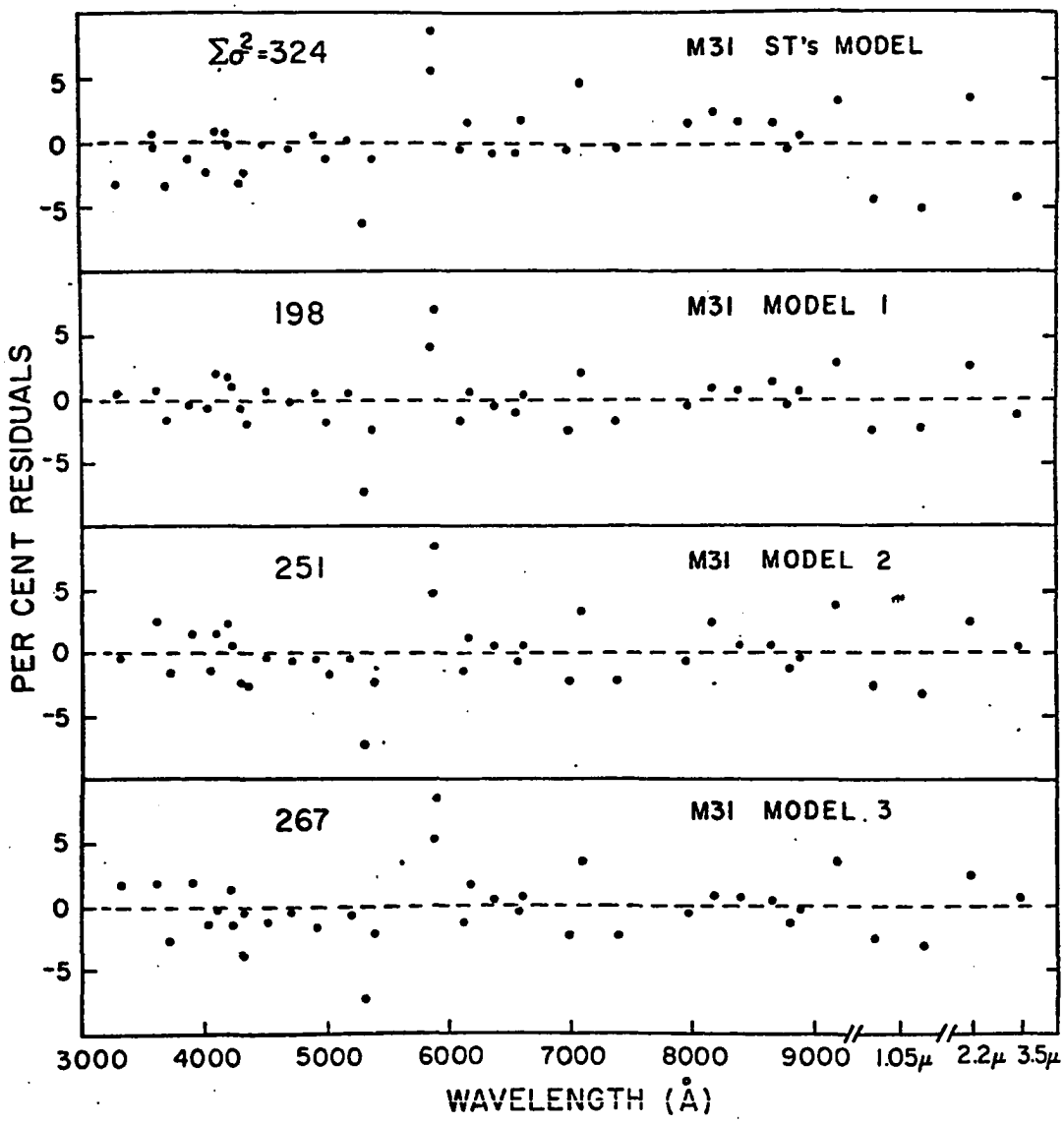

Fig. 1. Per cent residuals, in the sense (Model - Observed), for four models for the nucleus of M 31. Colors in all 38 filters were used.

Reproduced with permission of the copyright owner. Further reproduction prohibited without permission.

magnitude. The sum for 36 filters is 33.3 while for all 38 filters it is 282. The near equality of the latter number with the sums actually computed from the models might indicate that the attempt to duplicate the K and L colors precisely has caused the larger errors in these measurements to propagate backwards to shorter wavelengths. That this is not the case, however, is demonstrated by M 31 models based on only the first 36 filters, for all of which the run of the residuals is quite similar to that in Model 1. Hence, the large excess of the residuals in all M 31 models indicates clearly the presence of systematic deficiencies in either the choice of input stars, the assumed stellar colors, the galaxy colors, or all three.

The discontinuous nature of the solution in Model 1 is rather striking. Large numbers of one kind of star are present while stars of neighboring spectral type are omitted. The fact that a given x_k has been set to zero indicates that the residual sum would remain constant or decrease if a negative number of stars of that type could be added to the solution. This statement may be verified by assigning such a group a negative luminosity and then rerunning the calculation, in which case a positive number of such stars appears in the subsequent model. The discontinuous property of Model 1 demonstrates that smoothing constraints are an indispensable feature of the procedure if a smoothly-varying H-R diagram is

Reproduced with permission of the copyright owner. Further reproduction prohibited without permission.

desired. Such smoothing constraints for the main sequence were adopted in the form of various trial luminosity functions (Figure 2). Several of these were tested.

Functions III and IV yielded UV continua that were too faint and were rejected immediately. With Functions I and II, the number of Hyades giants always greatly exceeded the number of main sequence precursors. These giants were consequently eliminated from future models. Once this change was made, all subsequent models selected SMR giants exclusively. Because spectra of M 31 show that large numbers of upper main sequence stars cannot be present and because the light contributions from groups 1-5 in the initial models tested were always small, the upper main sequence through group 5 was set to zero. It was also found that a smooth giant branch would not arise automatically, but rather the solutions were discrete in a manner similar to Model 1. However, all solutions had giant branch luminosity functions that generally resembled that of M 67. Hence a luminosity function for the giants found by smoothing the counts of giant branch stars in M 67 was incorporated. This function is shown in Table 3. The quantity "Ratio" represents the number of stars in group A relative to the number in the corresponding group B. Here the two separate upper branches, one normal in abundance, the other composed of SMR stars, are imagined to grow out of a common subgiant branch. The number of subgiants relative to

Reproduced with permission of the copyright owner. Further reproduction prohibited without permission.

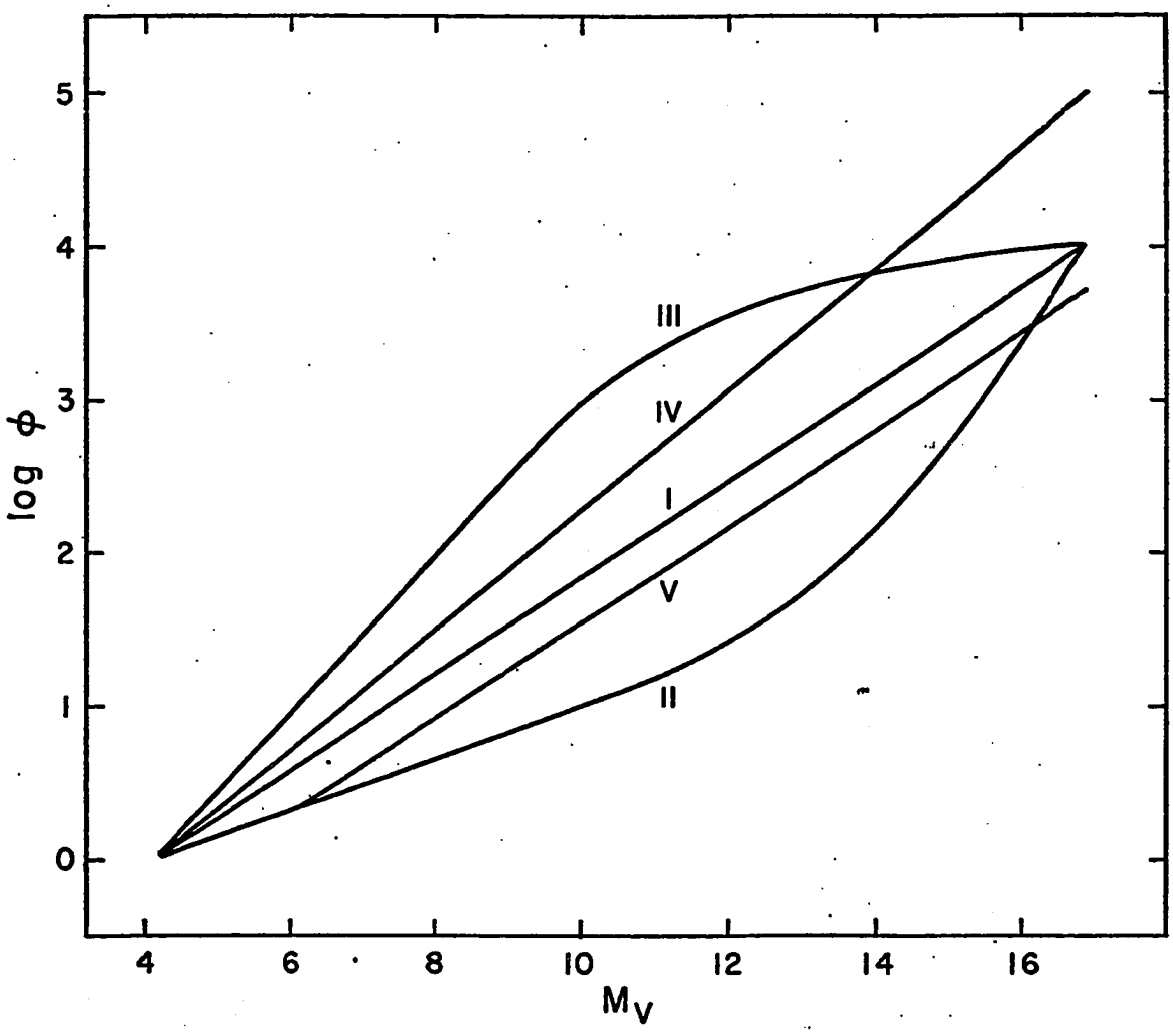

Fig. 2. Trial main-sequence luminosity functions used as smoothing constraints for the main sequence. The ordinate is the logarithm of the number of stars per unit magnitude, relative to an arbitrary zero-point.

Reproduced with permission of the copyright owner. Further reproduction prohibited without permission.

TABLE 3

ASSUMED LUMINOSITY FUNCTION ON THE GIANT BRANCH

Group A	Group B	Ratio A/B
Early G Subgt.	Early G Dwarf	Variable
Late G Subgt.	Early G Subgt.	.73
SMR K0-K1IV	Late G Subgt.	Freely Adjustable
SMR K2III-IV	SMR K0-K1IV	1.00
SMR K3III	SMR K2III-IV	0.29
SMR K4-5III	SMR K3III	0.33
Normal K0-K1IV	Late G Subgt.	Freely Adjustable
Normal G8-K0III	Normal K0-K1IV	1.00
Normal K1-K3III	Normal G8-K0III	0.29
Normal K4-K5III	Normal K1-K3III	0.33

Reproduced with permission of the copyright owner. Further reproduction prohibited without permission.

early G dwarfs can be varied, while the numbers of upper giant branch stars are left free in an effort to leave open the choice between normal or strong-lined stars. Use of an M 67 giant branch increased the residual sum by only 10 units.

With these added constraints it was possible to investigate the effect of using either Function I or Function II and of varying the number of subgiants from approximately one-third to twice the number of early G dwarfs. Because of their influence on the UV continuum, these alterations vary the turnoff from group 6 to group 8. They also have a drastic impact on the alternate sources of UV flux that were still allowed at this point in the calculations, namely white dwarfs and horizontal branch stars. On the other hand, the total number of giants on the SMR upper giant branch was quite insensitive to these changes, the ratio of K0-K4V stars to K0-K5III stars always lying between 5 and 15. Normal giants were never present in any of these models. For a given set of constraints, Function I always yielded a residual sum approximately 100 units larger than that of Function II, because the main sequence just below turnoff for the former is so steep that either the numbers of subgiants are unreasonable or the model UV continuum is too weak.

Model 2 in Table 2 represents one of the better models in this set. Function II was used, but the number of M8 dwarfs was freely adjustable. The number of early G sub-

Reproduced with permission of the copyright owner. Further reproduction prohibited without permission.

giants is two-thirds the number of early G dwarfs, though this ratio can be halved without appreciably affecting the residuals. If this is done, the resultant giant branch approximates almost exactly the luminosity function in M 67. In this model horizontal branch stars and white dwarfs were excluded, but similar models with fewer than 0.1 horizontal branch stars and/or 1000 white dwarfs containing 3 per cent or less of the total mass were equally acceptable. No statements concerning redder and fainter white dwarfs can be made since they were not included in the calculations. Ratios of numbers of giant stars in contiguous groups can also be altered by a factor of two without disturbing the residuals.

Though it is by now apparent that one is allowed considerable flexibility in fitting the galaxy intensities, all models tested with a residual sum within 50 units of Model 2 had certain characteristics in common. All relied exclusively on SMR giants. All had a main sequence turnoff between middle F dwarfs and early G dwarfs. The main sequence below turnoff was relatively flat, producing rather low ratios, between 5 and 15, of K dwarfs to K giants (the value for ST's model is 6.8). This property, together with the large numbers of M8V dwarfs, results in a luminosity function that turns upwards at small masses. In fact, the larger sum of residuals squared in the ST model, which otherwise does not differ drastically from Model 2, is caused by the use of a luminosity

Reproduced with permission of the copyright owner. Further reproduction prohibited without permission.

function too closely similar to Function I (see Figure 3). Function V was tried here but did not yield appreciably smaller residuals than Function I. Finally, because of the use of M dwarfs rather than M giants to supply the infrared luminosity, the mass-to-light ratios were invariably high, lying between 45 and 60.

The reality of these common characteristics can be tested by the methods suggested above. Model 2 was recomputed in several ways and the constraints and input data varied each time. If instead of imposing Function II, we require only that the numbers of stars along the main sequence in consecutive groups increase monotonically, the giant branch and residuals are largely unaffected, but the resultant main-sequence luminosity function is as shown in Figure 3. In addition, models computed with the line indices given double weight do not differ significantly from Model 2.

The stability of the model against the addition of anomalous elements can also be examined. As a test of uniqueness, the same example chosen by Spinrad and Taylor to illustrate such stability was selected. In that instance, 37 O9V stars were added to the best compromise model with the result that the UV continuum rose to unacceptably high levels, giving a residual of 8 per cent at 3300 Å. Such an example is not realistic, however, because it does not test the existence of models only slightly different from Model 2 that contain

Reproduced with permission of the copyright owner. Further reproduction prohibited without permission.

Reproduced with permission of the copyright owner. Further reproduction prohibited without permission.

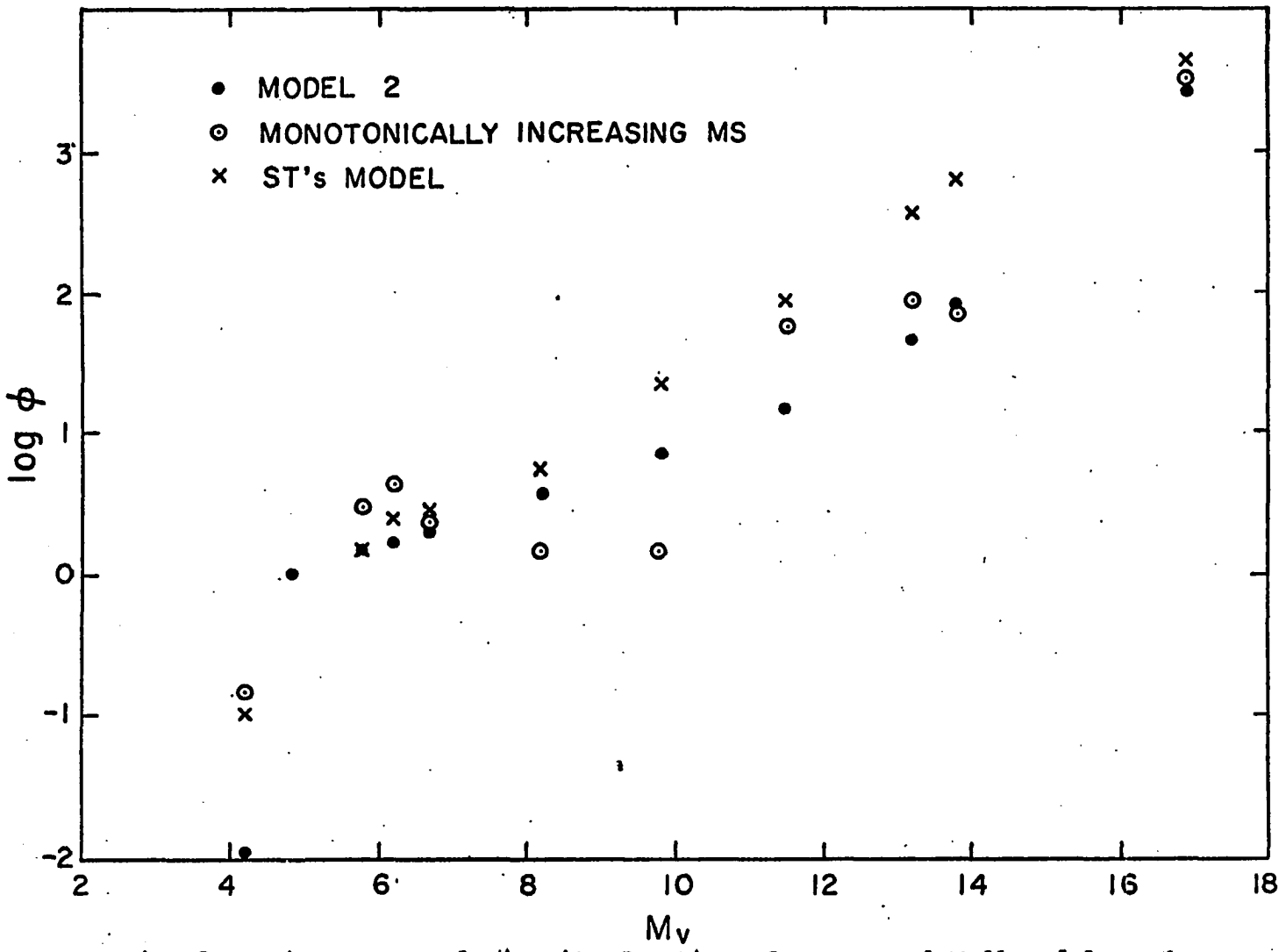

Fig. 3. Main-sequence luminosity functions from several M 31 models. The open circles represent the luminosity function that results when the numbers of stars in successively fainter synthesis groups are constrained to increase monotonically.

the so-called anomalous elements and still fit the observed colors. It is more reasonable to insist that 8 per cent of the UV flux be provided by O-B stars and then to see whether the basic model can adjust itself to accommodate this addition without raising the residuals to unacceptable levels. The result of such a test is provided by Model 3, the residuals for which are available in Figure 1. Although the scatter in the UV has increased marginally and the turnoff has moved down the main sequence one group, the resultant model is not markedly less acceptable than Model 2 in any way. Considerable experimentation suggests that if a given model is specified no more rigidly than Model 2, one may require that up to 10 per cent of the flux at any wavelength come from any given group, without disturbing the basic properties of the stellar population. This fact, together with the uncertainty in our knowledge concerning the sources of UV radiation to be expected in an old but strong-lined stellar population (white dwarfs, horizontal branch stars, blue stragglers, and a possible admixture of a metal-poor population), indicates that the location of the turnoff certainly cannot be known with an accuracy of better than plus or minus one stellar group. At group 7, this corresponds to a variation in the age of the stellar population of from 3 to 7 $\times$ 10^9 years for stars of solar abundance (Iben, 1967).

Reproduced with permission of the copyright owner. Further reproduction prohibited without permission.

The models have indicated clearly that the stars in the center of M 31 must be very strong-lined. The interpretation of this fact in terms of actual composition naturally depends upon the determination of metal abundance for the input stellar groups observed in our own galaxy. As pointed out by Spinrad and Taylor, one cannot determine whether a population having absorption lines of moderate strength is composed exclusively of objects with intermediate metal abundance or whether it contains a mixture of metal-poor and metal-rich populations. This is the ambiguity presented by M 32. Determination of helium content is probably beyond reach because of the possible spread in giant luminosities within M 31 itself and the ease with which giants may be shuffled about on the giant branches of the computed models.

Although all the acceptable models calculated for M 31 had mass-to-light ratios within rather well-defined limits, this third parameter is the least well-determined. The strong M8V contribution is required to fit exactly the assumed infrared colors K and L. If K and L are arbitrarily made bluer by an average of 0.32 magnitude, the M8V component totally disappears, and M/L falls to 20.0. M dwarfs are necessary because the $(K-L)_o$ index for M 31 assumed by Spinrad and Taylor is large, 0.39 magnitude. Only two groups of stars among the systhesis groups, M8V and M8-9III, have $(K-L)_o$ larger than this value, each having $(K-L)_o$ equal to 0.70. Since the great

Reproduced with permission of the copyright owner. Further reproduction prohibited without permission.

majority of synthesis groups has $(K-L)_o$ much smaller than 0.39, a large contribution from a group with high $(K-L)_o$ is necessary in order to bring the model $(K-L)_o$ up to the observed value for M 31. If the M giants are used to match the colors at K and L, their continua are so steep ($(V-K)_o$ equals 12.0) that they make very little contribution at 1μ, where the model is therefore too faint. Hence, M8V dwarfs must be used to match the continua precisely at 1, 2.2, and 3.5μ.

However, in view of the large observational errors associated with K and L, 0.04 and 0.17 magnitude any model that fits theobserved indices in these filters with errors smaller than these numbers has been unduly influenced by inherently inaccurate data. Consequently, there might exist M giant-dominated models with small M/L and red residuals that, though larger than the residuals for M dwarf models, are still no larger than the observational errors. By forcing M/L to equal 7.0, such a model was computed for M 31, which had residuals in the four reddest passbands that averaged 6 per cent. In view of the uncertainties in the K and L colors, this model and the dwarf-dominated models are equally acceptable.

More recent measurements of the infrared flux of M 31 and of MV stars have cast further doubt on the need for M dwarfs. Wolf 359 is the star used by Spinrad and Taylor as the type example for M8V. According to Greenstein, Neugebauer,

Reproduced with permission of the copyright owner. Further reproduction prohibited without permission.

and Becklin (1970), the infrared colors V-K and V-L for this object are 7.5 and 7.8 magnitude, differing greatly from the values 7.0 and 7.7 used by Spinrad and Taylor. In particular, K-L is only 0.3. The faintest known star, VB 10, measured by Greenstein, et al., has a K-L of only 0.5. These values are comparable to the K-L indices of M giants of similar overall color. Furthermore, Becklin (private communication) has recently remeasured the infrared colors of the M 31 nucleus through a 7".5 diaphragm. His new value for K-L is 0.11 ± 0.10 magnitude. This much smaller number removes the need for stars with large K-L indices. As a result, the infrared colors can now be duplicated equally well by M dwarfs or M giants.

The model computations described here will be repeated with these new data. However, several conclusions can be drawn from the calculations already performed. The models as they now stand fit the infrared data poorly. The new residuals for the ST model are +16 per cent at K and +19 per cent at L. The sense of the errors is such that future models will require fewer M stars of either high or low luminosity.

Since the infrared colors cannot be used to distinguish between M dwarfs and M giants, we are forced to rely on the luminosity discriminant at 8190 Å (Spinrad and Taylor 1970), which is in "emission " for M giants but not for M dwarfs. Because M stars contribute less than 25 per cent of

Reproduced with permission of the copyright owner. Further reproduction prohibited without permission.

of the light at 8190 Å, this index is not very sensitive to the relative numbers of dwarfs and giants. The computations in the following section, which use only the 36-color data on M 31, M 32, and M 81, show that M/L can be varied over wide limits without greatly increasing the residual at 8190 Å.

Spinrad and Taylor describe their best model as dwarf-enriched compared to the stellar population in the solar neighborhood. Nevertheless, the light at wavelengths shorter than 7000 Å in their model (and in the models presented in this paper) is produced largely by giants. At 5360 Å, the main sequence contributes only 20 per cent of the luminosity. This result necessarily means that the sensitivity to relative numbers of giants and dwarfs of spectral types G and K is small. Spinrad and Taylor have cited the strengths of the MgH and Na D indices as two criteria for estimating the dwarf contribution to the light. One can test this assertion,using their model, by computing the contribution to the model line indices arising from the dwarf and giant components. If the dwarf stars of types G5 through M2 are totally removed from the ST model, the strength of the MgH index decreases by only 3 per cent, and Na D decreases by only 1 per cent. Therefore, great caution should be exercised in drawing conclusions concerning the numbers of K dwarfs and K giants from the values of these two indices alone. This fact makes difficult the interpretation of positional variations in line-index strengths in gal-

Reproduced with permission of the copyright owner. Further reproduction prohibited without permission.

axies (see for example Spinrad, et al. 1971) unless adequate data on the continuum are also available.

Attention has been drawn to the present uncertainty in the M dwarf-M giant ratio in M 31. Since the models discussed above were computed with incorrect values of the K and L colors for both M dwarfs and M 31, it is of interest to examine a series of comparative models of M 31, M 32, and M 81 computed without the K and L colors. As is shown below, complete omission of the far infrared data renders the M giant contribution even more uncertain because no limits are placed on the allowable numbers of extremely red M8-9 giants. The following section discusses this point at greater length.

IV. COMPARATIVE MODELS FOR M 31, M 32, AND M 81

The data and discussion in ST have established that the nuclei of M 31, M 32, and M 81 consist of old stars. Therefore, a series of models for the three galaxies, all computed with identical constraints, can indicate clearly the relative nature of the stellar populations in the three nuclei. For example, M 32 is the bluest, while M 81 is the reddest. Does this fact indicate a sequence in mass-to-light ratio, metal abundance, or both?

Such a series of models should be as flexible as possible and yet produce a recognizable H-R diagram. The con-

Reproduced with permission of the copyright owner. Further reproduction prohibited without permission.

straints shown in Table 1 under Models A and B provide the best compromise between these two goals. The main sequence increases monotonically, the number of M8 dwarfs is freely adjustable, the number of early G subgiants is roughly one-third the number of early G dwarfs, an M 67 giant branch is adopted, and the upper main sequence and other subordinate groups of stars including globular clusters are omitted. Since far infrared colors for M 32 and M 81 are unavailable, only the 36-filter data are used. In Models A an asymptotically-decreasing M giant branch adjoined to the SMR giant branch can be selected, while all M giants redder than M2III are excluded from Models B. Table 4 contains the results of these calculations.

The inclusion of very late M giants clearly has a drastic effect on the models' M/L and lower-main-sequence luminosity functions. The change in M/L for M 32 has been made artificially small by forcing the number of M0-2III stars to adjoin smoothly to the SMR branch. In this galaxy, normal giants are present in greater numbers than SMR giants. The residuals for all Models A and B are displayed in Figure 4.

On the basis of the residual sums for the 36-filter data alone, we would conclude, though not firmly, that M8-9 giants contribute substantially to the infrared flux in M 31, whereas the K and L colors indicate the opposite. The residuals for Model A at K and L are over 100 per cent because of the

Reproduced with permission of the copyright owner. Further reproduction prohibited without permission.

Reproduced with permission of the copyright owner. Further reproduction prohibited without permission.

TABLE 4

COMPARATIVE MODELS FOR M 31, M 32, AND M 81

Gr. No.	Group Name	Number of Stars					
		M 31		M 32		M 81	
		A	B	A	B	A	B
1	O-B Dwarf						
2	Late B Dwarf						
3	Early A Dwarf						
4	Late A Dwarf						
5	Early F Dwarf	.583 E 01	.279 E 01			.442 E 03	
6	Middle F Dwarf	.583 E 01	.279 E 01			.246 E 04	.155 E 02
7	Late F Dwarf	.583 E 01	.279 E 01	.391 E 03	.230 E 03	.246 E 04	.798 E 02
8	Early G Dwarf	.798 E 03	.200 E 03	.391 E 03	.230 E 03	.246 E 04	.798 E 02
9	G5V-K0V	.127 E 04	.362 E 03	.391 E 03	.230 E 03	.246 E 04	.798 E 02
10	K1V-K2V	.127 E 04	.362 E 03	.391 E 03	.230 E 03	.246 E 04	.798 E 02
11	K3V-K4V	.127 E 04	.362 E 03	.391 E 03	.230 E 03	.246 E 04	.798 E 02
12	K5V-K7V	.127 E 04	.362 E 03	.391 E 03	.230 E 03	.167 E 05	.101 E 04
13	M0V-M2V	.127 E 04	.362 E 03	.391 E 03	.230 E 03	.242 E 06	.101 E 04
14	M3V-M4V	.127 E 04	.362 E 03	.391 E 03	.230 E 03	.242 E 06	.101 E 04
15	M5V-M6V	.495 E 06	.792 E 05	.391 E 03	.230 E 03	.242 E 06	.101 E 04
16	M7V	.495 E 06	.792 E 05	.997 E 05	.161 E 05	.242 E 06	.101 E 04
17	M8V		.839 E 06	.896 E 06	.982 E 06		.994 E 06
18	Early G Subgt.	.303 E 03	.762 E 02	.141 E 03	.828 E 02	.885 E 03	.287 E 02
19	Late G Subgt.	.224 E 03	.564 E 02	.101 E 03	.596 E 02	.638 E 03	.207 E 02
20	SMR K0-K1IV	.117 E 03	.317 E 02	.161 E 02	.687 E 01	.938 E 03	.329 E 02
21	SMR K2III-IV	.116 E 03	.314 E 02	.162 E 02	.694 E 01	.948 E 03	.333 E 02
22	SMR K3III	.324 E 02	.878 E 01	.487 E 01	.208 E 01	.284 E 03	.998 E 01
23	SMR K4-5III	.104 E 02	.281 E 01	.166 E 01	.707 E 00	.967 E 02	.339 E 01
24	Hyades G8III						
25	Normal G8-K0III			.295 E 02	.179 E 02	.397 E 02	
26	Normal K0-K1IV			.292 E 02	.177 E 02	.393 E 02	
27	K1III-K3III			.884 E 01	.502 E 01	.119 E 02	
28	K4III-K5III			.301 E 01	.161 E 01	.405 E 01	

Reproduced with permission of the copyright owner. Further reproduction prohibited without permission.

TABLE 4 continued

COMPARATIVE MODELS FOR M 31, M 32, AND M 81

Gr. No.	Group Name	M 31		M 32		M 81	
		A	B	A	B	A	B
29	M0III-M2III	.797 E-01		.166 E 01	.289 E 01	.820 E 02	.272 E 01
30	M3III-M4III	.797 E-01		.140 E 01		.107 E 01	
31	M5III-M6III	.797 E-01		.174 E 00		.107 E 01	
32	M8III-M9III	.797 E-01		.130 E-01		.107 E 01	
33	Carbon star						
34	WD A						
35	M15+M92						
36	M3+M5						
37	NGC 6356						
38	Hor. Branch						
	M/L	23.657	56.320	24.286	39.625	4.826	54.779
	$\Sigma\sigma^2$	213	231	72.5	74.0	126	178

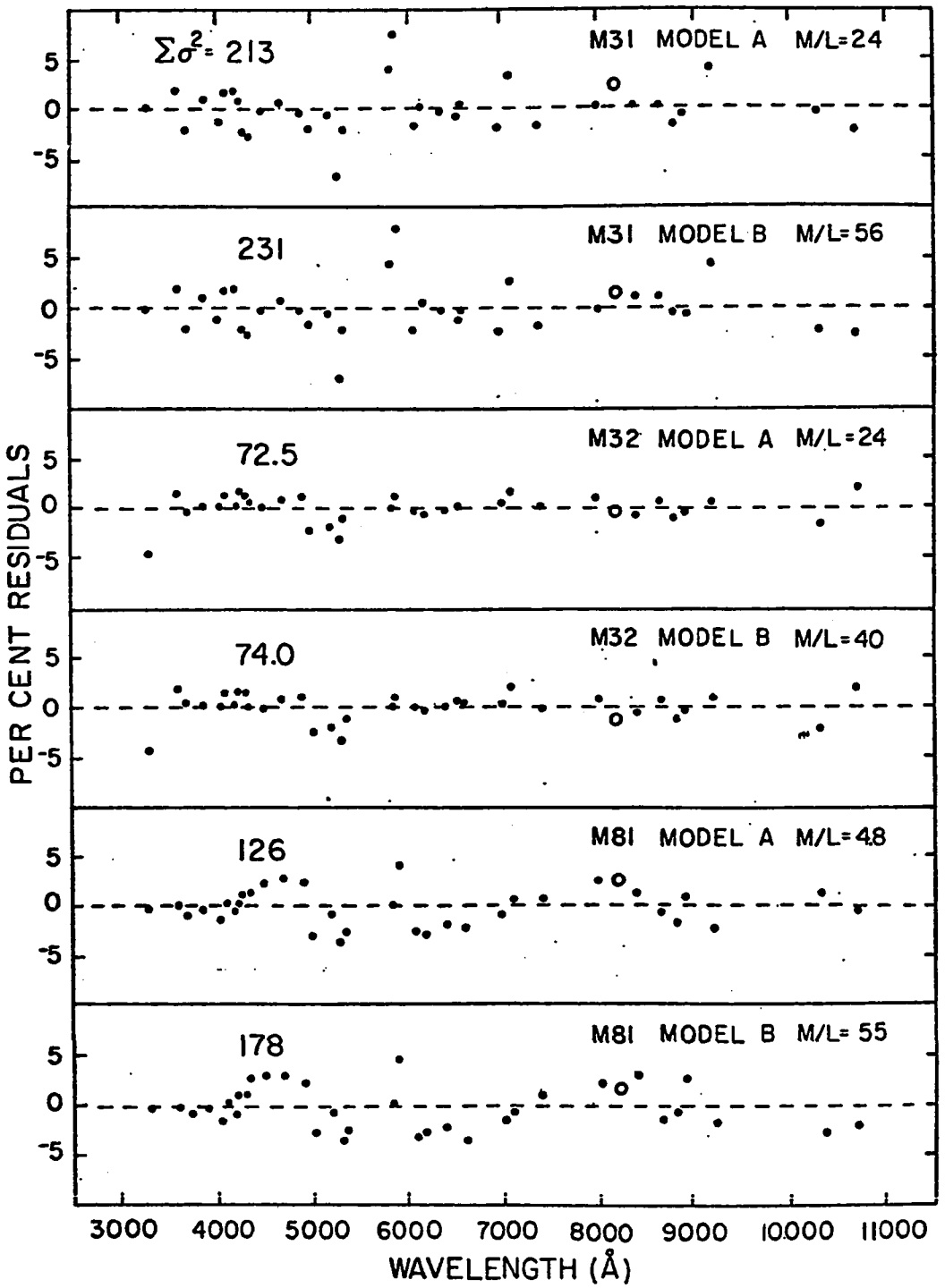

Fig. 4. Per cent residuals, in the sense (Model - Observed) for the comparative models for M 31, M 32, and M 81. In Models A, late M giants were allowed. In Models B, late M giants were excluded. The open circles denote the residuals at 8190 Å, an indicator of the M dwarf-M giant ratio.

Reproduced with permission of the copyright owner. Further reproduction prohibited without permission.

inclusion of M8 and M9 giants in the model. The 36-filter data however do not give any hint of this discrepancy at longer wavelengths. Therefore, continuum colors to the red of 1μ are essential in determining the number of M8-9 giants. Models lacking these data will not be well-determined. Moreover, as the model for M 31 with M/L equal to 7.00 has demonstrated, it is possible to achieve low mass-to-light ratios for M 31 without the use of M8-9 giants and without large residuals in the far infrared. An excellent model based on the moderately metal-poor globular cluster NGC 6356 can also be calculated for M 32 with extremely small red residuals and an M/L of 7.00, much smaller than the values of 24 and 40 computed for Models A and B.

Although the Na 8190 index does vary in the way one would predict from an M giant to an M dwarf model (see Figure 4), the index is not sensitive enough, given the scatter apparent in other residuals, to determine the M dwarf-M giant ratio with sufficient accuracy. M stars contribute only 25 per cent of the total model flux at this wavelength. Hence, an M dwarf-M giant discriminator must be placed at longer wavelengths. Frogel (private communication) has found that the 2.28μ band of CO can be used to distinguish M dwarfs from M giants. Observations of the strength of this CO band in galaxies would be most useful.

Reproduced with permission of the copyright owner. Further reproduction prohibited without permission.

Other features of this comparative series of models deserve mention. The model for M 32 having the smallest residual possessed an NGC 6356 cluster base providing 15 per cent of the visual light, together with roughly twice as many normal giants as SMR giants. M 81 models on the other hand always had SMR-dominated giant branches. The variations in turnoff point that appear in Table 3 are not meaningful since setting groups 5 and 6 to zero initially for all models makes virtually no change in the residuals. In short, the present set of calculations produces no evidence that suggests a systematic difference in age (based on the turnoff point) between M 31, M 32, and M 81.

V. ELLIPTICAL GALAXIES

The 10-color narrow-band photometric system used for photometry of elliptical galaxies is a hybrid of the systems developed by Wood (1966) and McClure and van den Bergh (1968a) for the study of stellar populations in galaxies. Table 5 contains a description of the passbands in the system. All measures discussed here have been made with an S-20 photomultiplier. The set of filters was designed to determine whether elliptical galaxies and globular clusters form a homogeneous system from the standpoint of their integrated energy distributions, but it was hoped that the data would also allow the construction of stellar population models.

Reproduced with permission of the copyright owner. Further reproduction prohibited without permission.

TABLE 5

PHOTOMETRIC SYSTEM

Filter	λ_{eff}	Half Width W_λ
35	3450 Å	390 Å
38	3803	140
41	4167	79
42	4257	82
45	4517	84
52	5162	54
55	5545	214
62	6222	108
67	6702	131
74	7415	188

Reproduced with permission of the copyright owner. Further reproduction prohibited without permission.

Reproduced with permission of the copyright owner. Further reproduction prohibited without permission.

TABLE 6

GROUP MEMBERS FOR E GALAXIES AND GLOBULAR CLUSTERS

Galaxies					Clusters		
Group 1	Group 2	Group 3	Group 4	Group 5	Group 1	Group 2	Group 3
NGC 205	NGC 221	NGC 584	NGC 2672	NGC 224	NGC 5024	NGC 5272	NGC 6356
3073	596	3193	2872	1332	6341	5904	
4627	1889	3226	3379	2300	7078	6205	
	2634	3608	4261	4472	7089	6254	
	3605	3613	4278	4486B		6779	
	4464	4283	4486	4649			
	6307	4478	5846A	5846			
		5982		7619			
				7626			

TABLE 7

MEAN COLORS OF E GALAXIES AND GLOBULAR CLUSTERS

	Galaxies					Clusters		
Color	Group 1	Group 2	Group 3	Group 4	Group 5	Group 1	Group 2	Group 3
$(35-55)_o$	1.605	2.167	2.249	2.368	2.468	1.529	1.680	1.995
$(38-55)_o$	1.169	1.892	1.961	2.049	2.171	1.074	1.237	1.777
$(41-55)_o$	.524	1.029	1.097	1.181	1.249	.592	.692	.986
$(42-55)_o$	.470	.953	.991	1.053	1.100	.556	.660	.913
$(45-55)_o$	.283	.509	.537	.558	.582	.370	.428	.539
$(52-55)_o$	.167	.292	.310	.354	.361	.124	.173	.293
$(62-55)_o$	-.127	-.187	-.195	-.208	-.223	-.170	-.189	-.139
$(67-55)_o$	-.282	-.343	-.367	-.386	-.400	-.261	-.301	-.314
$(74-55)_o$	-.376	-.543	-.599	-.625	-.637	-.377	-.436	-.524

Reproduced with permission of the copyright owner. Further reproduction prohibited without permission.

In order to increase accuracy and to minimize the effects of errors in corrections for galactic absorption, the galaxies and globular clusters were arranged in five and three groups respectively, according to the value of their reddening-corrected $(35-55)_o$ color index. It has been shown elsewhere (Chapter 2) that this quantity is also correlated with luminosity in the sense that the redder ellipticals are the most luminous. The group members are shown in Table 6 while mean colors for each group are presented in Table 7. With the exception of group 1 for the galaxies and group 3 for the globulars, the mean colors are accurate to better than 0.01 magnitude. Errors for the remaining two groups are less than 0.03 magnitude. Individual colors and diaphragm sizes for all of these objects are available elsewhere (Chapter 1 and Chapter 2), together with a more complete description of the photometric system.

The colors, masses, and absolute magnitudes of the stellar synthesis groups are given in Table 8, and the stars comprising each stellar group are listed in Table 9. For all groups except the late A-early F stars, the stellar colors were taken from Chapter 1. For the late A-early F stars, however, we used the mean colors given by Wood and McClure and van den Bergh, transformed to the present system. Because colors are not available for extremely late M dwarfs, the mass-to-light ratios in these models will be artificially low. Relative trends between groups of elliptical galaxies can still be studied however.

Reproduced with permission of the copyright owner. Further reproduction prohibited without permission.

Reproduced with permission of the copyright owner. Further reproduction prohibited without permission.

TABLE 8

GROUPS USED IN SYNTHESIS

Gr. No.	Name	Mass	M_V	Colors (35-55)	(38-55)	(41-55)	(42-55)	(45-55)
1	O-B	$10.0M_\odot$	-4.00	-0.44	-0.41	-0.46	-0.44	-0.33
2	Late BV-Early AV	$2.50^\odot$	0.70	1.03	0.37	-0.22	-0.21	-0.18
3	Late AV-Early FV	1.60	2.90	1.30	0.86	0.22	0.20	0.11
4	Late FV	1.20	4.20	1.34	1.00	0.44	0.44	0.24
5	Early GV	1.00	4.80	1.52	1.26	0.59	0.62	0.32
6	Late GV	0.85	5.30	1.73	1.54	0.72	0.76	0.36
7	Early KV	0.70	6.35	2.38	2.25	1.12	1.14	0.52
8	Late KV	0.55	7.70	3.29	2.99	1.71	1.79	0.80
9	Early MV	0.35	9.80	3.58	2.97	1.94	2.15	1.06
10	Middle MV	0.20	12.45	4.00	3.14	2.49	2.81	1.26
11	G0-5IV	1.20	3.00	1.78	1.51	0.68	0.68	0.33
12	G8-K0IV	1.20	2.60	2.45	2.21	1.17	1.10	0.57
13	G8-K0III	1.50	1.00	2.76	2.49	1.38	1.21	0.64
14	K3-5III	1.50	0.30	3.83	3.31	2.03	1.80	0.94
15	Early MIII	1.50	-0.30	4.72	3.71	2.34	2.23	1.24
16	Middle MIII	1.50	-0.50	4.03	2.72	1.41	1.54	1.21
17	Late MIII	1.50	-0.70	3.86	1.79	1.12	1.81	2.00
18	G-K SMR	1.20	0.55	3.42	3.11	1.82	1.49	0.78
19	Hyades Gt.	2.00	0.70	2.69	2.45	1.37	1.13	0.61
20	Pop. II Gt.	0.90	-0.80	2.39	1.73	1.09	1.04	0.68
21	G8-K0 Low Abund. Gt.	1.20	1.00	2.34	2.19	1.24	1.16	0.58
22	F Sd.	1.30	3.70	1.19	0.84	0.38	0.38	0.22
23	F9-G0 Sd.	1.10	4.60	1.38	1.10	0.54	0.58	0.31
24	Late G Sd.	0.70	5.60	2.15	1.94	1.05	1.03	0.53
25	Hor. Branch	0.50	0.50	1.29	0.39	-0.17	-0.15	-0.14
26	Group 1 Globular	10^5	-7.70	1.53	1.07	0.59	0.56	0.37
27	Group 2 Globular	10^5	-7.70	1.68	1.24	0.69	0.66	0.43
28	Group 3 Globular	10^5	-7.70	2.00	1.78	0.99	0.91	0.54

Reproduced with permission of the copyright owner. Further reproduction prohibited without permission.

TABLE 8 continued

GROUPS USED IN SYNTHESIS

Gr. No.	Name	Color					
		(52-55)	(62-55)	(67-55)	(74-55)	V-K	V-L
1	O-B	-0.12	0.21	0.35	0.50	-0.81	-0.86
2	Late BV-Early AV	-0.06	0.13	0.21	0.30	0.05	0.08
3	Late AV-Early FV	0.05	-0.02	0.04	0.07	0.73	0.80
4	Late FV	0.11	-0.07	-0.10	-0.13	1.20	1.38
5	Early GV	0.16	-0.11	-0.17	-0.22	1.37	1.55
6	Late GV	0.20	-0.14	-0.22	-0.28	1.60	1.80
7	Early KV	0.43	-0.22	-0.32	-0.42	2.11	2.19
8	Late KV	0.72	-0.32	-0.54	-0.79	3.03	3.18
9	Early MV	0.69	-0.19	-0.69	-1.44	3.95	4.15
10	Middle MV	0.66	0.09	-0.80	-2.09	5.17	5.54
11	G0-5IV	0.17	-0.12	-0.18	-0.23	1.49	1.67
12	G8-K0IV	0.30	-0.21	-0.34	-0.44	2.14	2.24
13	G8-K0III	0.31	-0.22	-0.36	-0.47	2.31	2.43
14	K3-5III	0.54	-0.29	-0.55	-0.78	3.09	3.24
15	Early MIII	0.50	-0.13	-0.71	-1.64	4.67	4.85
16	Middle MIII	0.05	-0.15	-0.91	-2.82	6.50	6.80
17	Late MIII	0.20	-0.54	-1.71	-4.05	10.88	11.49
18	G-K SMR	0.44	-0.26	-0.43	-0.55	2.68	2.83
19	Hyades Gt.	0.29	-0.20	-0.33	-0.41	2.22	2.34
20	Pop. II Gt.	0.23	-0.25	-0.39	-0.56	2.22	2.34
21	G8-K0 Low Abund. Gt.	0.27	-0.22	-0.34	-0.44	2.22	2.34
22	F Sd.	0.08	-0.08	-0.11	-0.16	1.09	1.27
23	F9-G0 Sd.	0.14	-0.11	-0.17	-0.23	1.35	1.53
24	Late G Sd.	0.30	-0.20	-0.32	-0.44	1.70	1.92
25	Hor. Branch	-0.05	0.08	0.15	0.21	0.13	0.16
26	Group 1 Globular	0.12	-0.17	-0.26	-0.38		
27	Group 2 Globular	0.17	-0.19	-0.30	-0.44		
28	Group 3 Globular	0.29	-0.14	-0.31	-0.52		

Reproduced with permission of the copyright owner. Further reproduction prohibited without permission.

TABLE 9

STARS IN SYNTHESIS GROUPS

Gr. No.	Name	Stars				
1	O-B V	1641	3454	6175	8622	
2	Late BV-Early AV	4468	2763	3410	4357	4386
		4534	5511			
3	Late AV-Early FV	Transformed from Wood (1966) and McClure and van den Bergh (1968a)				
4	Late FV	799	1543	4112	8969	
5	Early GV	483	660	937	1729	2047
		2721	4098	4845	4983	5911
		5968	6458	7503	7569	HD28068
		HD28099	HD28344	HD30649	HD115043	
6	Late GV	5544	7504			
7	Early KV	1084	1325A	8832		
8	Late KV	5568A	HD88230			
9	Early MV	5568B	HD95735	HD119850		
10	Middle MV	BD+4 3561				
11	G0-G5IV	5235	6212	6623		
12	G8-K0IV	1136	5535	6220	7602	8961
13	G8-K0III	2002	2035	2219	4287	4932
		5480	5709	7949	8255	
14	K3-K5III	224	4365			
15	Early MIII	2091	2286	4362	5154	8775
16	Middle MIII	867	4267	5589	6146	
17	Late MIII	3882	5080	HD126327		
18	G-K SMR III	1805	3369	3905	3994	5854
		7429	7576			
19	Hyades Giant	1346	1373	1409	1411	
20	Pop. II Giant	5270	HD2665	HD165195	HD221170	
21	G8-K0 Low Abund. Giant	1907	5681	HD26	HD201626	
22	F Subdwarf	5447	6775A	HD140283		
23	F9-G0 Subdwarf	5914	9088	HD22879	HD114762	HD148816
		HD152792	HD157089	HD160693		
24	Late G Subdwarf	4550	7477	HD25329		
25	Hor. Branch	HD86986	HD109995	HD161817		

This 10-color system is also insensitive to the M dwarf-M giant ratio since any M/L between 1.0 and 10.0 is consistent with the observed colors for galaxies in groups 2 through 5. Hence a comparative series of models was computed for the elliptical galaxies in a manner similar to that used for the ST photometry but with late M giants excluded. The constraints defining a representative set of these models are set forth in Table 10. The models themselves appear in Table 11 and the residuals in Figure 5. As before, for groups 2 through 5 the main sequence was constrained to be monotonic, an M 67 giant branch was assumed, and the number of M5 dwarfs was freely adjustable. For groups 4 and 5 the number of SMR giants was limited. Otherwise the SMR component became much too large. Since the line strengths for group 1 ellipticals suggested that a complete set of giants with the proper metal abundance was not available for synthesis, no constraints on the giant branch were imposed for this group. Otherwise the group 1 model was identical to those for groups 2 through 5.

These model ellipticals demonstrate a sequence that has several properties that correlate with integrated $(35-55)_o$ colors and therefore with luminosity. The dependence on a globular cluster base declines markedly from group 1 to group 5, while the number of SMR giants relative to normal giants rises until, in groups 4 and 5, normal giants are absent entirely. The subdwarf contribution also increases as the over-

Reproduced with permission of the copyright owner. Further reproduction prohibited without permission.

Reproduced with permission of the copyright owner. Further reproduction prohibited without permission.

TABLE 10

MODEL CONSTRAINTS FOR E GALAXIES

	Synthesis Groups set to zero	Light Contributors	Group A	Group B	Ratio A/B	M/L
Group 1:	1 17	None	3	4	0.00-1.00	None
	2 19	Specified	4	5	0.00-1.00	Specified
	16 25		5	6	0.00-1.00	
			6	7	0.00-1.00	
			7	8	0.00-1.00	
			8	9	0.00-1.00	
Groups 2-3:	1 17	None	22	23	0.00-1.00	None
	2 19	Specified	23	24	0.00-1.00	Specified
	16 25		27	7	0.00-1.00	
			3	4	0.00-1.00	
			4	5	0.00-1.00	
			5	6	0.00-1.00	
			6	7	0.00-1.00	
			7	8	0.00-1.00	
			8	9	0.00-1.00	
			11	24	0.50-1.00	
			11	5	0.50-1.00	
			12	11	0.54-0.56	
			14	12	0.12-0.14	
Groups 4-5:	Same as Groups 2-3	None Specified	Those for Groups 2-3 plus:			None Specified
			18	12	0.64-0.66	

Reproduced with permission of the copyright owner. Further reproduction prohibited without permission.

TABLE 11

E GALAXY MODELS

Gr. No.	Name	No. of Stars				
		Group 1	Group 2	Group 3	Group 4	Group 5
1	O-B·V					
2	Late BV-Early AV					
3	Late AV-Early FV	.132 E 05	.440 E 03	.355 E 03	.313 E 03	.226 E 03
4	Late FV	.132 E 05	.440 E 03	.355 E 03	.313 E 03	.226 E 03
5	Early GV	.132 E 05	.440 E 03	.355 E 03	.407 E 03	.482 E 03
6	Late GV	.132 E 05	.706 E 04	.253 E 04	.407 E 03	.482 E 03
7	Early KV	.132 E 05	.966 E 04	.545 E 04	.731 E 04	.701 E 04
8	Late KV	.451 E 06	.966 E 04	.545 E 04	.937 E 04	.701 E 04
9	Early MV	.451 E 06	.966 E 04	.545 E 04	.937 E 04	.701 E 04
10	Middle MV		.963 E 06	.979 E 06	.971 E 06	.976 E 06
11	G0-G5IV		.220 E 03	.177 E 03	.407 E 03	.482 E 03
12	G8-K0IV		.119 E 03	.957 E 02	.228 E 03	.270 E 03
13	G8-K0III		.198 E 03	.922 E 02		
14	K3-K5III	.486 E 03	.143 E 02	.115 E 02	.273 E 02	.324 E 02
15	Early MIII					
16	Middle MIII					
17	Late MIII					
18	G-K SMR III		.878 E 02	.125 E 03	.150 E 03	.178 E 03
91	Hyades Giant					
20	Pop. II Giant					
21	G8-K0 Low Abund. Giant					
22	F Subdwarf	.308 E 05			.817 E 02	
23	F9-G0 Subdwarf				.817 E 02	
24	Late G Subdwarf		.220 E 03	.177 E 03	.407 E 03	.482 E 03
25	Hor. Branch	.143 E 04				
26	Group 1 Globular					
27	Group 2 Globular					
28	Group 3 Globular	.201 E 01	.481 E-01	.447 E-01	.400 E-02	.902 E-02
	M/L	1.305	7.155	9.093	10.356	9.452
	$\Sigma\sigma^2$	35.7	3.2	5.7	11.7	15.0

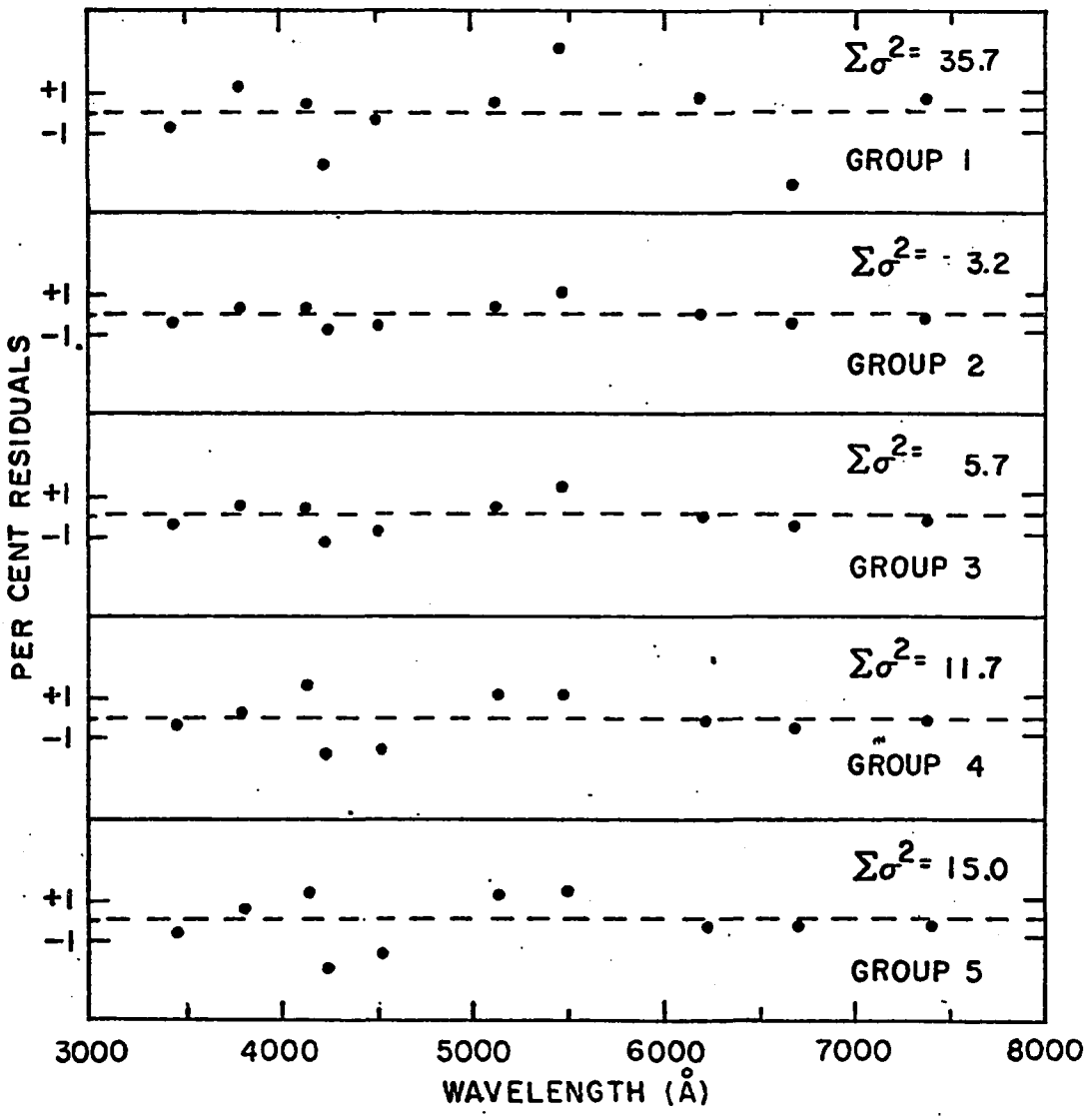

Fig. 5. Per cent residuals, in the sense (model - observed), for population models for elliptical galaxies. Increasing group number corresponds to increasing galaxy luminosity, redder continuum colors, and stronger absorption lines.

Reproduced with permission of the copyright owner. Further reproduction prohibited without permission.

all color reddens. At first this increase may seem paradoxical, but it results from the decline in the number of globular cluster stars, together with the presence of the same kind of UV continuum that was found in M 31. The subdwarfs therefore are used as increasingly important sources of UV flux. As in M 31, this need can be satisfied by other groups of relatively hot stars, and the rise in numbers of subdwarfs in redder ellipticals is therefore not a secure result.

The residual diagrams in Figure 5 demonstrate that the residuals from group to group are strongly correlated. Leaving aside group 1, for which the proper synthesis objects are probably not available, we see that the fit is best for group 2 and worsens increasingly as group 5 is approached. Clearly the set of synthesis objects and/or the assumed constraints are most appropriate for group 2 galaxies and increasingly inappropriate for the redder objects. As part of this trend, the computed CN indices (41-42) become progressively weaker than the observed galaxy indices for the redder objects. More stars with stronger CN are needed in the models.

The mass-to-light ratios also increase with increasing redness. This is an artificial effect, however, produced by the exclusion of M giants. A series similar to that in Table 10, but one that included M giants, showed no trend in M/L with color for groups 2 through 5, the values shifting randomly from group to group between 0.5 and 5.0. Johnson

Reproduced with permission of the copyright owner. Further reproduction prohibited without permission.

(1966) has published K and L photometry for NGC 4278, 4486, and 5846, which can be adjoined to the 10-color data for these galaxies. As for M 31, the results were inconclusive since either M dwarf or M giant models could fit the data within the observational errors for NGC 4278 and 4486, while no model could accurately fit the colors for NGC 5846. We conclude that the available data are insufficient to support Wood's (1966) assertion, made on the basis of 12-color photometry of elliptical galaxies similar to the 10-color data analyzed here, that M/L increases with increasing luminosity.

The models for groups 2 through 5 become increasingly red because more K stars have been included on the giant branch. In fact, the SMR giants for groups 4 and 5 were artificially constrained in order to prevent their number from becoming unreasonably large. If the models are presumed to represent a coeval stellar population, however, this inclusion of more giants is not strictly in accord with initial assumptions unless one also assumes (without justification) that giants evolve more slowly along the giant branch in groups 4 and 5 than in groups 2 and 3. The problem arises because the sample of giant stars in the synthesis groups does not include stars of a sufficient variety of compositions and ages. Therefore, although the actual galaxies in groups 4 and 5 may be redder because their giant branches are redder (due to increas-

Reproduced with permission of the copyright owner. Further reproduction prohibited without permission.

ing age or metal abundance, for example), the models become redder only through the inclusion of more giants that are redder than the mean star in the model. Clearly the matter of increasing redness and line strength with luminosity in elliptical galaxies is a subtle one. Attempts to understand the problem using the technique of population synthesis must employ a sufficiently varied mixture of stars of different ages and metal abundances.

VI. DISCUSSION

Since the photometric data alone do not provide accurate information about the mass-to-light ratio in M 31, M 32, M 81, and in elliptical galaxies, a summary of the available indirect evidence concerning this quantity is appropriate.

This evidence consists of two kinds, the first comprising our knowledge of the distribution of M giants in our own galaxy and in the Small Magellanic Cloud. The number of late M giants required by the giant-dominated models is small, approximately one-hundredth of the star density on the giant branch above the turnoff if M5-6 giants are used. Thus the lack of such stars in old galactic-cluster H-R diagrams cannot be used as evidence for the absence of similar stars in the extragalactic populations, since the cluster diagrams are simply too sparsely populated to show these stars. The K and L colors for M 31

Reproduced with permission of the copyright owner. Further reproduction prohibited without permission.

clearly preclude the presence of M5-6 giants in numbers sufficient to dominate the flux at 1μ, but because of the similarity in infrared colors between M8 dwarfs and M5-6 giants, the groups can be substituted for one another with relative ease as demonstrated by the model for M 31 with a mass-to-light ratio of 7.0. Therefore the basic question concerns the number of M5-6III stars present in these galaxies.

In his discussion of the origin of the infrared flux in elliptical galaxies, Tifft (1963) has noted that the colors of galaxies closely resemble the integrated colors of the old stellar population in the vicinity of NGC 121 in the Small Magellanic Cloud. His photometric study (Tifft, 1962) of this region revealed no significant number of very red giants. He cites this as weak but positive evidence for the absence of such stars in elliptical galaxies.

On the other hand, Wilson's (1959) color-magnitude diagram for stars in the solar neighborhood contains red giants with B-V nearly equal to 1.70, the mean color of M6 giants as tabulated by Mendoza and Johnson (1965). Tinsley (1971) has recently determined the giant-branch luminosity function for old-disk red giants, using the members of moving groups identified by Eggen. She finds that the old-disk giant branch does not end at M0III, as in M 67, but extends as far as M8III. The frequency of stars on the upper giant branch is approxi-

Reproduced with permission of the copyright owner. Further reproduction prohibited without permission.

mately 1 per cent of the frequency on the subgiant branch. The number of late M giants in the old-disk population is therefore similar to the number of such stars demanded by the giant-dominated models for M 31.

Studies of the space distribution of M5-6 giants indicate that the incidence of these stars increases towards the galactic center (Mavridis, 1971). Counts of M giants in the field of NGC 6522 by Nassau and Blanco (1958) revealed a strong maximum at M5-7 in the frequency distribution with spectral type. The number of these M giants versus apparent magnitude also displayed a strong peak at the apparent magnitude that would place them inside the nuclear bulge near the galactic center. van den Bergh's (1961) later study of the same field demonstrates that these M stars comprise 2 per cent of the total number of giants present. This is again similar to the relative number of M5-6 giants required by the model for M 31 with M/L equal to 7.0. The information available for M5-6 giants therefore indicates that they are a significant component of the stellar population near the center of our own galaxy.

Unfortunately the evidence from dynamical data concerning mass-to-light ratios for elliptical galaxies is very contradictory. Values of M/L for M 32 based on the nuclear rotation curve or the velocity dispersion have ranged from

Reproduced with permission of the copyright owner. Further reproduction prohibited without permission.

0.8-1.8 (Walker 1962) to 10 (Burbidge, Burbidge, and Fish 1961). Using velocity dispersions measured by Minkowski (1961), Fish (1964) derived a mass-to-light ratio of 23 for a mean elliptical galaxy. Against these fairly low values one must balance the estimate of 67 determined by Page (1965) from 28 double systems. The dynamical data on M 31 are equally confusing. Rubin and Ford (1970) have computed a value for M/L of 0.74 for the region within 3 kpc of the nucleus. In contrast, by assuming a constant M/L and an isotropic velocity dispersion of 225 km/sec, Kinman (1965) determined a mass-to-light ratio of 37 for the innermost 10 pc.

VII. SUMMARY

A method of matching synthesized populations to observed intensity distributions of galaxies has been developed that allows a more objective and accurate fit than has before been possible and at the same time affords more extensive methods of testing the reliability of the solution. This technique applied to both the 38-color data of Spinrad and Taylor and the 10-color data of Faber demonstrated that mean line-strengths of galaxy populations can be determined with considerable accuracy. The uncertainty in the turnoff from the main sequence is sufficiently large that with the presently available data, galaxy synthesis cannot provide a useful deter-

Reproduced with permission of the copyright owner. Further reproduction prohibited without permission.

mination of population ages. The dominant contributors to the computed spectra shortward of 8000 Å are invariably G and K giants, but the dwarf-giant ratio among M stars and thus the mass-to-light ratio remain highly uncertain. While dynamically determined values of M/L for elliptical galaxies and for M 31 are themselves very contradictory, an analogy with the stellar population in the nuclear bulge of our own galaxy suggests that M5-6 giants may be the most important contributor to the infrared continua in extra-galactic old stellar populations. This would imply that the mass-to-light ratios for these systems lie near the lower limits computed for M 31, M 32, and M 81. A photometric index that discriminates strongly between M dwarfs and M giants and is located at a wavelength longward of 1μ, together with highly accurate V-K and V-L colors for these objects, would be extremely valuable in distinguishing M dwarfs from M giants in old stellar populations.

Reproduced with permission of the copyright owner. Further reproduction prohibited without permission.

REFERENCES

Arp, H. C. 1962, Astrophys. J., 135, 311.

_____. 1966, Atlas of Peculiar Galaxies (Pasadena: California Institute of Technology).

Baum, W. A. 1959, Pub. Astron. Soc. Pacific, 71, 106.

Boot, J. C. 1964, Quadratic Programming (Amsterdam: North-Holland Publishing Company), p. 186.

Boyarchuk, M. E. 1960, Izv. Krymskoj Astrofiz Obs.,24, 115.

_____. 1962, Izv. Krymskoj Astrofiz Obs., 28, 94.

Burbidge, E. M., and Burbidge, G. R. 1965, Astrophys. J., 142, 634.

Burbidge, E. M., Burbidge, G. R., and Fish, R. A. 1961, Astrophys. J., 133, 393.

Cayrel, G. 1966, in I.A.U. Symp. No. 26, Abundance Determinations in Stellar Spectra, ed. H. Hubenet (London: Academic Press), p. 294.

_____. 1966, Ann. d'Astrophys., 29, 413.

Cayrel, R., and Cayrel, G. 1966, Annu. Rev. Astron. Astrophys., 4, 1.

Chaffee, F., Carbon, D., and Strom, S. E. 1971, Astrophys. J., 166, 593.

Danziger, I. J. 1966, Astrophys. J., 143, 591.

Deeming, T. J. 1964, Monthly Not. Roy. Astron. Soc., 127, 35.

Deutsch, A. J. 1964, Astrophys. J., 139, 532.

Fish, R. A. 1964, Astrophys. J., 139, 284.

Gratton, L. 1953, Mem. Soc. Roy. Sci. Liège, 14, 419.

Greenstein, J. L., and Keenan, P. C. 1958, Astrophys. J., 127, 172.

Greenstein, J. L., Neugebauer, G., and Becklin, E. 1970, Astrophys. J., 161, 519.

Reproduced with permission of the copyright owner. Further reproduction prohibited without permission.

Griffin, R. 1969, Monthly Not. Roy. Astron. Soc., 143, 223.

Hartwick, F. D. A. 1968, Astrophys. J., 154, 475.

Hayes, D. S. 1970, Astrophys. J., 159, 165.

Hazlehurst, J. 1963, Observatory, 83, 128.

Heeschen, D., and Wade, C. 1964, Astron. J., 69, 277.

Heiser, A. M. 1960, Astrophys. J., 132, 506.

Helfer, H. L., and Wallerstein, G. 1968, Astrophys. J. Suppl., 16, 1.

Helfer, H. L., Wallerstein, G., and Greenstein, J. L. 1963, Astrophys. J., 138, 97.

Herbig, G. H. 1965, Astrophys. J., 141, 588.

Hodge, P. W. 1963, Astron. J., 68, 237.

_____. 1971, Annu. Rev. Astron. Astrophys., 9, 35.

Holmberg, E. 1937, Ann. Lund Obs., No. 6.

_____. 1958, Lund Medd., Ser. II, No. 136.

Hoyle, F. 1962, in Proc. International School of Physics, Enrico Fermi, ed. L. Gratton (New York: Academic Press), p. 141.

Humason, M. L., Mayall, N. U., and Sandage, A. R. 1956, Astron. J., 61, 97.

Iben, I., Jr. 1967, Annu. Rev. Astron. Astrophys. 5, 571.

Johnson, H. L. 1966, Astrophys. J., 143, 187.

Jugaku, J. 1966, cited by Cayrel, R., and Cayrel, G., Annu. Rev. Astron. and Astrophys.,4, 1.

Kendall, M. G., and Stuart, A. 1966, Advanced Theory of Statistics, Vol. 3 (London: Charles Griffin and Company), p. 285.

King, I. R. 1962, Astron. J., 67, 471.

Reproduced with permission of the copyright owner. Further reproduction prohibited without permission.

_____. 1971, Publ. Astron. Soc. Pacific, 83, 377.

Koelbloed, D. 1967, Astrophys. J., 149, 299.

Krishna-Swamy, K. 1968, Astrophys. J., 154, 983.

Lasker, B. M. 1970, Astron. J., 75, 21.

Mannery, E., Wallerstein, G., and Welch, G. A. 1968, Astron. J., 73, 548.

Martin, W., and Bingham, R. 1970, Observatory, 90, 13.

Mavridis, L. N. 1971, in Structure and Evolution of the Galaxy, ed. L. N. Mavridis (New York: Springer-Verlag New York), p. 110.

McClure, R. D. 1969, Astron. J., 74, 50.

_____. 1970, Astron. J., 75, 41.

McClure, R. D., and Racine, R. 1969, Astron. J., 74, 1000.

McClure, R. D., and van den Bergh, S. 1968a, Astron. J., 73, 313.

_____. 1968b, Astron. J., 73, 1000.

Mendoza, E., V, and Johnson, H. L. 1965, Astrophys. J., 141, 161.

Mills, B., Slee, O., and Hill, E. 1958, Austral. J. Phys., 11, 360.

Minkowski, R. 1961, in Proceedings of the Fourth Berkeley Symposium on Mathematical Statistics and Probability, ed. J. Neyman (Berkeley: University of California Press), p. 245.

_____. 1962, in I.A.U. Symp. No. 15, Problems of Extra-Galactic Research, ed. G. C. McVittie (New York: The Macmillan Company), p. 112.

Moore, E. 1968, unpublished doctoral dissertation, University of Arizona.

Nassau, J. J., and Blanco, V. M. 1958, Astrophys. J., 128, 46.

Oke, J. B. 1964, Astrophys. J., 140, 689.

Reproduced with permission of the copyright owner. Further reproduction prohibited without permission.

Oke, J. B., and Sandage, A. R. 1968, Astrophys. J., 154, 21.

Oke, J. B., and Schild, R. E. 1970, Astrophys. J., 161, 1015.

Osterbrock, D. 1960, Astrophys. J., 130, 325.

Page, T. L. 1961, in Proceedings of the Fourth Berkeley Symposium on Mathematical Statistics and Probability, ed. J. Neyman (Berkeley: University of California Press), p. 277.

Page, T. L. 1965, SAO Special Report, No. 195.

Pagel, B. E. J. 1964, Roy. Obs. Bull., No. 87.

Powell, A. L. T. 1970, Monthly Not. Roy. Astron. Soc., 148, 477.

Rogstad, D., and Ekers, R. 1969, Astrophys. J., 157, 481.

Rood, H. J. 1969, Astrophys. J., 158, 657.

Rubin, V. C., and Ford, W. K., Jr. 1970, Astrophys. J., 159, 379.

Sandage, A. R. 1969, Astrophys. J., 157, 514.

Sandage, A. R., and Wallerstein, G. 1960, Astrophys. J., 131, 598.

Schild, R., and Oke, J. B. 1971, Astrophys. J., 169, 209.

Schwarzschild, M., Schwarzschild, B., Searle, L., and Meltzer, A. 1957, Astrophys. J., 125, 123.

Spinrad, H. 1966, Publ. Astron. Soc. Pacific, 78, 367.

_____. 1970, Quarterly J. Roy. Astron. Soc., 11, 188.

Spinrad, H., Gunn, J., Taylor, B., McClure, R., and Young, J. 1971, Astrophys. J., 164, 11.

Spinrad, H., and Peimbert, M. 1972, in Galaxies and the Universe, ed. A. and M. Sandage (Chicago: University of Chicago Press), in press.

Spinrad, H., and Taylor, B. J. 1969, Astrophys. J., 157, 1279.

_____. 1971a, Astrophys. J. Suppl., 22, 445.

_____. 1971b, Comments on Astrophys. and Space Sci., 3, 40.

Reproduced with permission of the copyright owner. Further reproduction prohibited without permission.

Spite, F. 1966, Ann. d'Astrophys., 29, 601.

Strom, S. E., Strom, K. M., and Carbon, D. 1971, Astron. and Astrophys., 12, 177.

Tifft, W. G. 1962, Monthly Not. Roy. Ast. Soc., 125, 199.

_____. 1963, Astron. J., 68, 302.

_____. 1969, Astron. J., 74, 354.

Tinsley, B. M. 1971, Astrophys. Letters, 9, 105.

van den Bergh, S., 1960, Astrophys. J., 131, 558.

_____. 1967, Astron. J., 72, 70.

_____. 1970, Nature, 225, 503.

Vaucouleurs, G. de 1961, Astrophys. J. Suppl., 5, 233.

Vaucouleurs, G. de and Malik, G. 1969, Monthly Not. Roy. Astron. Soc., 142, 429.

Vaucouleurs, G. de, and Vaucouleurs, A. de 1964, Reference Catalogue of Bright Galaxies (Austin: University of Texas Press).

Walker, M. F. 1962, Astrophys. J., 136, 695.

Wallerstein, G. 1961, Astrophys. J. Suppl., 6, 407.

Wallerstein, G., Greenstein, J. L., Parker, R., Helfer, H. L., and Aller, L. H. 1963, Astrophys. J., 137, 280.

Warner, B. 1965, Monthly Not. Roy. Astron. Soc., 129, 263.

Webb, C. J. 1964, Astron. J., 69, 442.

Whitford, A. E. 1958, Astron. J., 63, 201.

_____. 1971, Astrophys. J., 169, 215.

Wilson, O. C. 1959, Astrophys. J., 130, 496.

Wood, D. B. 1966, Astrophys. J., 145, 36.

_____. 1969, Astron. J., 74, 177.

Zwicky, F. 1964, Astrophys. J., 125, 451.

Reproduced with permission of the copyright owner. Further reproduction prohibited without permission.